PL-TR-97-2076

HIGH RESOLUTION MID-INFRARED SPECTROSCOPY OF CELESTIAL SOURCES

John H. Lacy

University of Texas at Austin
Austin, TX 78712

1 May 1997

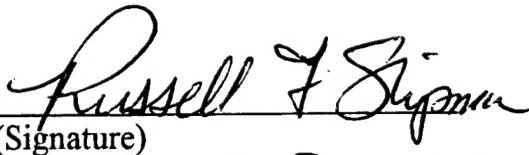Final Report
1 April 1994 - 31 January 1997

DTIC QUALITY INSPECTED 2
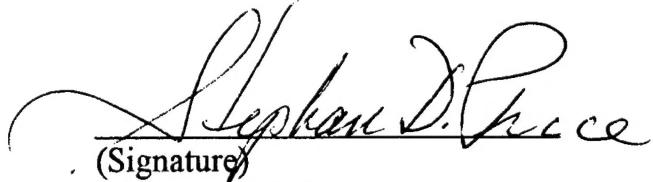
19980129 029

"This technical report has been reviewed and is approved for publications "

Russell F. Shipman
(Signature)
~~Dr.Frank Clark~~ Dr Russell F. Shipman
Contract Manager

Stephan D. Price
(Signature)
Dr.Stephan D. Price
Branch Chief

Duane E. Paulse
(Signature)
Dr.William A.M. Blumberg
Division Director

REPORT DOCUMENTATION PAGE

Public reporting burden for this collection of information is estimated to average 1 hour per response, including the time for reviewing instructions, searching existing data sources, gathering and maintaining the data needed, and completing and reviewing the collection of information. Send comments regarding this burden estimate or any other aspect of this collection of information, including suggestions for reducing this burden, to Washington Headquarters Services, Directorate for Information Operations and Reports, 1215 Jefferson Davis Highway, Suite 1204, Arlington, VA 22202-4302, and to the Office of Management and Budget, Paperwork Reduction Project (0704-0188), Washington, DC 20503.

1. AGENCY USE ONLY (Leave blank)	2. REPORT DATE May 1, 1997	3. REPORT TYPE AND DATES COVERED Final Technical Report 4/1/94–1/31/97

4. TITLE AND SUBTITLE

High Resolution Mid-Infrared Spectroscopy of Celestial Sources

5. FUNDING NUMBERS

F19628-93-K-0011
PE62101F
PR3054 TA GG
WU AA

6. AUTHOR(S)

John H. Lacy

7. PERFORMING ORGANIZATION NAME(S) AND ADDRESS(ES)

University of Texas at Austin
Austin, TX 78712

8. PERFORMING ORGANIZATION REPORT NUMBER

9. SPONSORING / MONITORING AGENCY NAME(S) AND ADDRESS(ES)

Phillips Laboratory
29 Randolph Rd.
Hanscom, MA 01731-3010

Contract Manager: Russell Shipman/GPOB

10. SPONSORING / MONITORING AGENCY REPORT NUMBER

PL-TR-97-2076

11. SUPPLEMENTARY NOTES

12a. DISTRIBUTION / AVAILABILITY STATEMENT

Approved for public release;
distribution unlimited

12b. DISTRIBUTION CODE

13. ABSTRACT (Maximum 200 words)

This contract supported high resolution telescopic observations of a wide variety of celestial sources at wavelengths between 5 and 25 μm. The observations were made to provide information about targets to be observed by the Infrared Space Observatory Short Wavelength Spectrometer and to provide data relevant to the Air Force Celestial Background Scene Descriptor. Observations made at the European Southern Observatory and the NASA Infrared Telescope Facility are described.

14. SUBJECT TERMS

Infrared Spectroscopy, Celestial Background

15. NUMBER OF PAGES
118

16. PRICE CODE

17. SECURITY CLASSIFICATION OF REPORT	18. SECURITY CLASSIFICATION OF THIS PAGE	19. SECURITY CLASSIFICATION OF ABSTRACT	20. LIMITATION OF ABSTRACT
Unclassified	Unclassified	Unclassified	SAR

NSN 7540-01-280-5500

Standard Form 298 (Rev. 2-89)
Prescribed by ANSI Std. Z39-18
298-102

CONTENTS

1. INTRODUCTION

This final report is for a project entitled, "High Resolution Mid-Infrared Spectroscopy of Celestial Sources".

The project involved mid-infrared spectroscopy of astronomical sources. These observations had two primary purposes: to provide information to the Infrared Space Observatory (ISO) Short Wavelength Spectrometer (SWS) team in preparation for the flight of ISO, and to provide information about the spectral content of the celestial background in support of the Air Force Celestial Background Scene Descriptor.

The SWS is a moderate to high resolution (R = 1000-2000 with a grating or 25,000 with a Fabry-Perot) mid-infrared (2.4-45 μm) spectrometer which is now in use on the ISO spacecraft. Because it observes in a spectral region which had been relatively little explored, especially at high spectral resolution, it was important to make exploratory observations of potential targets before its flight. Much of the spectral region observed by the SWS is inaccessible from ground-based telescopes, but observations can be made through several atmospheric windows, at 3-4μm, 4.5-5.5μm, 7.5-13.5μm, and to some extent at 17-25μm. The best instrument for observations in the latter two windows is the University of Texas Irshell spectrograph (Lacy *et al.* 1989), which was used for this project.

Irshell is a grating spectrograph that uses a 10×64 pixel Si:As detector array to measure a 64-point spectrum at each of 10 positions along a slit projected onto the sky. Depending on the grating used, Irshell can achieve a spectral resolution ranging between 1000 and 20,000. On a 3-m telescope its pixels are separated by $1''$. Because of the small detector array used, the instantaneous spectral coverage is relatively small, $\lambda/40$ to $\lambda/300$. However, wider spectral regions can be observed by stepping the grating angle during observations.

2. OBSERVATIONS

Most of the observations for this project were made with the 3.6 m telescope of the European Southern Observatory, with some additional observations made with the 3 m NASA Infrared Telescope Facility. They were made over a period of three years between April 1992 and January 1995. Dates of observing runs relevant to this project are listed in Table 1. Several of these runs were shared with other projects, and the first few runs were made before contract funding began (data reduction was supported by this contract).

1

Table 1: Observing Dates

Date	Telescope	Weather	Observers
17 Apr 1992	ESO 3.6m	cloudy, unable to focus TV	
18 Apr 1992		cloudy, dewar focus bad	Lacy, Achtermann, de Graauw, Helmich
19 Apr 1992		clear after midnight	
20 Apr 1992		clear until midnight	
21 Apr 1992		clear 12-2 AM only	
22 Apr 1992		clear	
23 Apr 1992		clear	
08 Aug 1992	NASA IRTF	4 hr. (shared night)	Lacy, Parmar
09 Aug 1992		4 hr. (shared night)	
10 Aug 1992		4 hr. (shared night)	
18 Aug 1992	NASA IRTF	clear	Lacy, Luhman
19 Aug 1992		clear	
20 Aug 1992		clear	
05 Oct 1992	ESO 3.6m	cloudy, instrument and telescope problems	
06 Oct 1992		clear	Lacy, Parmar, de Graauw, van der Hulst
07 Oct 1992		clear	
08 Oct 1992		clear	
09 Oct 1992		clear	
10 Oct 1992		clear	
02 Apr 1993	ESO 3.6m	clear	Lacy, Kelly, van der Hulst, Waters
03 Apr 1993		clear	
04 Apr 1993		clear	
05 Apr 1993		clear	
06 Apr 1993		clear	
29 Apr 1993	ESO 3.6m	2 hr. clear, loose grating	Kelly, van Dishoeck
30 Apr 1993		mostly clear	
01 May 1993		1 hr. clear	
02 May 1993		3 hr. clear	
03 May 1993		mostly open with cirrus	
04 May 1993		mostly open with cirrus	
04 Jun 1993	NASA IRTF	2 hr. (shared night)	Lacy, Kelly, Achtermann
09 Jun 1993		4 hr. (shared night)	
10 Jun 1993		2 hr. (shared night)	
02 Jun 1994	NASA IRTF	mostly clear	Lacy, Kelly, Clayton
03 Jun 1994		mostly clear	
22 Oct 1994	NASA IRTF	cloudy	Kelly, Richter
23 Oct 1994		clear (shared)	
24 Oct 1994		clear (shared)	

Table 1 Continued

Date	Telescope	Weather		Observers
25 Jan 1995	ESO 3.6m	3 hr.	clear	Lacy, Kelly, de Graauw, van der Hulst, Waters
26 Jan 1995		2 hr.	clear	
27 Jan 1995		8 hr.	poor conditions	
28 Jan 1995		clear		
29 Jan 1995		clear		
30 Jan 1995		clear		
31 Jan 1995		clear		
12 May 1995	NASA IRTF	cloudy (shared)		Kelly, Richter
13 May 1995		clear		
14 May 1995		4 hr.	(shared)	
15 May 1995		3 hr.	(shared)	
16 May 1995		3 hr.	(shared)	
17 May 1995		3 hr.	(shared)	

Data were taken in two modes, high resolution (single line) mode and low resolution (grating scan) mode.

In high resolution mode, an echelle grating was used which gave a dispersion of about $\lambda/20,000$ pixel^{-1} and $\sim \lambda/300$ spectral coverage, well suited for observations of single emission or absorption lines. The slit was generally opened to 2 pixels, giving a resolution of $\lambda/\Delta\lambda \approx 10,000$. The telescope pointing was nodded to alternately observe sources at two positions along the spectrograph entrance slit. During data reduction the two sets of observations were subtracted, resulting in a positive signal at one position along the slit and a negative signal at the other. These signals were then subtracted to give the source flux with sky emission subtracted. Along with each set of nodded source observations, a measurement was made of an ambient temperature card (essentially a blackbody) for flux calibration and flat-fielding of the array. The data were reduced with the snoopy data reduction program (Achtermann 1994). For high resolution data, the data reduction procedure involved spike removal, subtraction of spectra from the two nod positions, addition of nod sets, flat-fielding, and flux calibration.

In low resolution mode, one of two first-order gratings was used, and for one set of observations (18-20 Aug 1992) a lens was installed in front of the detector to further lower the resolution. The two gratings gave dispersions of $\sim \lambda/6000$ pixel^{-1} and $\sim \lambda/2000$ pixel^{-1}, with the lens decreasing the dispersion by a factor of 2.4. With a 2-pixel slit opening the resolution was $\lambda/\Delta\lambda \approx 1000-3000$. For this project, low resolution mode was used when wide spectral coverage was desired. In this case, short integrations (~ 20 s.) were made at each grating setting and the grating was automatically stepped to shift the spectrum on the array by 5-25 pixels between integrations. In this way the entire 7.5-13.5μm spectral region could be observed over a period of about two hours. The data reduction for each grating setting was essentially the same as for high resolution mode. This was followed by patching sequential spectra together, using the relative fluxes in the overlap region to scale the spectra to correct for guiding and seeing variations.

Resolutions, spectral coverages and sources observed are listed in Table 2.

Table 2: Sources Observed

Date Object	Resolution Coverage/Feature	Object	Coverage/Feature
17-23 Apr 1992	R = 2500		
α CMa	7.5-13.0μm	α Cen	8.5-13.0μm
λ Sgr	10.7-13.0μm	η Car	8.0-13.0μm
HD 44179	7.5-10.5μm	HR 4049	10.5-13.0μm
WR 48A	8.5-13.0μm	IRC +10420	8.5-13.5μm
AFGL 4176	8-10, 11-13μm	NGC 6302	8.5-13.0μm
He2-113	8.5-13.0μm	NGC 6240	[Ne II]
NGC 3256	H_2, [Ne II], [Ar III]	NGC 4038	[Ar III], H_2
Cen A	[Ar III], H_2	W33 A	10.7-13.0μm
Sgr A West	8.5-9.5, 10.5-13μm		
8-14 Aug 1992	R = 10,000		
W3 IRS5	SiO, CS, H_2S	W33 A	SiO, CS, H_2S, HCO^+
NGC7538 IRS1	C_2H_2	NGC7538 IRS9	C_2H_2
AFGL 2591	H_2S, HCO^+		
18-20 Aug 1992	R = 1000		
α Cas	12.0-13.5μm	α Ari	8.3-10.8, 12.0-13.5μm
α Tau	12.0-13.5μm	α Aur	7.3-13.5μm
W3 IRS5	8.3-10.8, 12.0-13.5μm	W33 A	8.3-9.5μm
NGC7538 IRS1	8.3-13.5μm	NGC7538 IRS9	8.3-13.5μm
Sgr A West	7.3-13.5μm	NGC 7027	7.3-13.5μm
5-10 Oct 1992	R = 10,000		
LMC N11A	[Ne II]	LMC N12	[Ne II]
LMC N27	[Ne II]	LMC N81	[Ne II], [S IV]
LMC N83A	[Ne II], [S IV]	LMC N83B	[Ne II], [S IV]
LMC N88	[Ne II], [S IV]	LMC N159	[Ne II], [S IV]
LMC N160	[S IV]	30 Dor	[S IV]
He3-1333	[Ne II]	AFGL 5356	[Ne II]
NGC 6302	[Ne II], [Ar III], [S IV]	IC 481	[Ne II]
WR 104	[Ne II]	WR 125	[Ne II]
α PsA	[S IV]	ε PsA	[S IV]
γ Phe	[S IV]	α Eri	[S IV]
γ Ret	[S IV]		
Ori IRc2	SiO, H_2S, HCO^+		

4

Table 2 Continued

Date Object	Resolution Coverage/Feature	Object	Coverage/Feature
2-6 Apr 1993	R = 10,000		
α Ara	Pfβ, Huβ, [S IV]	ι Ara	Pfβ, Huβ, [S IV]
η Car	[Ne II]	AG Car	[Ne II]
HR Car	[Ne II]	β Cen	Pfβ, [S IV]
δ Cen	Huβ, [S IV]	η Cen	[S IV]
χ Oph	Pfβ, Huβ, [S IV]	66 Oph	[S IV]
δ Sco	Pfβ	τ Sco	[S IV]
γ Vel	[Ne II]	α Vir	Huβ, [S IV]
HD 44179	11.3μm PAH	He 2-10	[Ne II], [S IV]
NGC 3256	[Ar III]	NGC 3783	[Ne II], [S IV]
NGC 5236	[Ne II], [Ar III]	NGC 5253	[Ar III], [S IV]
NGC 5506	[Ne II]	NGC 6240	[Ne II]
Cen A	[S IV]	Circinus	[Ne II]
LMC N11A	[Ne II], [Ar III], [S IV]	LMC N160	[Ne II], [Ar III], [S IV]
IRAS 07027	[Ne II]		
29 Apr - 4 May 1993		R = 10,000	
α Ara	Pfβ	β Ara	Pfβ, Huε
α Cen	CO, HCO+	δ Cen	Pfβ
η Cen	Pfβ	μ Cen	Pfβ
θ Cen	Pfβ	α CMa	CO
R CrA	CO	χ Oph	Pfβ
66 Oph	Pfβ	51 Oph	CO
δ Sco	Pfβ	ζ Sco	Pfβ
λ Sco	Pfβ	σ Sco	Pfβ
τ Sco	Pfβ	ε Sgr	Pfβ, Huε
σ Sgr	Pfβ	μ Sgr	CO, Pfβ
NGC 3576	CO	NGC 4176	CO, HCO+
HR 4049	Pfβ		
3-10 Jun 1993	R = 10,000		
G34.3	C₂H₂	NGC 7027	fine-structure lines, 7-25μm
IRAS 1525+36	[Ne V]	Arp 220	[Ne II], [Ne V], [S IV], [Ar III]
NGC 4102	[Ne II], [S IV], [Ar III]	NGC 5253	[Ne V]
NGC 6946	[Ne II], [S III], [S IV], [Ar III]		

Table 2 Continued

Date Object	Resolution Coverage/Feature	Object	Coverage/Feature
2-3 Jun 1994	R = 1000		
V845 Cen	C_{60}	R CrB	C_{60}
β Her	C_{60}	γ Leo	C_{60}
σ Lib	C_{60}	δ Sgr	C_{60}
τ Sgr	C_{60}	RY Sgr	C_{60}
IRC +10216	C_{60}		
22-24 Oct 1994	R = 10,000		
IC 443	H_2 J=4-2		
NGC 7027	[Mg V], [Al VI], [Ar V]		
25-31 Jan 1995	R = 2000		
ϵ Car	[Ne II], [Ar III]	θ Car	[S IV], Pfβ, Grβ
α Cen	Pfβ, Grβ	β Cen	Huα
δ Cen	Pfβ, Grβ	ζ Cen	Pfβ
ν Cen	Pfβ	γ Cha	[Ne II][S IV]
ϵ CMa	Grβ	γ CMa	[S IV]
α Cru	Pfβ, Grβ	ι Ori	Grβ
β Pic	11.3μm PAH, CO	α Pix	Grβ
γ Ret	[Ar III]	τ Sco	Huα, Pfβ, Grβ, HI 8δ
γ Vel	[Ar III], [S IV], Huα	λ Vel	HI 8δ
α Vir	Huα, Grβ	ψ Vir	Huα
HR 3734	Pfβ, HI 8δ	HR 4532	HI 8δ
HR 5192	[S IV]	HR 5261	[S IV]
LMC N88	[Ne II], [Ar III]	LMC N159	[Ne II]
LMC N160	[Ne II]		
NGC 1068	[Ne II], [Ar III]	NGC 1365	[Ar III]
NGC 3256	[S IV]	NGC 4038	[S IV]
NGC 4039	[S IV]	NGC 4945	[S IV]
NGC 5236	[S IV]	NGC 5253	[S IV]
He 2-10	[Ar III], [S IV]	Circinus	[S IV]
Hd 8	[Ne II]	He 3	[Ne II]
12-17 May 1995	R = 10,000		
NGC 4151	[Ne II], [S IV]	NGC 4214	[Ne II], [S IV]
NGC 4861	[S IV]	He 2-10	[Ne II], [Ar III], [S IV]
W33	[Ne II], [Ar II], [Ar III]	IRC +10261	HCO^+
NGC 6334 IRS1	C_2H_2, HCN	W51 IRS2	C_2H_2

3. RESULTS

The primary results of this project are a set of low resolution spectra, shown in Figures 1-15. They are also available in digital form from the author (lacy@astro.as.utexas.edu) on request. These spectra and the high resolution spectra of individual lines are described here briefly.

3.1 SPECTRA OF INTERSTELLAR ICES

Some of the most prominent features in the infrared spectra of stars embedded in molecular clouds are a series of broad absorption bands, which have been attributed to icy coatings on dust grains. A few of these have been positively identified (those due to H_2O and CO most notably), but many are still unidentified, and bands of several expected molecules have not been detected. Many of the most interesting bands are at wavelengths which are inaccessible from the ground (notably CO_2 which has now been detected by ISO at 4.3 and 15 μm), but two important molecules, CH_3OH and NH_3, should be observable in the 8-13 μm atmospheric window. We included a number of infrared sources embedded in molecular clouds in our low resolution survey for the purpose of searching for these molecules, as well as any others that might be observed fortuitously. The 7.5-13 μm spectra of W3 IRS5, W33 A, NGC 7538 IRS 1, and NGC 7538 IRS 9 are shown in Figures 1-4. The most prominent feature in these spectra is the broad silicate absorption centered at 9.7 μm. The strength of the silicate feature makes it difficult to identify weaker ice features, but comparison of the different source spectra shows strong evidence for additional absorption at 9.0, 9.4, and 9.8 μm toward NGC 7538 IRS 9 and possible W33 A. These are the expected wavelengths of bands of NH_3 (9.0 μm) and CH_3OH (9.0 and 9.4 μm). Preliminary results of this work are reported by Faraji (1994) and Lacy and Faraji (1996). A more detailed description is in preparation.

3.2 PAH EMISSION SOURCES

A number of astronomical sources show emission bands at wavelengths of 3.3, 3.4, 6.2, 7.7, 8.6, and 11.3 μm. These are generally attributed to polycyclic aromatic hydrocarbon molecules (PAHs) excited by ultraviolet radiation to fluoresce in the infrared. We observed four of these sources, HR 4049, HD 44179, He 2-113, and NGC 7027 in the 8-13 μm region. The spectra are shown in Figures 5-8. The goal of the observations was to find previously unobserved structure which might be diagnostic of which specific PAHs are present and whether they are individual gas-phase molecules or are attached to dust grains. Largely because of wiggles in the spectra due to interference fringing in the detector array, we were not able to improve on previous constraints on structure in the emission bands.

3.3 SILICATE EMISSION AND ABSORPTION SOURCES

Although not a primary goal of this project, spectra were observed of a number of sources whose 8-13 μm spectra are dominated by silicate emission or absorption. In addition to the sources observed to search for ice absorption, η Car and IRC +10420 (Figures 9, 10) are dominated by silicate emission, and Sgr A West IRS 3, Sgr A West IRS 10, AFGL 4176, and WR 48a (Figures 11-14) show silicate absorption.

3.4 FINE-STRUCTURE LINE SURVEY

Modern infrared instrumentation and telescopes are capable of measuring many faint lines in the mid-infrared spectra of stars and galaxies. The lines are widely spaced throughout the 8-25 μm region, so it is much more efficient with most instruments to observe only a narrow wavelength region around each line rather than obtaining full spectral coverage. It is therefore essential to have accurate wavenumbers for the lines, both to make sure the lines are not missed and to provide accurate wavenumber standards for velocity measurements. The wavenumbers are also very useful for atomic physicists, who cannot detect these lines under laboratory conditions. We used the bright, high temperature planetary nebula NGC 7027 (Figure 8) as our line source and measured wavenumbers for 13 fine structure lines. Many of these lines are also seen in a second planetary nebula observed, NGC 6302 (Figure 15). Our new measurements are good to 0.0025%, which is as much as 50 times better than previously published numbers. We also made the first observation of hyperfine splitting in the [Na IV] 1106 cm^{-1} line. The results are published in Kelly & Lacy (1995).

3.5 EXTRAGALACTIC OBSERVATIONS

Mid-infrared fine structure lines act as the primary cooling mechanism for warm gas in galaxies. As such, these lines have great value for studying both the physical properties of the gas clouds and the nature of the sources that heat the gas. We conducted several studies of the emission-line properties of galaxies. In our study of starburst galaxies, we found that infrared line ratios indicate that high mass stars are present in only a few of these galaxies. We are currently modeling the data to see if the presence of high mass stars could be masked by geometrical effects, high densities, or unusual metallicities. Two papers have resulted from this work so far (Beck et al. 1996; Beck, Kelly & Lacy 1997), and a third paper (Kelly et al. 1997) is in preparation. We have also studied the emission line properties of Seyfert galaxies and found line ratios indicative of unusual physical conditions or metallicities. Models are being constructed to examine the physical characteristics of the emission line regions. A paper is planned (Kelly 1997).

3.6 SEARCHES FOR MOLECULAR ABSORPTION

One of the primary interests of the ISO SWS team is the detection of infrared absorption lines of interstellar molecules, particularly those which cannot be observed from ground-based telescopes. In preparation for these observations we made observations of a variety of promising sources in the vibration-rotation bands of CO, HCO$^+$, C_2H_2, and HCN, with a few sources also observed in bands of SiO, H_2S, and CS. The results were entirely negative. Although CO, SiO, C_2H_2, and HCN had previously been observed toward two sources, they were not seen toward other sources that were being considered for ISO observations. HCO$^+$, H_2S, and CS, although frequently observed at millimeter wavelengths are still undetected in the infrared. These observations served primarily as a warning about how difficult it would be to observe interstellar molecules with ISO. Although CO has been easily observed and CH_4, and possibly CO_2, seen toward some sources, other molecules have not yet been reported.

An attempt was also made to detect the molecule C_{60} in the outflows around carbon-rich stars. This very interesting molecule (Buckminsterfullerene) was first found in the lab in experiments aimed at duplicating the process of molecule formation in stellar outflows, it has never been detected in space. We also failed to detect it, but set some interesting limits (Clayton, et al. 1995).

8

Fig, 1.— 8-13 μm spectrum of W3 IRS5, a young star embedded in a molecular cloud. The absorption centered at 9.7μm is due to interstellar silicate dust. The upper curve is scaled up by a factor of five to show the spectrum better near the bottom of the silicate feature. The region between 10.9 and 11.8 μm was not observed.
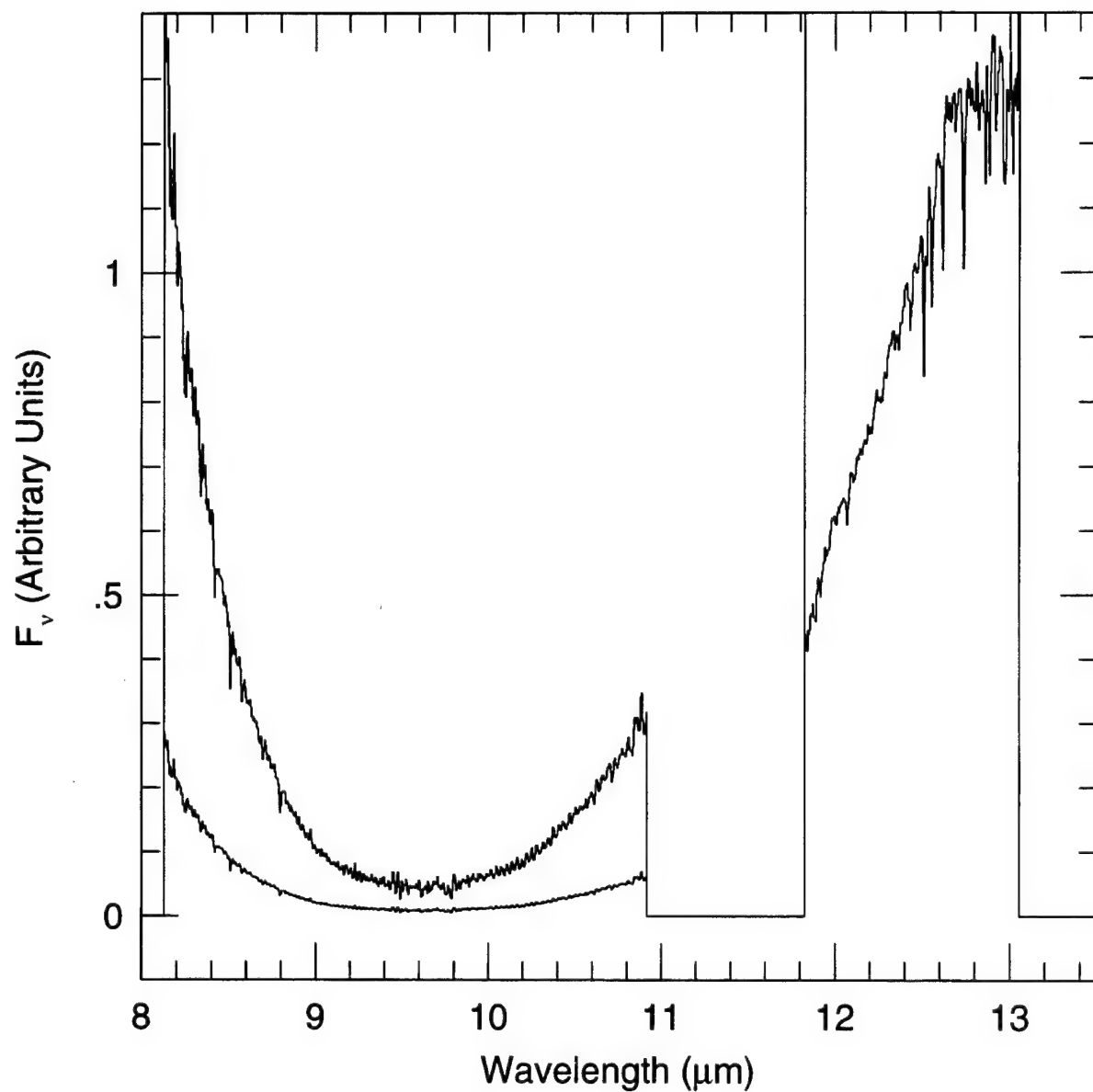
Fig. 2.— 8.2-13.2 μm spectrum of W33 A, a young star embedded in a molecular cloud. The absorption centered at 9.7μm is due to interstellar silicate dust, and the shoulder near 9.0 μm is probably due to NH_3 ice coating the dust. The upper curve is scaled up by a factor of five to show the spectrum better near the bottom of the silicate feat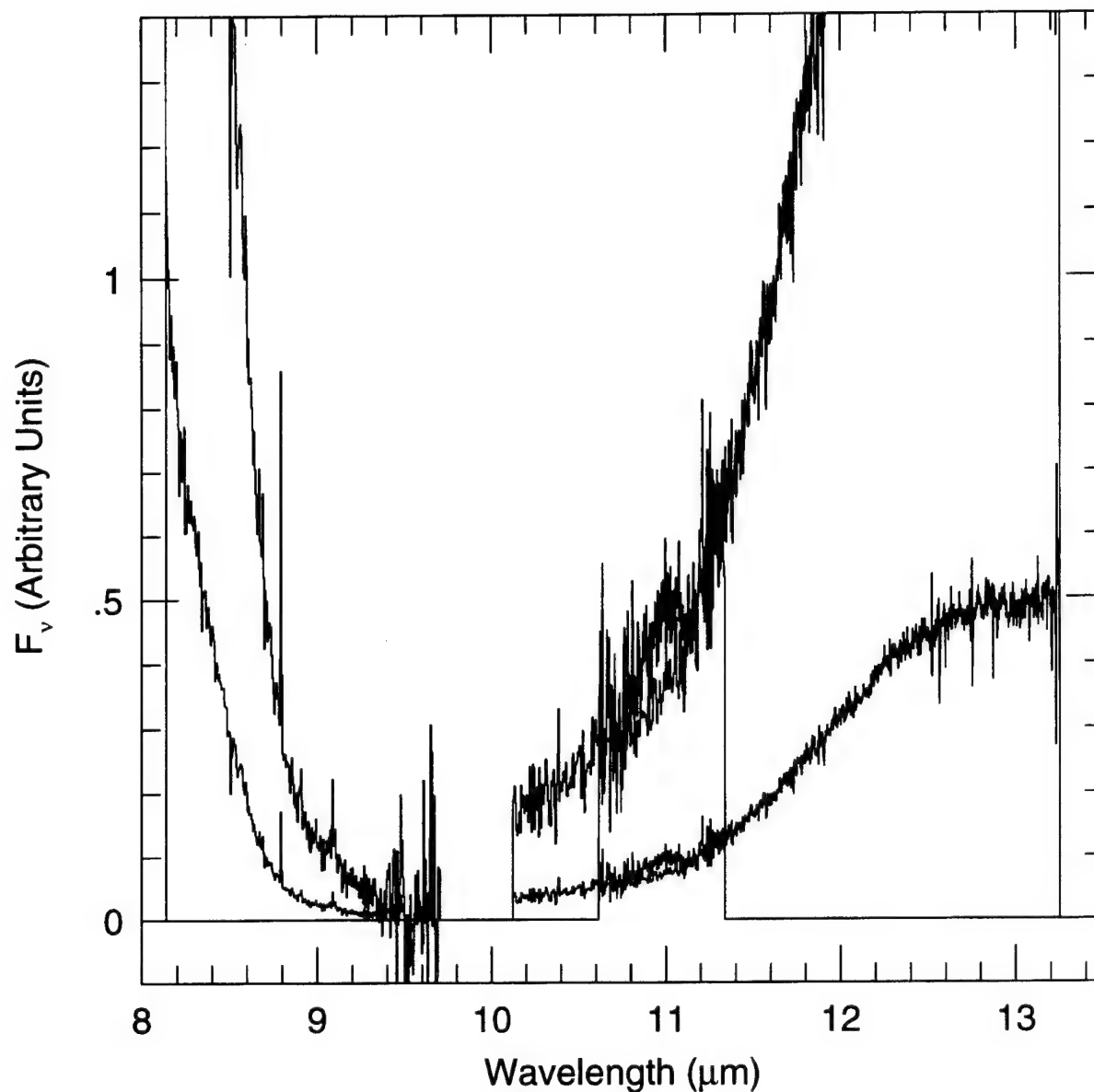ure. The region between 9.7 and 10.1 μm was not observed, and the source was not detected between 9.4 and 9.7 μm.

Fig. 3.— 8.2-13.4 μm spectrum of NGC 7538 IRS 1, a young star embedded in a molecular cloud. The absorption centered at 9.7μm is due to interstellar silicate dust. The upper curve is scaled up by a factor of five to show the spectrum better near the bottom of the silicate feature.
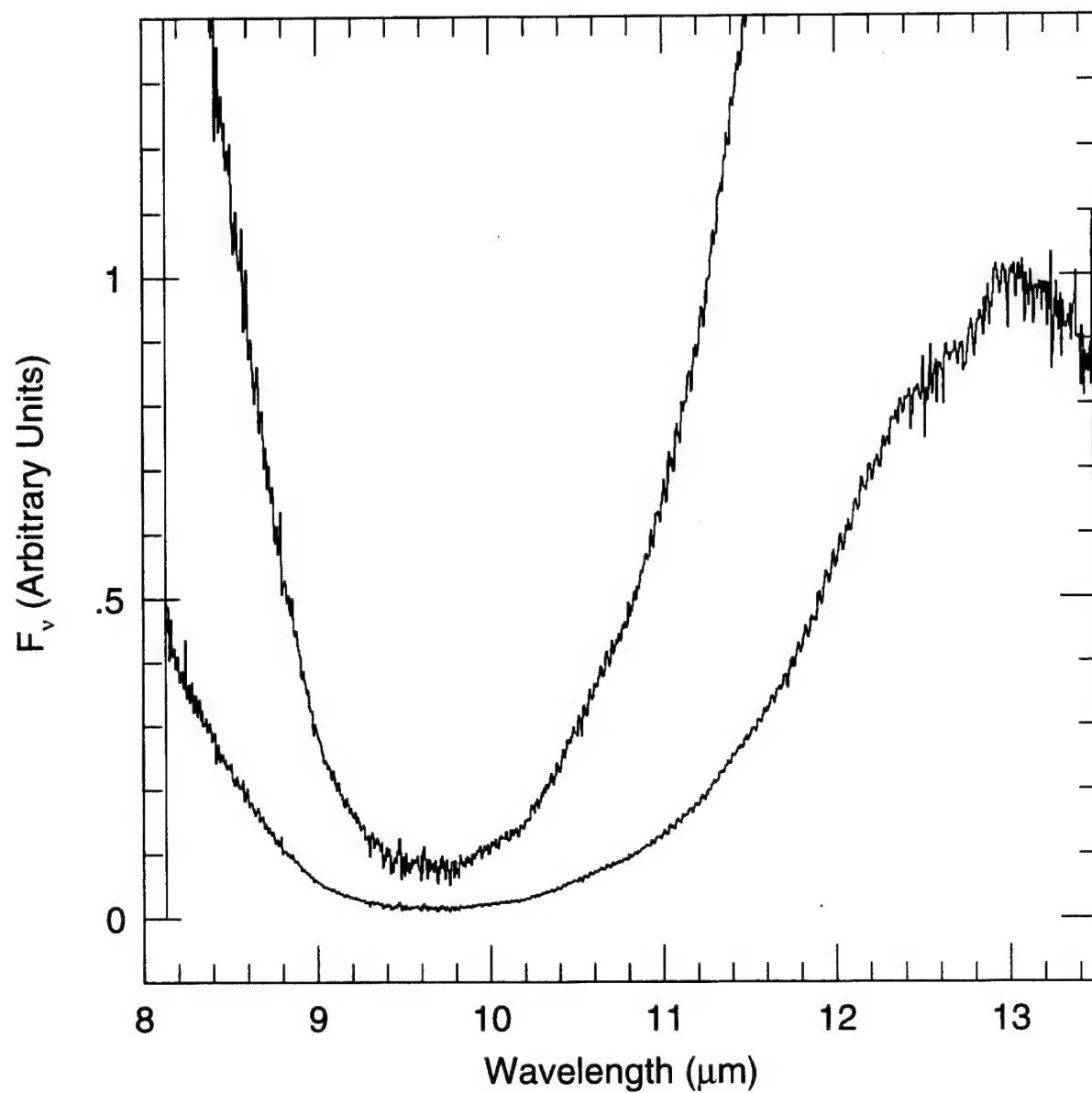
Fig. 4.— 8.2-13.4 μm spectrum of NGC 7538 IRS 9, a young star embedded in a molecular cloud. The absorption centered at 9.7μm is due to interstellar silicate dust, and the shoulder near 9.0 μm is probably due to NH$_3$ ice coating the dust. The upper curve is scaled up by a factor of five to show the spectrum better near the bottom of the silicate feature.

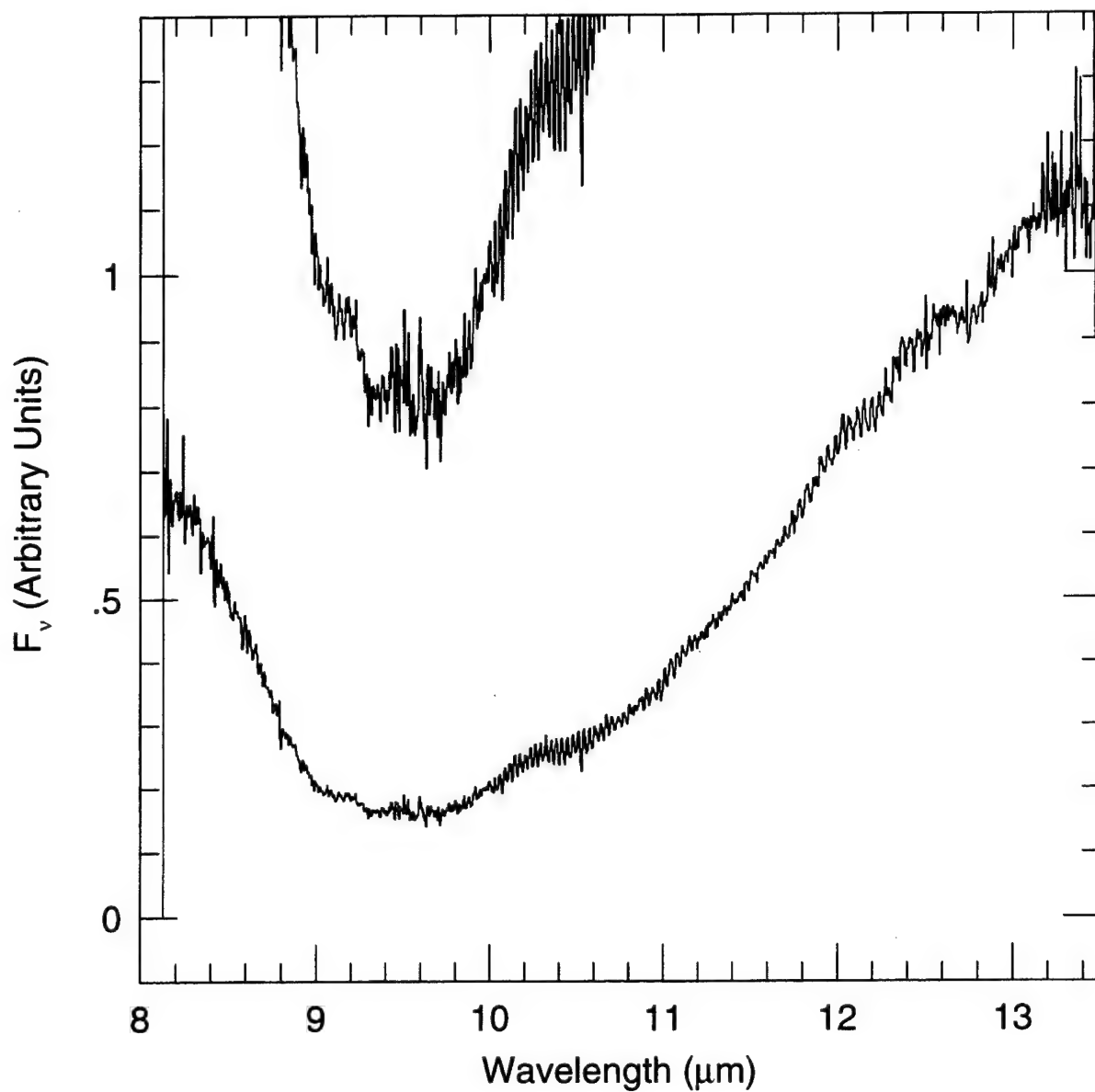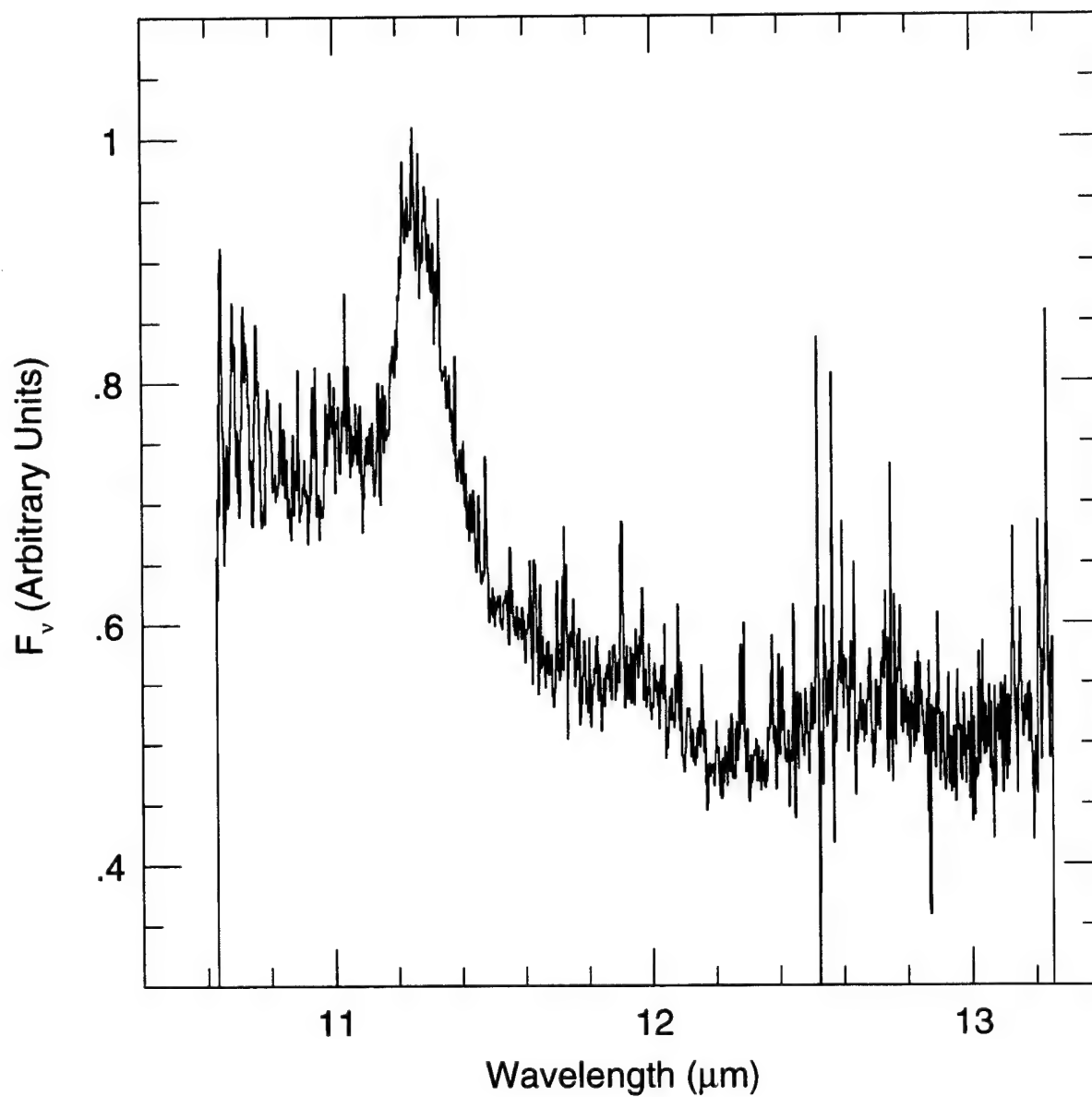Fig. 5.— 10.6-13.2 μm spectrum of HR 4049, a hot star illuminating nearby interstellar gas and dust. The peak near 11.3 μm has been attributed to emission by polycyclic aromatic hydrocarbon (PAH) molecules in their C-H out-of-plane bending mode.
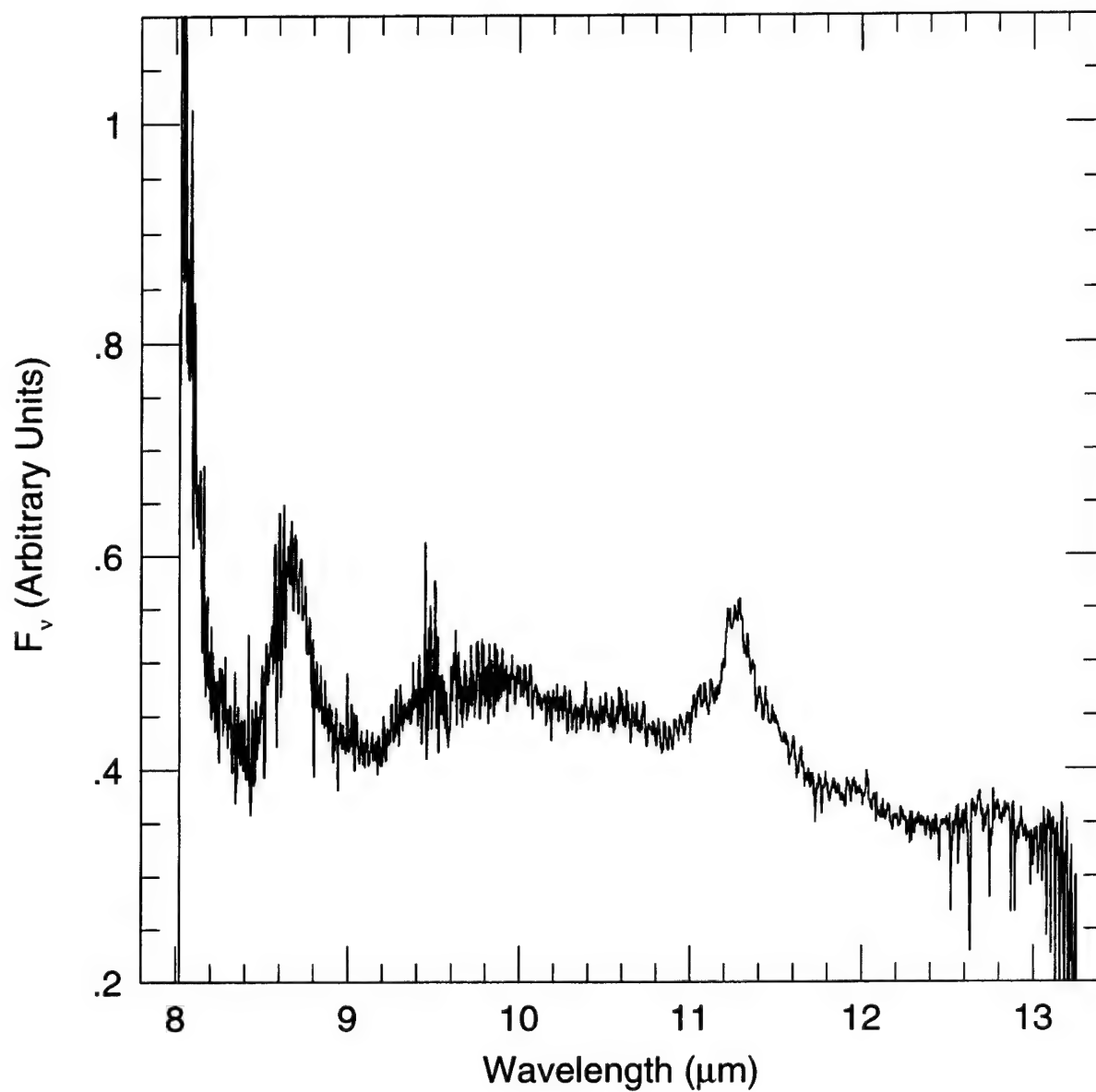
Fig. 6.— 8.0-13.2 μm spectrum of HD 44179 (the "Red Rectangle"), a hot star illuminating nearby interstellar gas and dust. The peaks near 8.0, 8.6, and 11.3 μm have been attributed to emission by polycyclic aromatic hydrocarbon (PAH) molecules.

14
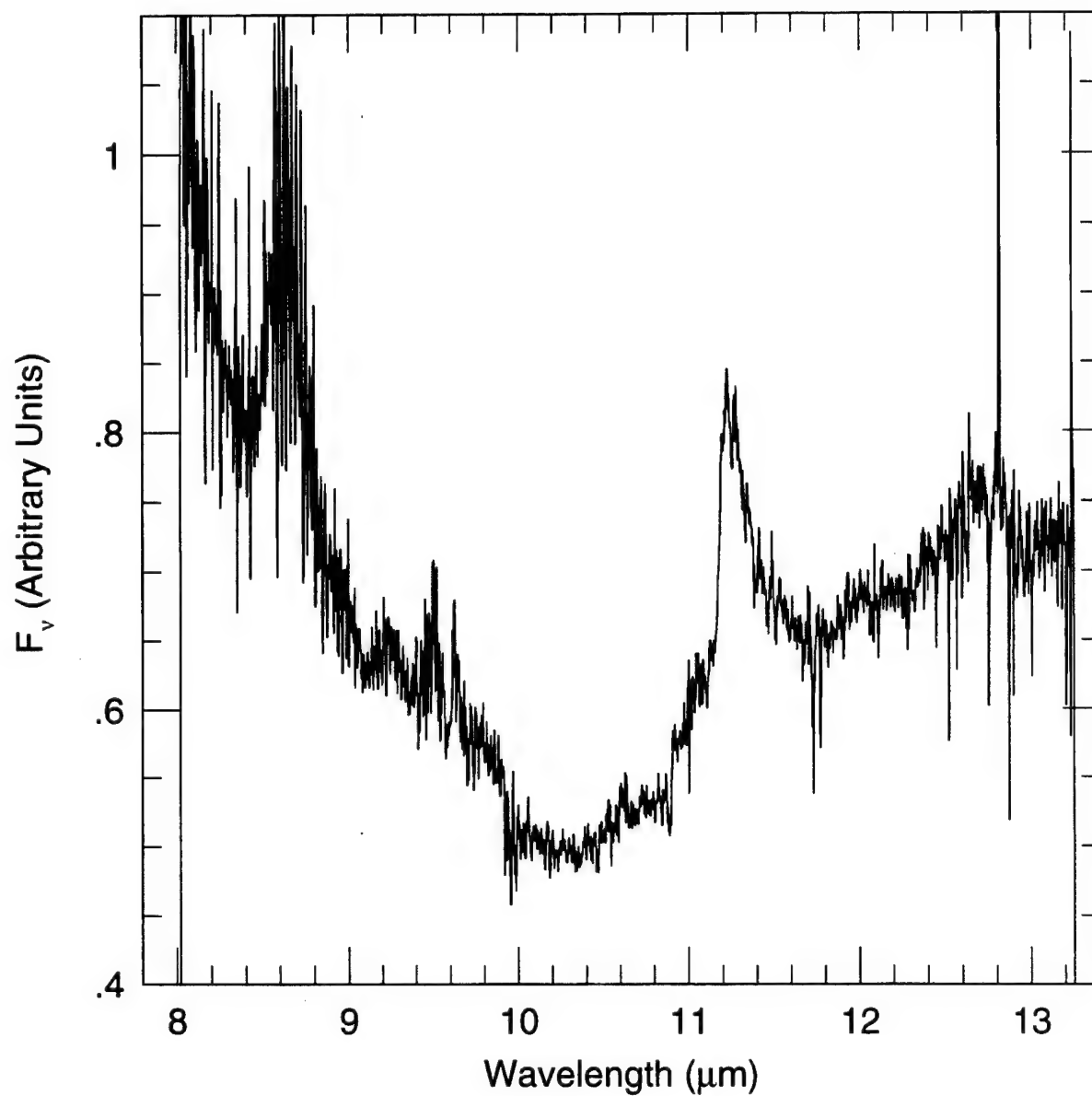
Fig. 7.— 8.0-13.2 μm spectrum of He 2-113, a hot star illuminating nearby interstellar gas and dust. The peaks near 8.0, 8.6, and 11.3 μm have been attributed to emission by polycyclic aromatic hydrocarbon (PAH) molecules.
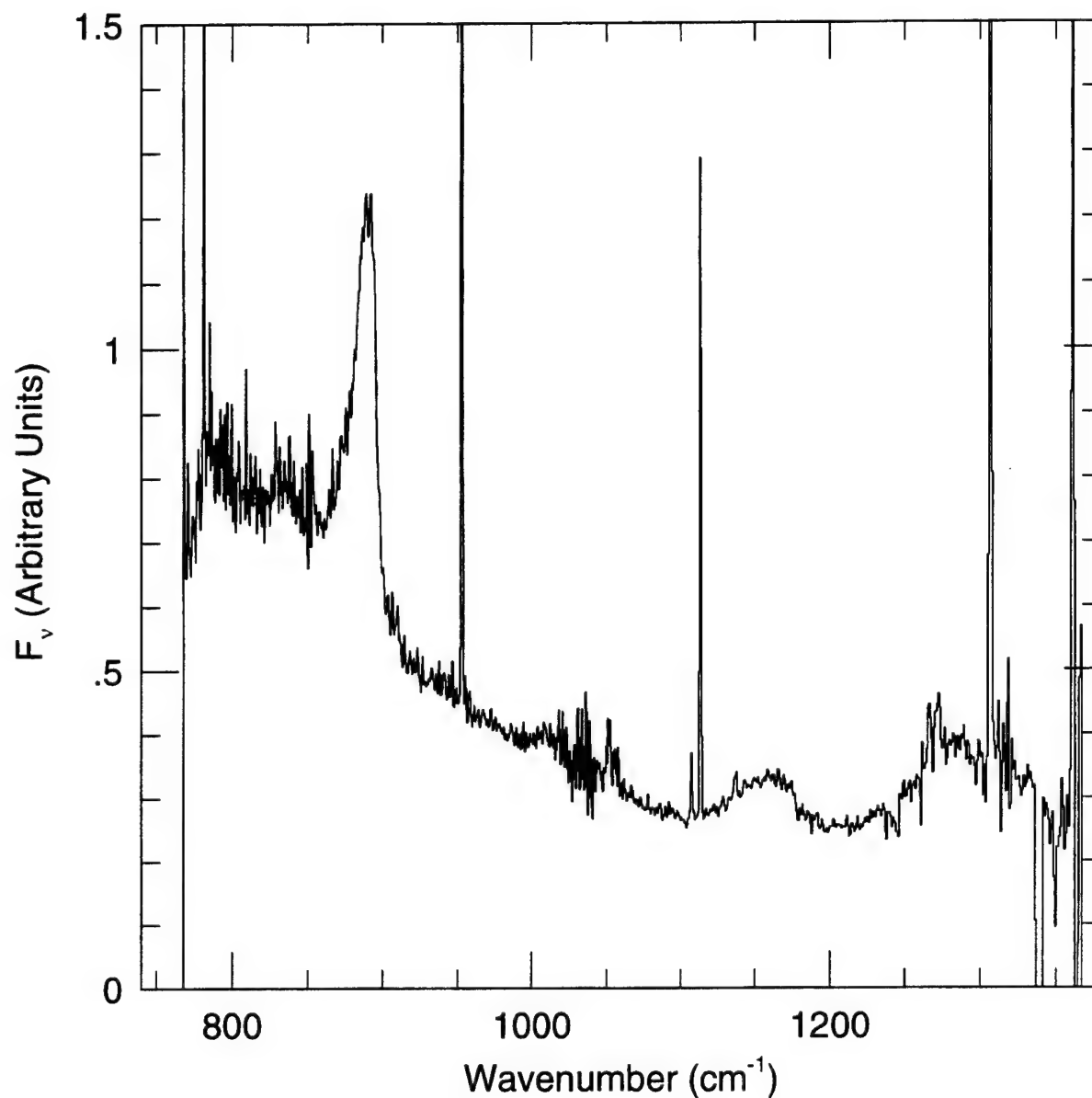
Fig. 8.— 760-1360 cm^{-1} (13.2-7.6 μm) spectrum of NGC 7027, a planetary nebula (a dying star illuminating its ejected gas). Broad features near 910, 1160, and 1300 cm^{-1} are attributed to emission by polycyclic aromatic hydrocarbon (PAH) molecules. Narrow features are fine-structure emission lines of various ions.
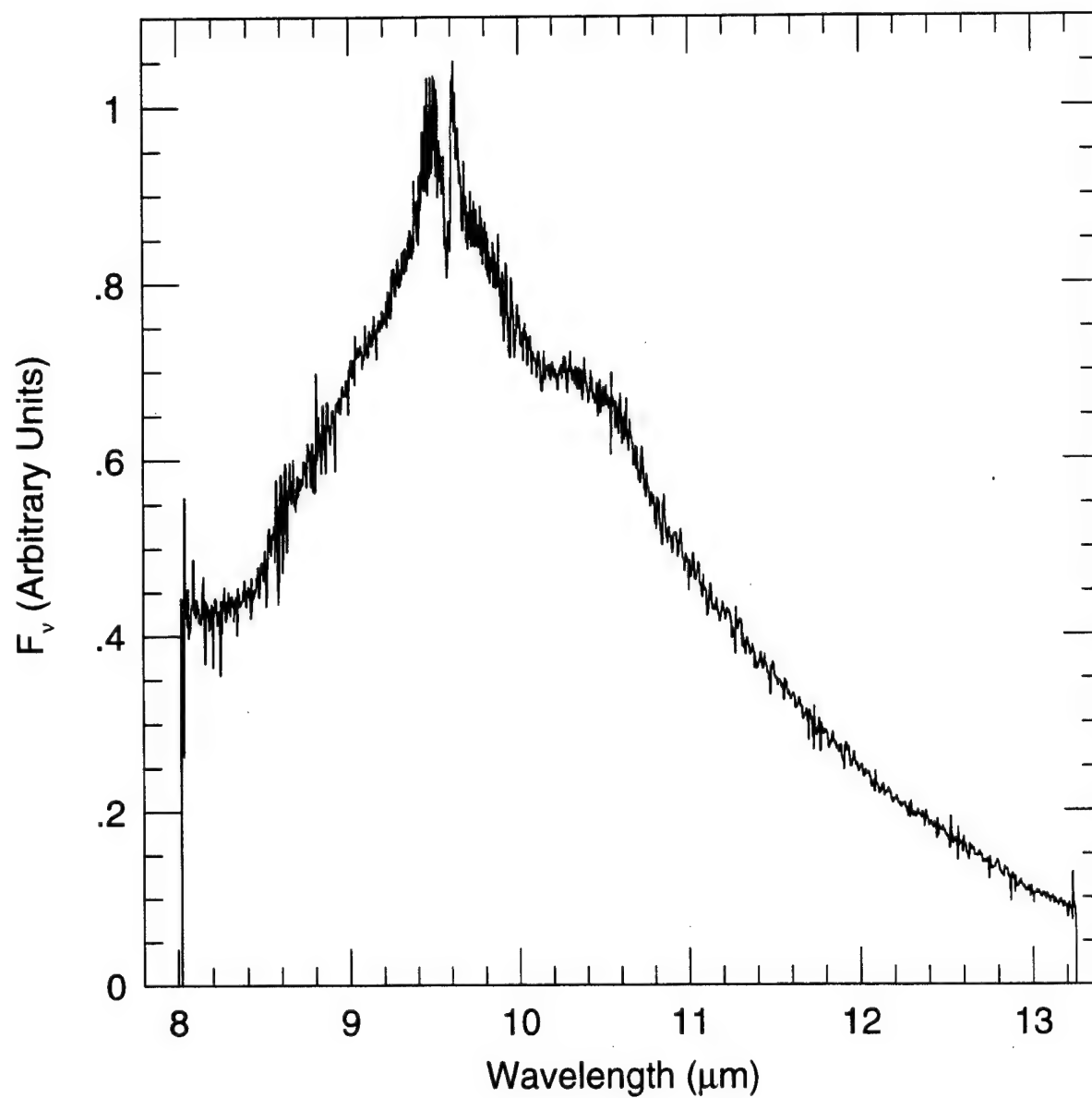
Fig. 9.— 8.0-13.2 μm spectrum of η Carinae, a very massive and luminous star illuminating gas it has ejected. The spectrum is dominated by emission from silicate dust.
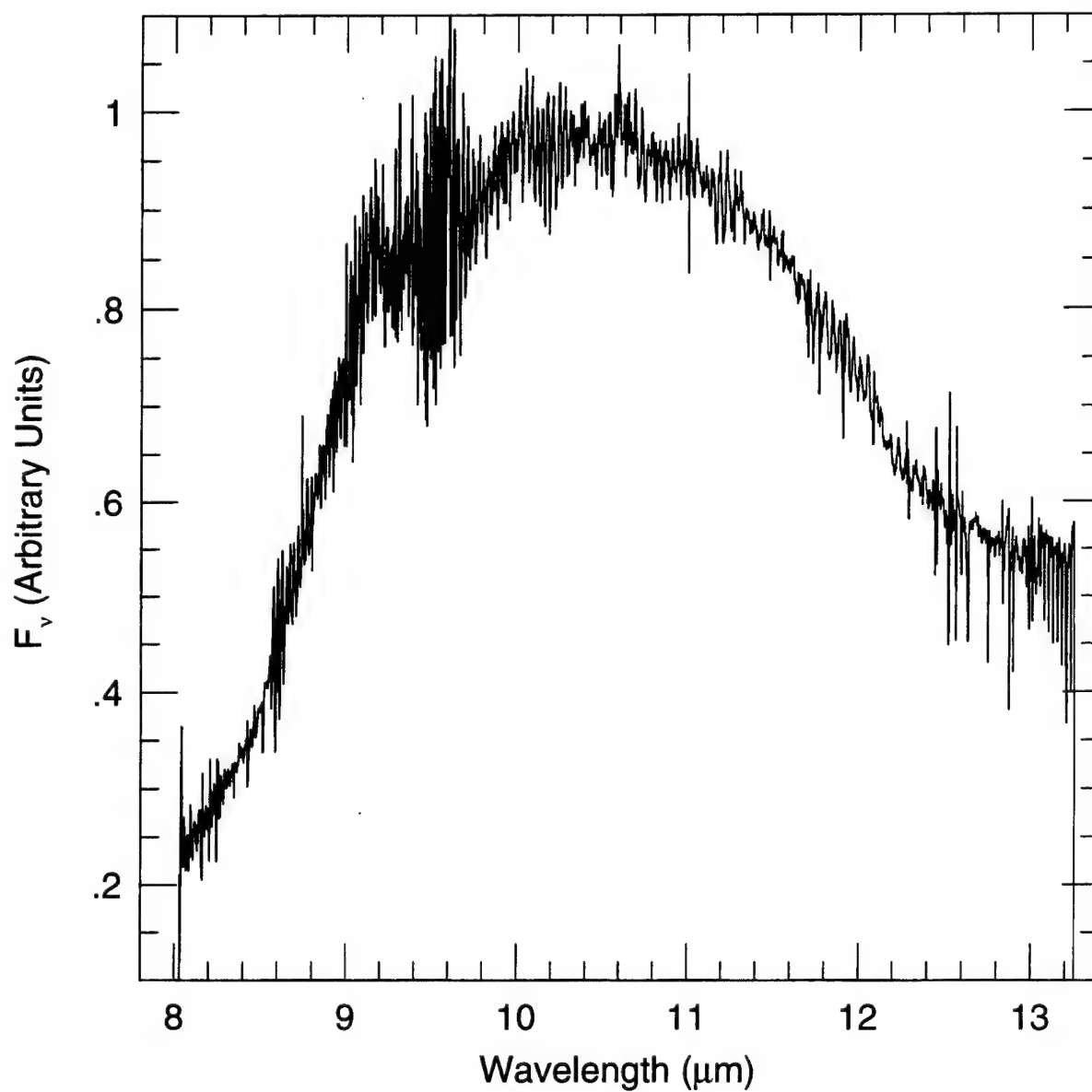
Fig: 10.— 8.0-13.2 μm spectrum IRC +10420, a star with a dense dust shell. The spectrum is dominated by emission from optically thick silicate dust.
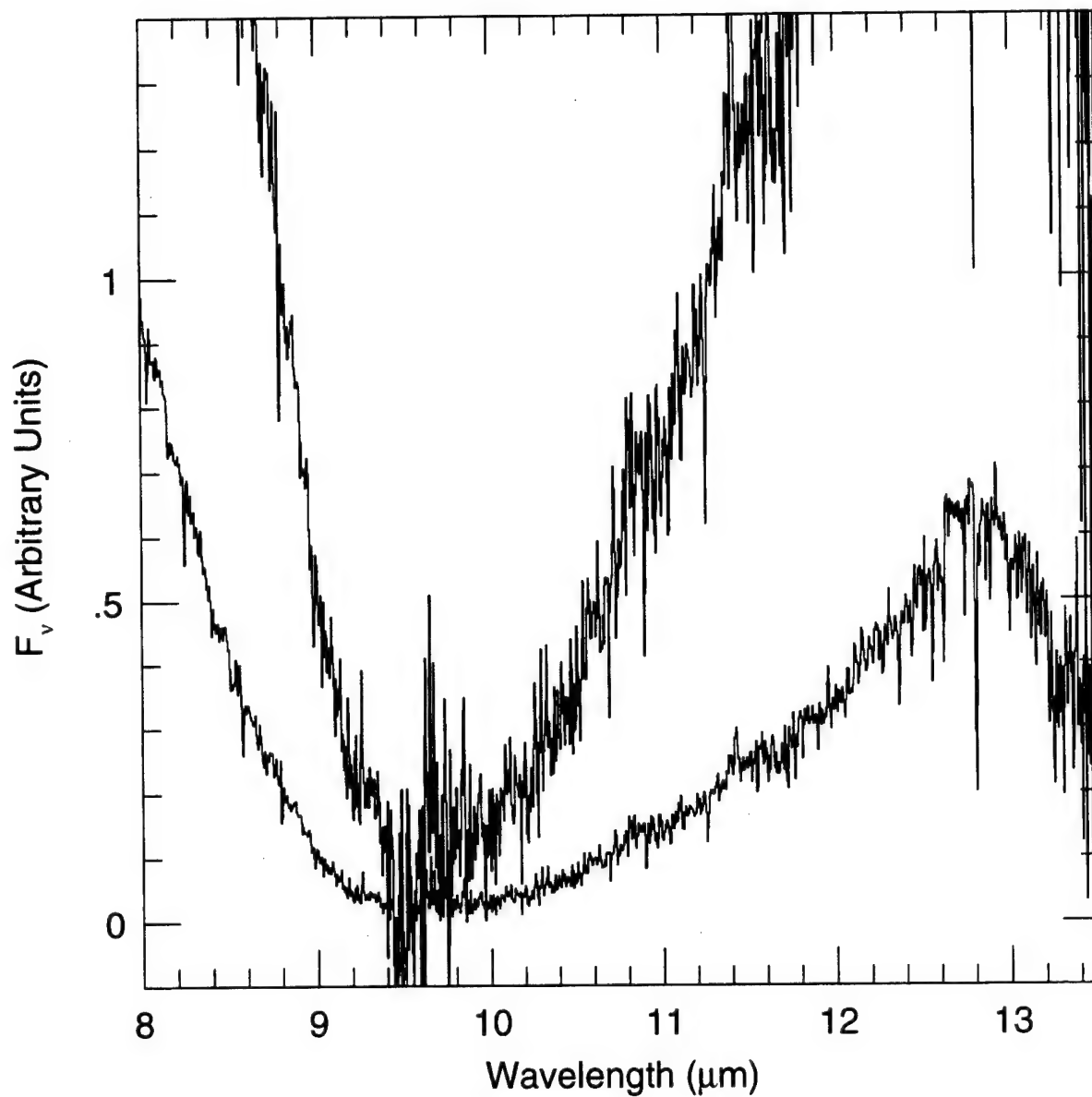
Fig. 11.— 8.0-13.5 μm spectrum of Sgr A West IRS 3, a star near the Galactic Center, embedded in a molecular cloud. The absorption centered at 9.7μm is due to interstellar silicate dust. The upper curve is scaled up by a factor of five to show the spectrum better near the bottom of the silicate feature.
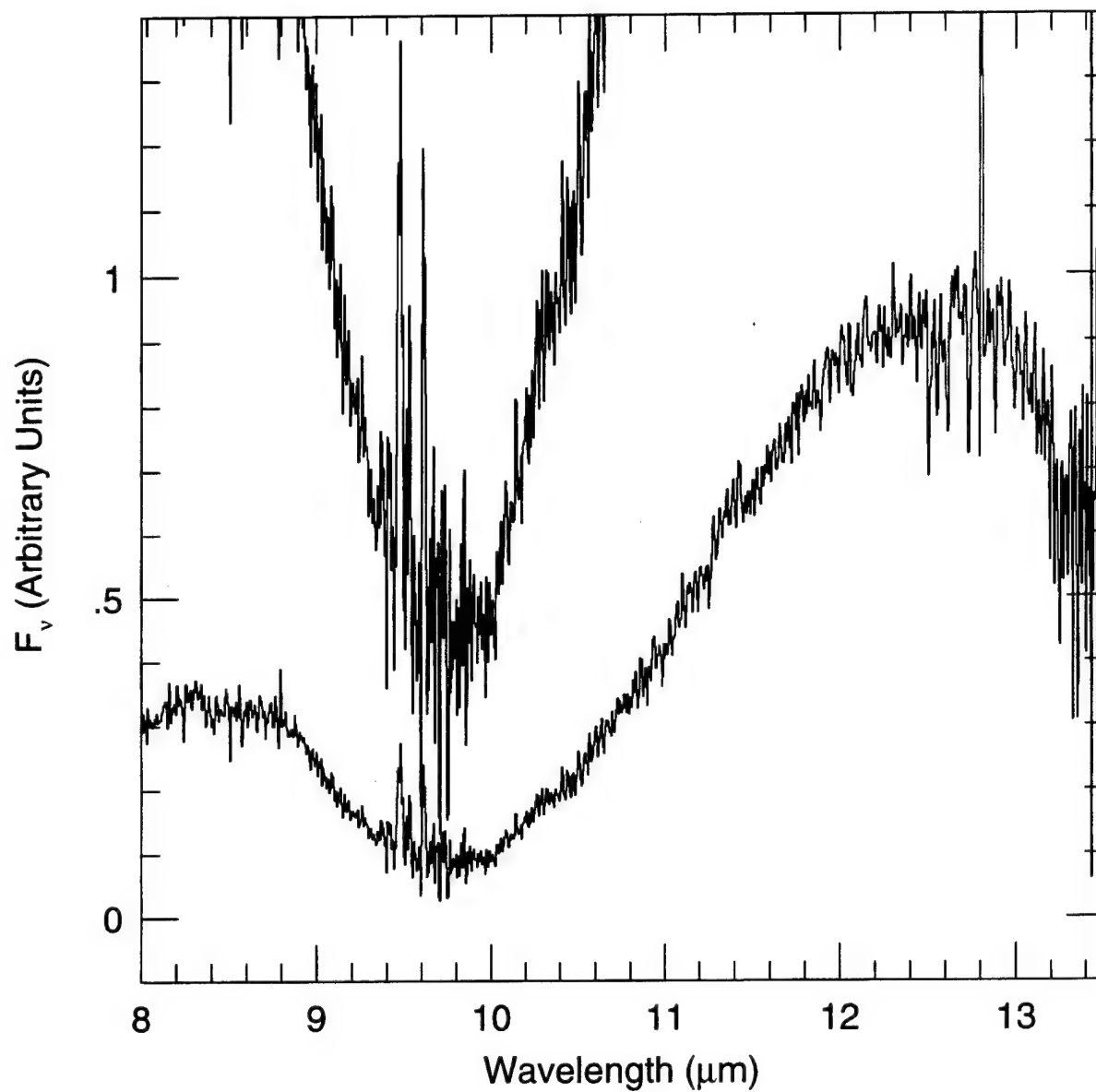
Fig. 12.— 8.0-13.5 μm spectrum of Sgr A West IRS 10, a dense clump of ionized gas and dust in the Galactic Center. The absorption centered at 9.7μm is due to interstellar silicate dust. The upper curve is scaled up by a factor of five to show the spectrum better near the bottom of the silicate feature.

20
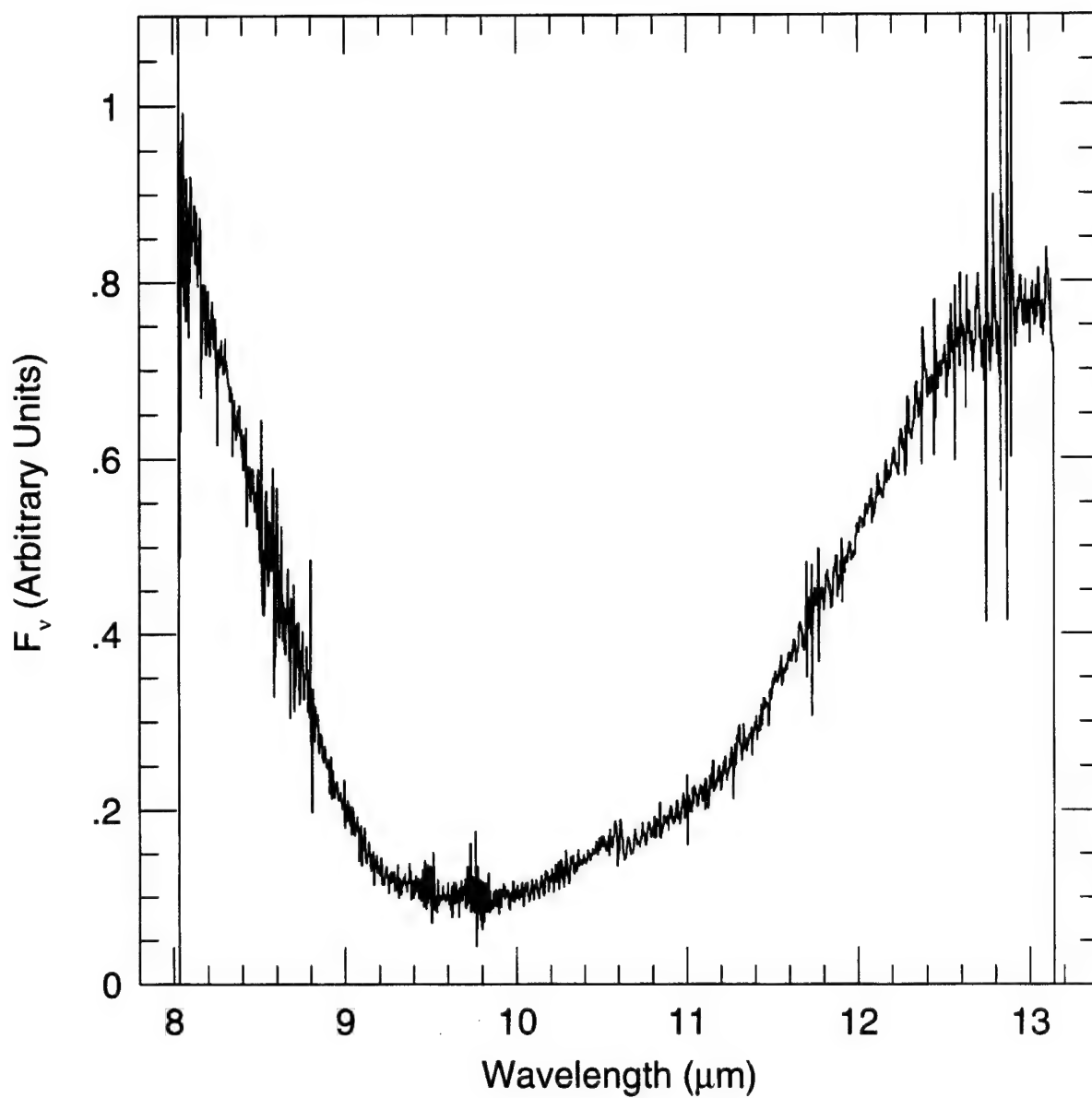
Fig. 13.— 8.0-13.2 μm spectrum of AFGL 4176, an obscured infrared star. The absorption centered at 9.7μm is due to interstellar silicate dust.
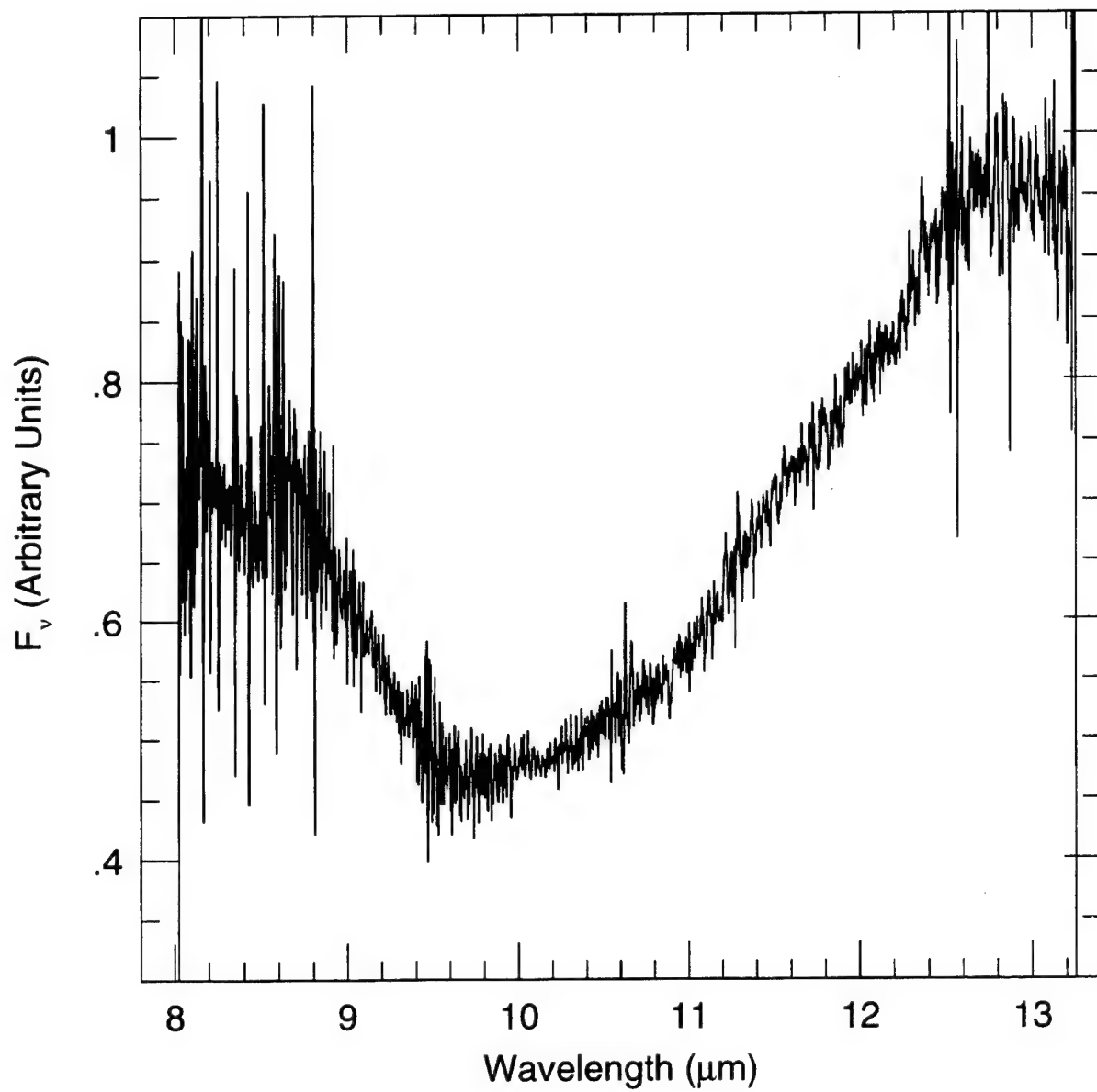
Fig. 14.— 8.0-13.2 μm spectrum of WR 48a, an obscured infrared star. The absorption centered at 9.7μm is due to interstellar silicate dust.
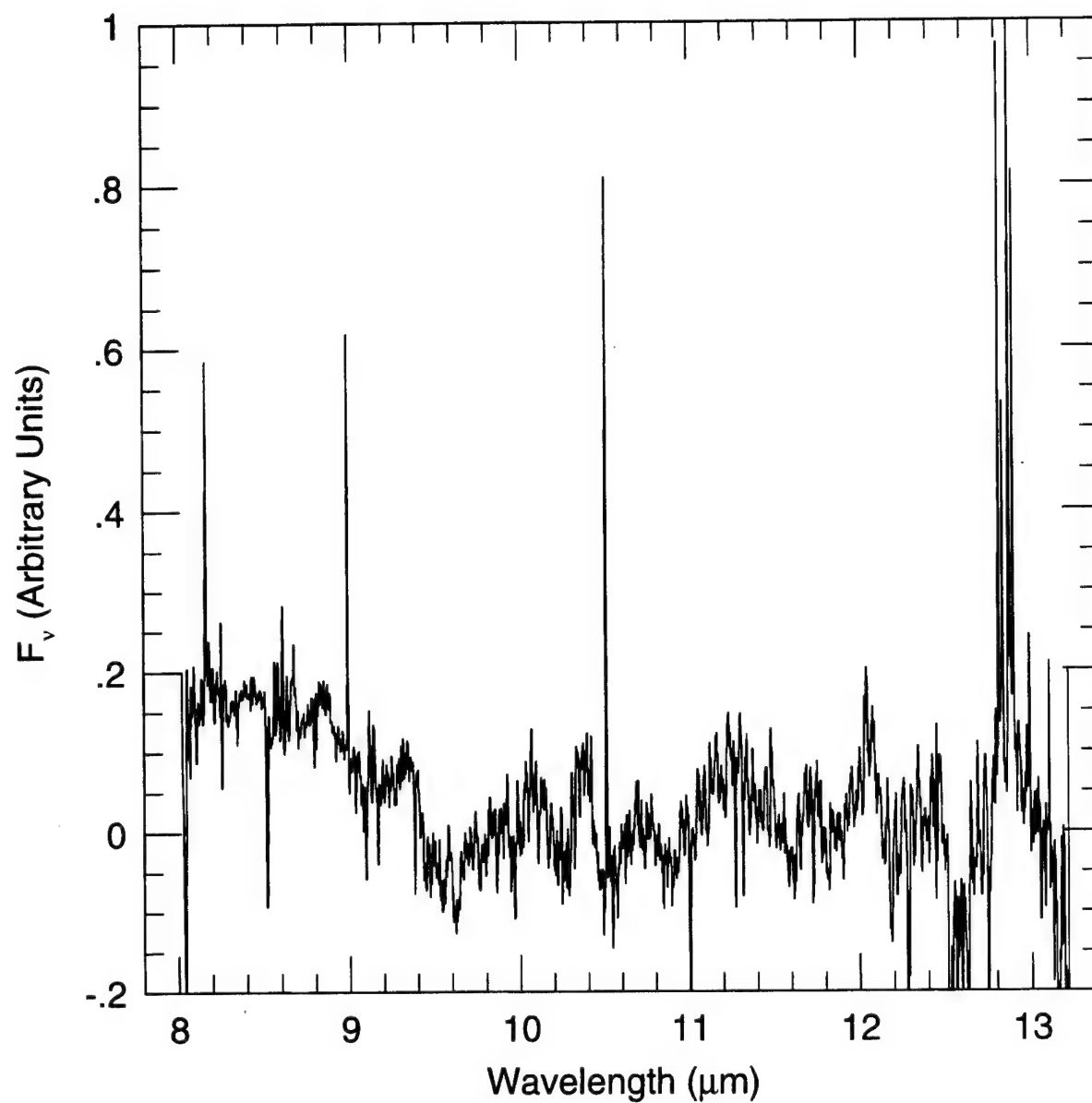
Fig. 15.— 8.0-13.2 μm spectrum of NGC 6302, a planetary nebula (a dying star illuminating its ejected gas). Narrow features are fine-structure emission lines of various ions.

4. REFERENCES

Achtermann, J.M. 1994, PASP, 106, 173-181.

Beck, S.C., Turner, J.L., Ho, P.T.P., Lacy, J.H., & Kelly, D.M. 1996. "The Central Star Cluster of the Star-Forming Dwarf Galaxy NGC 5253", Astrophys. J., 457, 610.

Beck, S.C., Kelly, D.M., & Lacy, J.H. 1997. "The Infrared Star Cluster of the Wolf-Rayet Galaxy Henize 2-10", Astron. J., in press.

Clayton, G. C., Kelly, D. M., Lacy, J. H., Little-Marenin, I. R., Feldman, P. A., and Bernath, P. F. 1995. "A Mid-Infrared Search for C60 in R Coronae Borealis Stars and IRC +10216", Astron. J., 109, 2096.

Faraji, H. 1994. "Infrared Spectroscopy of Icy Grain Mantles in Interstellar Clouds From 7 to 13 Microns", M. S. Thesis, University of Texas, Austin.

Kelly, D.M., Lacy, J.H., van der Hulst, J.M., & Achtermann. J.A. 1997, in preparation

Kelly, D.M. 1997, in preparation

Lacy, J. H., Achtermann, J. M., Bruce, D. E., Lester, D. F., Arens, J. F., Peck, M. C., and Gaalema, S. D. 1989. "Irshell: A Mid-Infrared Cryogenic Echelle Spectrograph" Publ. Astr. Soc. Pac., 101, 1166-1175.

Lacy, J. H., and Faraji, H. 1996. "High Resolution Mid-Infrared Spectroscopy of Interstellar Ices", in International Astronomical Union Symposium 178, 158-159.

5. TRAVEL

Most of the travel supported by this contract was to observatories for astronomical observations. John Lacy made two trips to the European Southern Observatory in Chile, in April 1993 and January 1995, and one trip to the NASA Infrared Telescope Facility in Hawaii, in June 1994. Doug Kelly traveled three times to Chile, in April 1993, May 1993, and January 1995, and four times to Hawaii, in July 1994, October 1994, June 1995, and November 1995. In addition, John Lacy attended three meetings, in Los Angeles in July 1993, in Colorado in June 1995, and in the Netherlands in June 1996. Doug Kelly attended one meeting, in Mexico City in April 1994, and Matthew Richter attended one meeting, in the Netherlands in June 1996.

6. PERSONNEL

Three researchers were supported by this contract. John Lacy, the principal investigator was supported in August 1994 and June 1995. Douglas Kelly, a postdoctoral scientist was supported for a total of 18 months between May 1993 and July 1995. A second postdoctoral scientist, Matthew Richter, was supported for a total of 10 months between October 1995 and November 1996.

7. EQUIPMENT PURCHASED

One piece of equipment was purchased with funds from this contract: a diffraction grating to allow low resolution observations.

8. PUBLICATIONS RESULTING FROM THIS CONTRACT

Lacy, J. H., and Achtermann, J. M. 1994. "Astronomy with a Mid-Infrared Echelle Spectrograph", Infrared Astronomy With Arrays, ed. I. McClean, 85.

Kelly, D. M., and Latter, W. B. 1995. "Spectroscopy of Evolved Stars in the Near Infrared: Explorations beyond the AGB", Astron. J., 109, 1320.

Clayton, G. C., Kelly, D. M., Lacy, J. H., Little-Marenin, I. R., Feldman, P. A., and Bernath, P. F. 1995. "A Mid-Infrared Search for C60 in R Coronae Borealis Stars and IRC +10216", Astron. J., 109, 2096.

Richter, M. J., Graham, J. R., Wright, G. S., Kelly, D. M., and Lacy, J. H. 1995. "Detection of Pure Rotational H2 Emission from the Supernova Remnant IC 443: Further Evidence for a Partially Dissociating J-Shock", Astrophysical J. Letters, 449, L83-86.

Kelly, D. M., and Lacy, J. H. 1995, "Accurate Wavenumbers for Mid-Infrared Fine-Structure Lines", Astrophysical J. Letters, 454, L161-164.

Beck, S. C., Turner, J. L., Ho, P. T. P., Lacy, J. H., and Kelly, D. M. 1995. The Central Star Cluster of the Star-Forming Dwarf Galaxy NGC 5253", Astrophysical J., 457, 610-615.

Lacy, J. H., and Faraji, H. 1996. "High Resolution Mid-Infrared Spectroscopy of Interstellar Ices", International Astronomical Union Symposium 178, 158-159.

van Dishoeck, E. F., *et al.* 1996. "A Search for Interstellar Gas-Phase CO_2", Astron. Astrophys., 315, L349-352.

Beck, S. C., Kelly, D. M., and Lacy, J. H. 1997. "The Infrared Nucleus of the Wolf-Rayet Galaxy Henize 2-10", Astron. J., in press.

Smith, H. A., Strelnitski, V., Miles, J. W., Kelly, D. M., and Lacy, J. H. 1997. "Mid-Infrared Hydrogen Recombination Line Emission from the Maser Star MWC 349A", Astron. J., in press.

ASTRONOMY WITH A MID-INFRARED ECHELLE SPECTROGRAPH

Exploiting its Advantages; Overcoming its Limitations

J. H. LACY and J. M. ACHTERMANN

Department of Astronomy, University of Texas, Austin

Abstract. Irshell, a mid-infrared echelle spectrograph developed through a collaboration between the University of Texas, the University of California Space Sciences Laboratory, and Hughes Aircraft, has been in regular use for astronomical observations for about five years. It is optimized for high spectral resolution (R~10,000) observations of narrow spectral regions ($\Delta\lambda/\lambda \sim 1/300$) and compact sources (a few arcsec), and is sensitive in the 5-25μm region. A wide variety of astronomical objects have been studied. Observing techniques have been developed to achieve maximum sensitivity in those observations for which Irshell is best suited and to allow observations of wide spectral regions and extended objects. We discuss the observing techniques and show some of the data obtained.

Key words: Infrared–Instrumentation–Spectra

1. Irshell

Irshell is an 0.75m focal-length liquid-helium-cooled spectrograph. It is normally used with a 10×22.5cm echelle grating and an 11×64 pixel Si:As impurity-band detector array, provided by Hughes Aircraft. With the echelle grating, the (2-pixel) resolving power can be varied between about 4000 and 24,000, with different options for the imaging optics. With a low-resolution grating, a resolving power as low as 1000 can be obtained. The instrument is sensitive between about 5 and 25μm. The detector array is oriented to observe a 64-point spectrum at each of 11 positions along an entrance slit. The spatial samples are separated by $0.4 - 2.4''$ on a 3m telescope. The instrument is described in more detail by Lacy et al. (1989), and the data reduction procedure is described by Achtermann (1991).

Irshell is most often used with the echelle grating and an image scale of $1''$ per pixel, giving a resolving power $\approx 10,000$. It is then best suited for observations of relatively compact sources, a few arcseconds, and moderately narrow lines, a few 100 km s^{-1}, so that many of the pixels in the array are used, but only a single grating and slit setting is required. Such observations are rare, however; the majority of sources and spectral regions of interest are either more compact or more extended that this. Different combinations of source size and spectral width are best observed with different observing strategies. The strategies that have been developed for use with Irshell, and examples of sources observed, are discussed in this paper.

85

2. Observations of Small Spatial and Spectral Regions

The observation for which Irshell is best suited cover a small enough spatial and spectral region to require only one slit and grating setting. They are often done with the traditional "chop and nod" mode of observing, in which chopping is done with the telescope's chopping secondary, with occasional nodding of the telescope to place the source in the other chop position. Alternatively, we have found that the use of the chopping secondary is usually not necessary; in good weather simply nodding the telescope every few seconds works as well. Representative spectra of sources obtained with a single slit and grating setting are shown in Figure 1.

The flat-fielding and intensity calibration procedures are similar for all types of observations. Flat fielding is first done by dividing the chopped source signal by the normalized difference between sky (from the off-source position) and dark (from a measurement with the grating slit closed, done once each night). This procedure removes instrumental features due to the detector non-uniformities and interference fringing. However, using the sky as a flat field enhances atmospheric absorption features, since the sky is brightest at those wavelengths where the atmosphere absorbs the source radiation. A second step largely corrects for atmospheric absorption. Before each integration set, a dome-temperature card is inserted into the field of view of the spectrograph. The flat-fielded source spectrum is divided by a flat-fielded chopped difference between the card and the sky (and telescope), and the result is multiplied by the calculated black-body intensity of the card. The flat-fielding cancels in this step, so could in principal have been left out, but allows shifting of the source spectrum relative to the card in cases where the grating shifted between the two measurements. To within the approximation that the card, telescope, and atmosphere are at the same temperature, this procedure results in an intensity-calibrated source spectrum, with telescope losses and atmospheric absorption features removed. Inevitably, the sky is colder than the card, however, resulting in undercorrection for atmospheric features; typical residual absorption is ~30% of the original depth. In addition, the procedure works best on a telescope with baffling around the secondary, which eliminates the card-sky chopped signal from edges of the instrument's's field of view which miss the secondary. On an infrared-optimized telescope, the card-sky calibration overestimates our response to sources. On the IRTF this causes a multiplicative error of 0.6-0.7. If better atmospheric division is required, a comparison star spectrum is observed, reduced in the same way, and divided into the object spectrum. However, some instrumental problems, notably interference fringing, vary with source extent and position on the array, making division of extended sources by point source somewhat problematical. Unfortunately, there are few if any truly uniform extended sources in the sky.
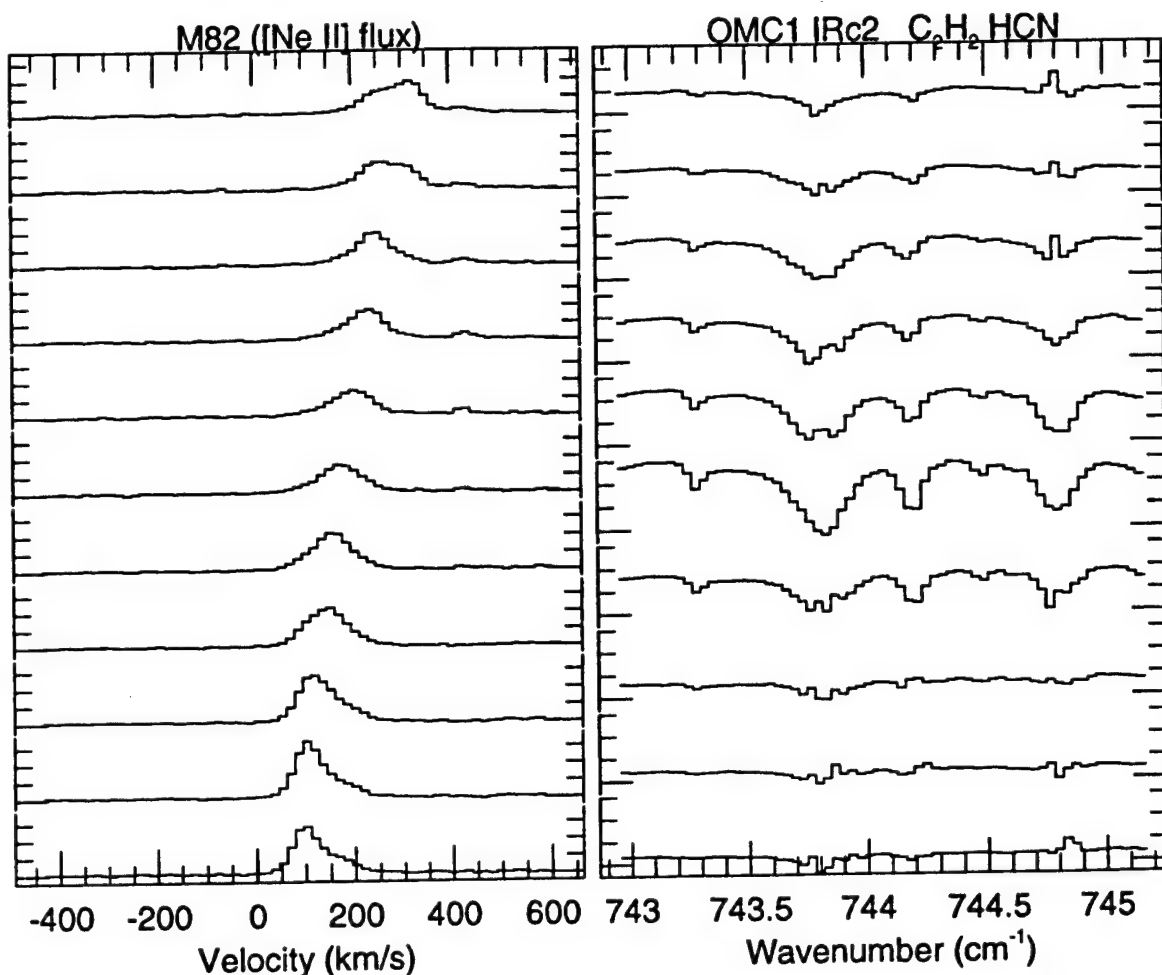
Fig. 1. Single spatial and grating position observations. (left) [Ne II] spectra of M82, with the slit centered on the nucleus and parallel to the major axis. (right) Spectra of C_2H_2 and HCN absorption toward Orion KL. The slit runs across IRc7 (spectra 3-4) and IRc2 (spectra 5-6). The C_2H_2 R(5) and HCN R(10) lines are at 743.3 and 744.5 cm^{-1}; other features are telluric. (The spectra have been divided by card-sky, but not by a comparison star.)

3. Observations of Narrow Spectral Regions in Point Sources

Point sources could be observed with the same chop-and-nod or nod observing procedures used for slightly extended sources. However, several variation on these procedures have some advantages.

For relatively bright sources, for which high-quality spectra are desired, it is possible to exploit an interesting feature of the Hughes array: the first six columns are offset from the last five by 1/2 pixel in the 64-pixel (spectral) direction. As a result, it is possible to obtain (128-point) Nyquist sampled spectra by centering sources to split their light between columns 6 and 7. An example of such a spectrum is shown in Figure 2.

If instead more efficient observing is required, it is possible to nod a point source between two positions along the slit, so that it is observed all of the
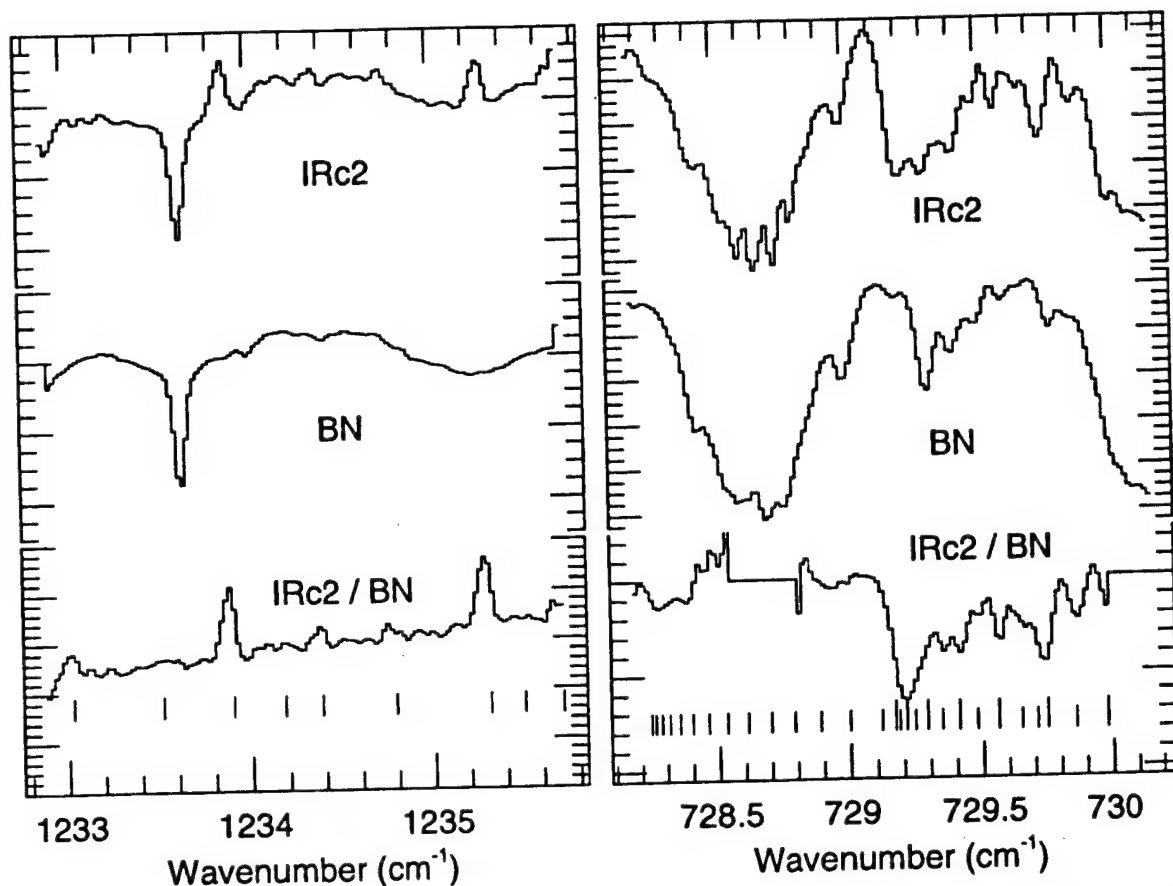
Fig. 2.   Nyquist-sampled spectra of point sources. (left) Spectra of IRc2 and BN (divided by card-sky), and their ratio, showing SiO emission in IRc2. Positions of several isotopic lines are marked with ticks. (right) Spectra of IRc2 and BN showing C_2H_2 Q-branch absorption in IRc2.

time. This improves the observing efficiency by a factor of two, or the S/N by $\sqrt{2}$. It also suppresses sky noise, since both source and sky are observed all of the time. In principal, it should be possible to gain nearly another factor of $\sqrt{2}$ by nodding the source between a number of positions along the slit. (We have not yet been able to try this procedure due to the narrow array used.) The relative merits of different nodding procedures can be seen by comparing different procedures all with the same total observing time. We assume white (photon) noise, so that the noise integrates up as the square root of time. Consider the reference case to be that of staring at a source, and take the signal and noise each to equal 1 in this case. In the case of chopping off of the array, the source is observed only 1/2 of the time, and the on-source and off-source noise each accumulate for 1/2 of the time, but must be added in quadrature, giving:

$$\text{chopping}: \quad S = 1/2, \ N = \sqrt{(\sqrt{1/2})^2 + (\sqrt{1/2})^2} = 1, \text{ or } S/N = 1/2. \quad (1)$$

If the source is nodded between two positions along the slit, each position provides the same S/N (1/2) as with chopping, but can be added (with noise added in quadrature) to give:

$$\text{nodding along slit}: \quad S/N = 1/\sqrt{2}. \tag{2}$$

If instead, the source is nodded between 4 positions along the slit (e.g.), the S/N for each position can be calculated using the fact that the source is observed 1/4 of the time and the sky 3/4 (so 1/3 of the total sky signal is subtracted from the source to get on-off). Again, the noise contributions from source and sky must be added in quadrature. For each position the result is:

$$S = 1/4, \; N = \sqrt{(\sqrt{1/4})^2 + (1/3\sqrt{3/4})^2} = \sqrt{1/3}, \text{ or } S/N = \sqrt{3}/4. \tag{3}$$

When the signals from the four positions are combined the S/N becomes:

$$\text{four} - \text{position nod}: \quad S/N = \sqrt{3/4}, \tag{4}$$

or an efficiency 3/4 that of staring. In general, nodding between n positions gives $S/N = \sqrt{(n-1)/n}$, approaching the S/N of staring as $n \to \infty$. It should be emphasized that these calculations assume white (photon) noise. If 1/f noise is present, or if more rapid readout of an array is required by the multiple position nod procedure, and increases readout noise, it may not be possible to achieve the calculated gain.

4. Observations of Broad Spectral Regions

The most straightforward method of observing a wide spectral interval with Irshell is to measure a series of spectra, moving the grating between the spectra by perhaps 1/2 the spectral coverage of the array, to allow scaling of the spectra from the relative signals in the overlap region. This procedure was found to have several problems: the inevitable difference in grating settings on an object and a comparison star result in poor correction for atmospheric features and instrumental problems such as interference fringing; and particularly the poorly corrected interference fringing results in systematic problems in the scaling procedure.

Much better results have been obtained by using a procedure in which the grating is automatically moved by small steps, so that each pixel scans a nearly completely sampled spectrum. Typically only ~10 seconds are spent at each grating setting, allowing coverage of the 8-13μm region in one to several hours. A card spectrum is automatically measured at each grating setting, and the individual spectra are shifted spectrally to patch them
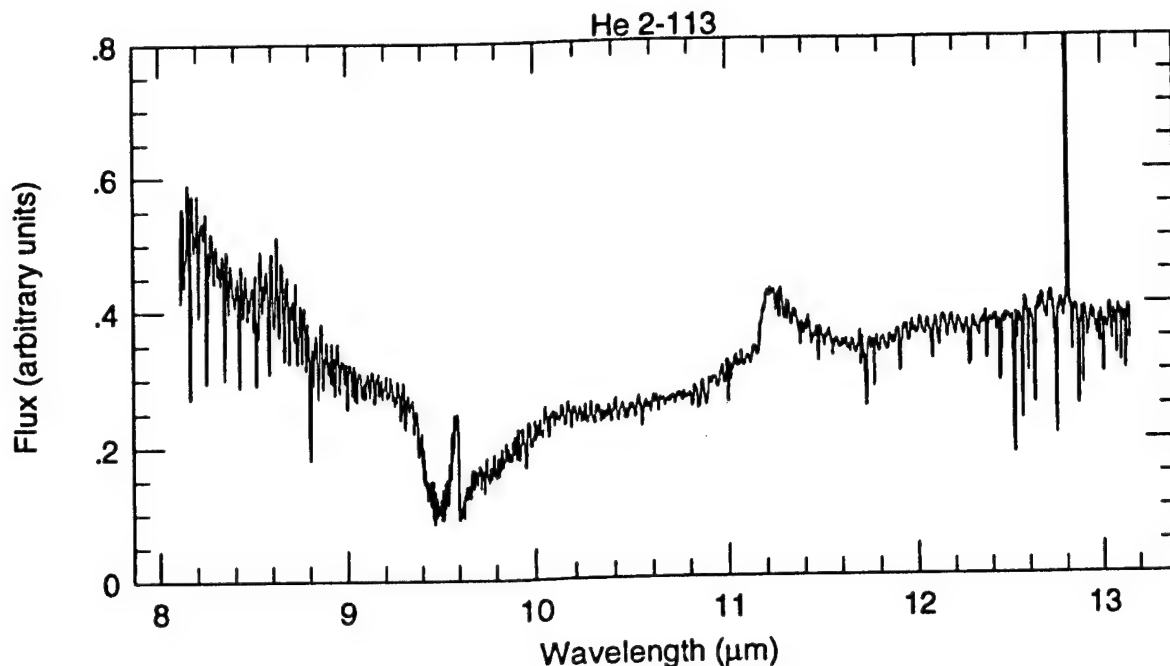
Fig. 3.   8-13μm spectrum of He 2-113. Spectra have been scaled and patched together, after dividing by card-sky. Residual atmospheric absorption is apparent, especially in the O_3 band, and residual detector fringing can be seen. Both are removed by division by a comparison star. The 7.7, 8.6, and 11.3μm UIR features and [Ne II] can be seen.

together by matching atmospheric features. A point-source spectrum is extracted before patching to avoid any problems caused by wandering of the source along the slit. Because the interference pattern shifts in phase along the length of the array, the combination of the spectra measured by different pixels has much less fringing than an individual spectrum. A spectrum obtained in this way is shown in Figure 3.

For observations of even moderately extended sources, measurement of broad spectral regions becomes very difficult, as guiding errors can have different effects on sources at different positions along the slit, making scaling and patching of the overlapping spectra problematical at best.

5. Imaging in a Line

For faint extended sources, for which long integration times are required at each position observed, it is generally easiest to measure a number of slit positions, with chop-and-nod or nod-mode observing. However, for sources bright enough that it is feasible to observe a large region, it is more efficient to automatically drive the telescope while recording spectra. One way to do this is to scan the telescope while taking data with a chopping procedure. As long as a frame is recorded in less time than is required to scan by a slit width, it is not very relevant whether the telescope is stepped or scanned continuously. Different telescopes require different scanning or stepping pro-

cedures. For example, on the IRTF we trigger a constant-speed "line scan", whereas on the ESO 3.6m we command steps over a serial communication link. It is generally best to scan a distance twice the chopper throw, so that subtracting the two halves of the scan is equivalent to nodding. We normally choose to scan in both the forward and reverse directions, although a fly-back could also be used.

Analogously with simply nodding, rather than chopping and nodding, it is frequently better to scan without chopping. In this mode, each position is stored as a DC measurement, and in data reduction the ends or low points of the scan are used as sky measurements and subtracted from all frames of the scan. We typically scan at a rate of about $1''\text{sec}^{-1}$, and may cover $\sim 1'$. The advantage to this procedure over chopping while scanning is similar to that of nodding between many points along a slit: almost all of the observing time is spent on the source, but yet several sky positions can be averaged to reduce their contribution to the noise, resulting in an efficiency nearly equal to that of staring. The problem with the procedure is that the sky may be measured up to ~ 1 minute in time from the object (and one sky measurement is used for all object positions), increasing the susceptibility to sky noise. We have found that about 1/2 of the time on Mauna Kea (2/3 of the clear time) the sky is sufficiently stable to allow scanning without chopping. In addition, on sources with narrow lines, the off-line spectral pixels can be used to monitor the sky, allowing removal of sky noise during data reduction.

Data cubes of emission lines from Sgr A West, M82 and several other objects have been obtained using a telescope-scan observing procedure. An image of Sgr A West in [Ne II] (summed over the resolved line) is shown in Figure 4.

6. Photometric Observations of Point Sources

The telescope-scan procedure can also be used to obtain photometric observations of point sources. With a simple pointed observation, guiding uncertainty with the narrow ($\sim 2''$) entrance slit makes photometry almost impossible, but by integrating the intensity in a map, this problem can be overcome. Perhaps surprisingly, the efficiency of this procedure is not much worse than that of chopping or nodding, since the decreased S/N on source is compensated by the increased S/N on sky (see the discussion of nodding along a slit).

7. Acknowledgements

A large number of people have contributed to the development, maintenance, and use of Irshell. D.E. Bruce and D.F. Lester (UT), J.F. Arens and M.C.
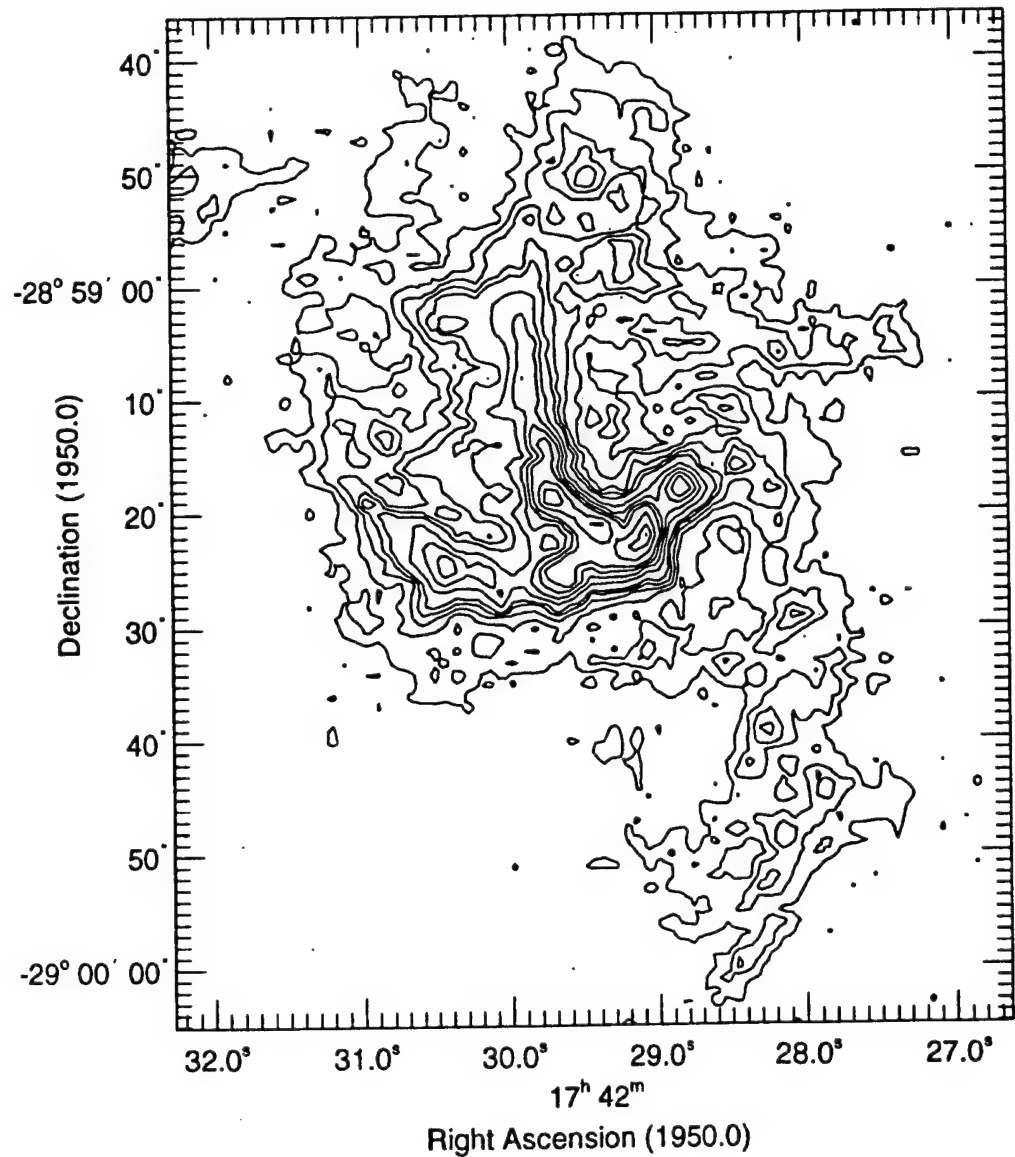
Fig. 4.   [Ne II] emission-line map of Sgr A West. The flux summed over the spectral channels containing the line is shown with quadratic contouring.

Peck (UCB SSL), and G. Kramer (Hughes) were particularly important in bringing it into existence. The development of and observations with Irshell have been supported primarily by the NSF.

References

Lacy, J.H., Achtermann, J.M., Bruce, D.E., Lester, D.F., Arens, J.F., Peck, M.C., and Gaalema, S.D.: 1989, *P.A.S.P.* **101**, 1166

Achtermann, J.M.: 1991, in Warrall, D.M., Biemesderfer, C., and Barnes, J., eds., *Astronomical Data Analysis Software*, Astronomical Society of the Pacific:San Francisco, 451

SPECTROSCOPY OF EVOLVED STARS IN THE NEAR INFRARED: EXPLORATIONS BEYOND THE AGB

Douglas M. Kelly

Department of Astronomy, University of Texas, Austin, Texas 78712
Electronic mail: dkelly@astro.as.utexas.edu

William B. Latter

National Radio Astronomy Observatory,[1] 949 N. Cherry Avenue, Campus Building 65, Tucson, Arizona 85721
Electronic mail: wlatter@nrao.edu

ABSTRACT

We present spectra taken between $\lambda = 0.9-1.3$ μm for a sample of evolved stars ranging from Mira variable stars to planetary nebulae. An evolution can be seen from the absorption spectra of the late-type stars to the emission line spectra of the planetary nebulae. We compare emission line strengths for objects ranging from $T_{eff} = 30\,000$ to $200\,000$ K, and we use infrared and visible line ratios to determine densities and temperatures in the emission line regions. We examine the four factors that are most important to determining relative ion strengths—stellar temperature, evolutionary status, excitation mechanism, and clumpiness. It is found that clumps appear to be common, and that shocks are very important to the excitation and shaping of planetary nebulae. We also find that the strength of the low ionization and molecular emission lines decreases with age, and we use a filling factor analysis to show that this evolution is caused by a decrease in the amount of low ionization material close to the star.

1. INTRODUCTION

Recent imaging studies are providing important insights into the formation and evolution of planetary nebulae (PN; e.g., Schwarz *et al.* 1992; Balick *et al.* 1992, 1993; Graham *et al.* 1993; Latter *et al.* 1993; Kastner *et al.* 1994; Latter *et al.* 1994). Stars with initial masses of roughly $\mathscr{M}_* \approx 1-8$ $\mathscr{M}_\odot$ build up a carbon–oxygen degenerate core while on the asymptotic giant branch (AGB). Mass is driven from the surface by a combination of pulsations and radiation pressure (Jura 1986). When the core mass approaches $0.6 \mathscr{M}_\odot$, the efficiency of radiation-driven mass loss increases rapidly and most of the remaining envelope material is ejected during a $\tau \approx 1000-10\,000$ yr period. Since the density in the stellar atmosphere is high and the temperature is low, the ejected material is predominantly molecular. When the envelope mass drops to $\mathscr{M}_{env} \approx 0.01 \mathscr{M}_\odot$, the pulsations cease, the mass loss rate drops by a factor of 100, and the star evolves off the AGB (Schönberner 1987). As the envelope of the star contracts and rises in temperature, the luminosity of the star remains nearly constant. The momentum of the wind is undiminished and the low mass wind is accelerated to very high velocities ($v \sim 1500$ km s^{-1}). This fast wind plows into the slower red giant wind and sweeps the material into shells (see Kwok *et al.* 1978). As the central star and nebula evolve, a photodissociation front moves through the gas and the circumstellar envelope changes from molecular to atomic to ionized. The gross morphology of the nebula depends mainly on its age and on the isotropy of mass loss on the AGB (see Balick 1987). By studying details of the morphology and spectra of PN and protoplanetary nebulae (PPN), we can learn more about the nature of AGB mass loss and the shaping and excitation of PN envelopes.

In this paper, we investigate the origin and evolution of planetary nebulae by tracing the evolution of their $\lambda = 0.9-1.3$ μm spectra. Our study begins with AGB stars and other highly evolved stars (WX Ser, IRC+10°420, IRC+10°216, AFGL 915). We also observed four of the PPN candidates identified by Kwok (1993) (IRAS 04296+3429, IRAS 23304+6147, AFGL 618, AFGL 2688), two symbiotic stars (HM Sge, V1016 Cyg), as well as several young and more evolved PN (Hubble 12, NGC 6790, Vy 2−2, NGC 7027). The Orion Nebula is presented as a comparison object.

The $\lambda = 0.9-1.3$ μm region has several attributes that make it a good choice for this study. It offers low attenuation, numerous molecular features, including high vibrational transitions of H_2, and good sensitivity to blackbody sources as cool as $T = 2000$ K. It also contains electronic transitions for many ions, including the Paschen series of hydrogen. We searched for new lines and species in our target objects and traced their atomic, molecular, and continuum emission. As we discuss in later sections, these observations give us a better understanding of the distribution and excitation of gas in PN.

A number of papers have been written over the last three decades about the infrared spectra of post-main sequence stars. The reader is referred to the following references for $\lambda = 0.9-1.35$ μm spectra of giants, supergiants, and oxygen- and carbon-rich AGB stars. Wing (1967) compared $\lambda = 0.75-1.1$ μm spectra of dwarfs, giants, and supergiants of various spectral types. He found that TiO and ZrO are the dominant features in the spectra of oxygen-rich post-main sequence stars, with VO becoming important for late-M

34

TABLE 1. Log of observations.

Object	Obs. Date	Ref. Star	Sp. Type
WX Ser	4/9/90	HR 5659	G5 V
IRC+10°420	6/9/90	HR 7354	F6 V
IRC+10°216	5/12-15/90	HR 3998	F7 V
AFGL 915	10/27/90	HR 2313	F8 V
IRAS 04296+3429	10/27-28/90	HR 1489	G0 V
IRAS 23304+6147	10/27/90	HR 8853	F8 V
AFGL 2688	10/27-28/90, 11/4/90	HR 8170	F8 V
V1016 Cyg	11/5/90	HR 7550	F4 V
HM Sge	11/3/90	HR 7560	F8 V
Hubble 12	10/27-28/90, 11/3-5/90	HR 8853	F7 V
NGC 6790	10/27/90	HR 7354	F6 V
Vy 2-2	10/28/90, 11/4/90	HR 7354	F6 V
NGC 7027	11/14/89	HR 8170	F8 V
Orion Neb.	11/14-16/89, 10/28/90, 11/3/90	HR 2007	G4 V

stars. He also found that CN bands are the dominant features in carbon-rich stars. Lockwood (1969) measured the 0.96–1.08 μm spectra of oxygen-rich Mira variables and found a relationship between TiO band strength and temperature. Thompson et al. (1969a,b) detected ^{13}CO in the λ=1.2–4.2 μm spectra of carbon-rich stars and presented evidence that the $\Delta v = 2$ and $\Delta v = 3$ bands of ^{12}CO are saturated in these stars. Miller (1970) observed the CN bands in the λ=0.7–1.1 μm spectrum of IRC+10°216. Lockwood (1973) made improved measurements of TiO and VO band strengths in the λ=0.96–1.04 μm spectra of M-type stars. Finally, Goebel et al. (1981) confirmed that CN bands are the dominant features in the λ=0.7–1.5 μm spectra of carbon-rich stars and showed that more complex molecules such as HCN and C_2H_2 are the dominant features in the λ=1.5–8.0 μm region.

There have been several recent studies of the infrared spectra of PN and PPN. The λ=0.84–1.35 μm spectrum of the bipolar PPN AFGL 618 is discussed by Latter et al. (1992) and Kelly et al. (1992). They found that the infrared spectrum is dominated by low-ionization, shock-heated lines, including strong H2 emission. The $T_{eff} \sim 30\,000$ K central star excites fluorescent O I and H2 lines in the λ=1.11–1.23 μm spectrum of that region. Rudy and collaborators presented a series of papers on the λ=0.8–1.3 μm spectra of PN, including IC 4997 (Rudy et al. 1989), V1016 Cyg (Rudy et al. 1990), NGC 6572 (Rudy et al. 1991a), BD+30°3639 (Rudy et al. 1991b), NGC 7027 (Rudy et al. 1992), and Hubble 12 (Rudy et al. 1993). They found that the infrared O I lines are excited by Lyβ fluorescence in IC 4997 and V1016 Cyg and by UV continuum fluorescence in the other sources. They devised a method for removing the nebular

TABLE 2. Line identifications and relative fluxes.

ID	λ(μm)	GL618	V1016Cyg	HMSge	Hb12	N6790	Vy 2-2	N7027	Orion
Fe II?	0.8930	-	.030	.023	-	-	-	-	-
?	0.8975	.025	-	-	-	-	.020	-	-
He I	0.8997	-	-	.015	.0082	-	-	-	-
Pa 10	0.9015	.106	.072	.145	.106	.052	.145	.121	.079
[FeII]	0.9034	.088	-	-	-	-	-	-	-
[S III]	0.9069	.106	.15	.77	.81	.53	1.88	1.68	1.32
C I	0.9112	.34	-	-	-	-	-	-	-
Pa 9	0.9229	.136	x	x	x	x	x	.176	.128
[Fe II]									
He II	0.9345	-	x	x	x	x	x	.055	-
?	0.9362	-	x	x	x	x	x	.008	-
?	0.9449	-	-	-	-	-	.026	.012	.017
He I	0.9464	-	-	-	.023	.028	.042	*	*
?	0.9495	-	-	.013	-	-	-	-	-
?	0.9516	-	-	-	.14	-	-	-	-
[S III]	0.9531	.66	.32	1.97	3.16	1.48	4.37	5.29	7.02
Pa 8	0.9546	.14	.064	.29	.23	.27	x	-	.029
He I	0.9604	-	x	x	x	x	x	-	.008
He I	0.9703	-	x	x	x	x	x	.003	-
[Fe II]	0.9756	-	x	x	x	x	x	.006	-
?	0.9770	-	x	x	x	x	x	.010	.006
[C I]	0.9824	.91	x	x	x	x	x	.035	.020
[C I]	0.9850	2.6	x	x	x	x	x	.011	.006
C II	0.9904	-	x	x	x	x	x	-	.0059
?	1.0014	-	-	-	x	x	x	*	.027
He I	1.0031	.022	-	-	x	x	x	.35	.38
Pa 7	1.0049	.28	.19	.28	x	x	x	-	.0030
N I	1.0109	.12	-	-	x	x	x	.82	-
He II	1.0124	-	.35	.83	x	x	x	-	.0027
?	1.0212	-	-	.0088	x	x	x	-	-
[S II]	1.0286	.34	.015	.15	.011	.015	.026	.072	.097
He I	1.0311	-	-	-	.0053	-	-	-	-
[S II]	1.0320	.47	.024	.20	.015	.029	.035	.105	.137
[S II]	1.0336	.34	.019	.13	.0096	.021	.020	.079	.109
[S II]	1.0370	.16	.013	.088	.0035	.0077	.011	.036	.053
[N I]	1.0398	1.69	.020	.18	.011	.0059	.012	.029	.016
[N I]	1.0408	1.16	.015	.14	.0068	.0053	.011	.024	.0072
He II	1.0420	-	-	-	-	-	-	-	.015
?	1.0447	-	-	.046	-	-	-	-	-
?	1.0519	-	x	x	.003	x	x	.006	.007
C I	1.0685	.06	x	x	-	x	x	.015	.013
C I	1.0754	-	x	x	-	x	x	-	.005
He I	1.0830	.75	3.01	6.48	6.30	9.11	7.67	8.10	4.98
H2	1.0848	.34	-	-	-	-	-	-	-
?	1.0858	-	.065	-	-	-	-	-	-
He I	1.0913	.084	.036	.059	.045	.077	.063	.030	.011
Paγ	1.0938	.375	.351	.527	.411	.507	.729	.566	.495
H2	1.0997	.13	-	-	-	.0011	-	-	-
H2	1.1172	.27	-	x	-	x	-	-	-
H2	1.1201	.059	-	x	-	x	-	-	-
H2	1.1208	.062	-	x	-	x	-	-	.011
O I	1.1287	.059	.17	x	.0081	x	.017	-	.011
H2	1.1301	.066	-	x	-	x	-	-	.0091
C I	1.1330	-	-	x	-	x	-	-	-
?	1.1344	-	-	x	-	x	-	.0076	.006
[P II]	1.1468	.075	x	x	.001	x	x	.016	.006
H2	1.1619	.23	x	x	-	x	x	.182	-
He II	1.1626	-	x	x	-	x	x	.025	-
He II	1.1673	-	x	x	.001	x	x	.002	.015
C I	1.1754	.022	x	x	.001	x	x	.002	.015
[Fe II]	1.1831	.025	x	x	.001	x	x	-	-
H2	1.1854	.16	x	x	.002	x	x	.051	.012
[Fe II]	1.1882	.21	x	x	.001	x	x	-	-
[P II]									
H2	1.1892	.081	x	x	.0015	x	x	.013	-
C I	1.1894	-	x	x	-	x	x	.012	.015
He I	1.1969	-	x	x	.015	x	x	.002	.004
?	1.2292	-	x	x	.002	x	x	.011	.003
H2	1.2327	.14	x	x	.002	x	x	.001	.002
H2	1.2380	.19	x	x	-	x	x	.003	-
H2	1.2416	.088	x	x	-	x	x	.014	.021
He I	1.2528	-	x	x	.027	x	x	.007	.014
[Fe II]	1.2567	.72	x	x	.010	x	x	.033	.030
He I	1.2785	.138	*	.035	.055	.073	.079	.033	.030
Paβ	1.2818	1.00	1.00	1.00	1.00	1.00	1.00	1.00	1.00
H2	1.2870	.072	-	-	-	-	-	-	-
?	1.2893	-	-	.012	-	-	-	.005	-
He II	1.2914	-	-	-	-	-	-	-	-
H2	1.2929	.034	-	-	.0022	-	.0042	.0022	.0047
[Fe II]	1.2943	.100	:	-	-	-	-	-	-
C I	1.2950	.012	-	-	.0037	.0050	-	.0033	.0044
He I	1.2968	-	-	-	.0046	x	x	.0027	.0036
He I	1.2985	-	x	x	.024	x	x	.003	.038
O I	1.3165	.13	x	x	.0035	x	x	.0026	.0089
[Fe II]	1.3205	.22	x	x	.0012	x	x	.0011	.0063
[Fe II]	1.3278	.062	x	x	-	x	x	-	-

Notes to Table 2

- observed, line not clearly detected
x spectra do not include this wavelength
* line probably present but cannot be deblended from adjacent features
: highly uncertain line flux due to uncertain continuum level and fluxing

All line ratios are listed relative to Paβ and have been dereddened. The uncorrected Paβ fluxes (erg s⁻¹ cm⁻²) and Av (mag) values are as follows: AFGL 618 – 1.9×10^{-13}, 2.1; V1016 Cyg – 3.45×10^{-11}, 1.15; HM Sge – 1.16×10^{-11}, 1.3; Hubble 12 – 1.8×10^{-11}, 2.0; NGC 6790 – 1.09×10^{-11}, 2.2; Vy 2-2 – 6.6×10^{-12}, 3.4; NGC 7027 – 3.6×10^{-11}, 2.5; Orion – 6.3×10^{-12}, 1.0.
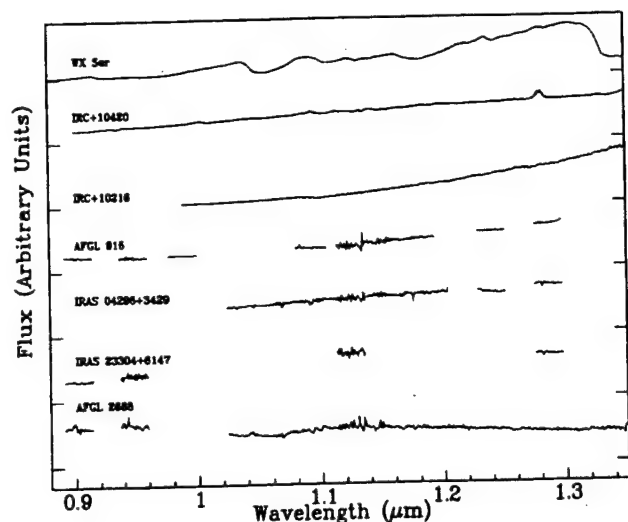
FIG. 1. The $\lambda=0.9-1.35$ μm spectra of continuum dominated sources. These data were acquired with the Steward Observatory 2.3 m telescope and a germanium diode spectrometer. See Sec. *3.1*.

FIG. 2. The $\lambda=0.9-1.35$ μm spectra of emission line objects, acquired with the Steward Observatory 2.3 m telescope and a germanium diode spectrometer. See Sec. *3.2*. Identifications for many of the prominent lines can be found in Fig. 3.

continuum emission from a spectrum and used this technique to isolate the spectra of the central stars. They determined densities and temperatures in the emitting regions of the nebulae, and derived new abundances for several of the objects.

2. OBSERVATIONS AND DATA REDUCTION

The spectra presented in this paper were measured at the Steward Observatory 2.3 m telescope on Kitt Peak, Arizona using the GeSpec, a $\lambda=0.9-1.6$ μm spectrometer with a 2×32 pixel germanium photodiode array. The twin apertures of the GeSpec are 6″ in diameter and are separated by 1′. With the 600 l/mm grating the resolution is $\lambda/\Delta\lambda\approx1000$ and the spectral coverage of each segment is $\Delta\lambda\approx0.022$ μm. With the 150 l/mm grating (used for WX Ser and IRC +10°420), the resolution is $\lambda/\Delta\lambda\approx300$ and the spectral coverage of each segment is $\Delta\lambda\approx0.1$ μm. F and G dwarf stars were used to remove telluric absorption features and to provide flux calibration. Observing and data reduction procedures are discussed by Rix *et al.* (1990). All sources were centered in the 6″ apertures, and up to 20% intensity variations resulted from pointing and guiding fluctuations. Since the data collection was very time consuming, we only made complete spectral scans of the spectroscopically most interesting objects. For the others, we observed the hydrogen recombination lines and several other diagnostic lines. The observations are summarized in Table 1, line identifications of the emission line objects are included in Table 2, and the resulting spectra are presented in Figs. 1 and 2. A more detailed version of the Orion Nebula spectrum is shown in Fig. 3. Only 5σ and better detections are listed in Table 2. See Kelly (1993) for additional (less certain) line identifications in the spectra of Hubble 12, NGC 7027, and the Orion Nebula.

3. COMMENTS ON INDIVIDUAL SOURCES

3.1 Absorption Spectra

3.1.1 WX Serpentis

WX Serpentis is a Mira variable star with spectral type M8.5. Its infrared spectral features are similar to but stronger than those found in late M dwarfs (see Kirkpatrick *et al.* 1993). The strong VO absorption bands at $\lambda=1.06$ and 1.18 μm and the deep H_2O feature at 1.34 μm are especially noticeable in the spectrum of WX Ser.

3.1.2 IRC +10°420

IRC+10°420 is an OH/IR star (spectral type F8 Ia), but it appears to be a high mass supergiant rather than a late-AGB star (Jones *et al.* 1993). It has an infrared spectrum similar to
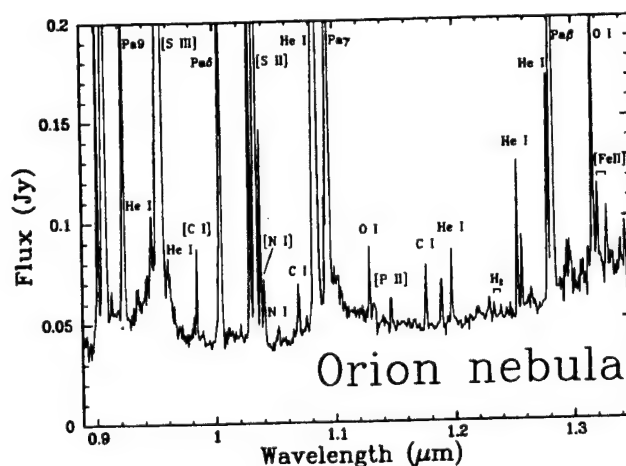

FIG. 3. The $\lambda=0.89-1.35$ μm spectrum of the Orion Nebula, acquired with the Steward Observatory 2.3 m telescope and a germanium diode spectrometer. This spectrum is shown for comparison and line identifications only. There is no analysis of the Orion Nebula in the text.

those of the early M dwarfs. Of the stars studied by Kirk-patrick *et al.* (1993), IRC+10°420 is most similar to the un-published M1 dwarf GL 15A. IRC+10°420 has weaker FeH 0.99 μm absorption than GL 15A, as expected because of the lower density atmosphere (Allard 1992), and it has stronger ZrO (0.93–0.94, 1.166, 1.177, 1.187 μm) and VO (1.05 μm) bands. IRC+10°420 also produces weak Paβ emission. Oudmaijer *et al.* (1994) presented slightly blueshifted line profiles for Brγ, Brα, and Pfγ and a double-peaked profile for Hα, and they argued that the H I lines come from a bipolar outflow that developed in the past ten years.

3.1.3 IRC+10°216

The 1.0–1.5 μm spectrum of the carbon star IRC −10°216 has few easily discernable features other than shallow CN absorption at 1.1 μm. Among the numerous faint absorption features, there are acetylene (C_2H_2) bands at 1.04 and 1.17 μm, CN bands at 1.0926, 1.0968, 1.0996, and 1.1244 μm, and dozens of what appear to be molecular absorption features scattered throughout the spectrum. The λ=1.0–1.5 μm spectrum is dominated by thermal dust emission and is well fit by a $T_c\approx$900 K blackbody. Miller (1970) reported that the λ=0.7–1.1 μm spectrum has the energy distribution of a $T_c\approx$1250 K blackbody, Becklin *et al.* (1969) fit the 1–5 μm spectrum with a $T_c\approx$650 K blackbody, and Le Bertre (1988) matched 0.55–25 μm photometry with blackbodies in the temperature range $T_c\approx$530–670 K, depending on the phase of pulsation. From Le Bertre's work, it is clear that the large range in dust temperatures cannot be accounted for by pulsations alone. Instead, one can fit the broadband photometry and our data simultaneously by invoking a two component model composed primarily of $T_d\approx$650 K dust but with 0.055% of the dust having a temperature $T_d\approx$1185 K. The maximum dust temperature is probably closer to the $T_d\approx$1250 K determined from the λ=0.7–1.1 μm spectra of Miller (1970). This value is similar to the continuum temperatures of $T_c\approx$1000–1200 K found at the onset of dust emission in carbon-rich novae (Gehrz 1988).

3.1.4 AFGL 915

The protoplanetary nebula AFGL 915 (the "Red Rectangle") has an interesting near-infrared spectrum. Our 6″ beam captured both the binary exciting star HD 44179 and some of the surrounding nebulosity. The blue end of our infrared spectrum is dominated by the photosphere of HD 44179, including weak absorption lines of H I, He I, C I, and N I. HD 44179 has been classified as a B9 to A0 III (Cohen *et al.* 1975), but the strong helium absorption lines near 0.9 μm indicate a spectral type of A1 III. Cool dust contributes to the emission from AFGL 915 starting at about 0.7 μm (Cohen *et al.* 1975), and it veils most of the atmospheric features longward of 1 μm. Brγ (Thronson 1982) and Paβ are completely obscured, and Paγ appears only weakly in absorption.

The most interesting feature in the infrared spectrum of AFGL 915 is He I at 1.0830 μm, which appears prominently in emission. Cohen *et al.* (1975) also found narrow Hα and Na D emission lines. The presence of He I recombination

emission normally indicates a central star temperature of at least $T_{eff}\approx$ 20 000 K, but given the cool photospheric temperature of AFGL 915, an alternative excitation mechanism such as chromospheric or coronal emission is required. Such activity is common in mid-F through late-K stars, but it is unexpected in an early-A star (Zirin 1976; O'Brien & Lambert 1986).

3.1.5 IRAS 04296+3429, IRAS 23304+6147, AFGL 2688

IRAS 04296+3429, IRAS 23304+6147, and AFGL 2688 (the "Egg Nebula") are carbon-rich PPN and have similar near-IR spectra. Their near-infrared spectra include a large number of absorption features, mostly from C I and CN. Other possible absorbers are Si I and He I. In addition, there is H I absorption in the spectrum of IRAS 04296+3429, consistent with the results of Hrivnak *et al.* (1994). The lack of emission lines in these spectra might be due in part to our large aperture size. With a narrow slit, Hora & Latter (1994) find CN and C_2 emission in a fairly isolated region of AFGL 2688, and C_2 Swan band emission is prominent in the visible spectrum of this object (Humphreys *et al.* 1976).

3.2 Emission Line Sources

The line strengths for the emission line sources are presented in Table 2, with all fluxes dereddened and listed relative to the Paβ flux. Paβ fluxes and visual extinctions are listed in the footnotes. Line fluxes from a bright knot in the Orion Nebula are presented for comparison. In examining Table 2, the reader should be aware of uncertainties in reddening corrections in addition to the $\approx$20% uncertainty in line flux measurements. Still, it is easy to see that there are significant differences in the relative line strengths of the various objects.

3.2.1 AFGL 618

The PPN AFGL 618 has an emission line spectrum dominated by low ionization, predominantly shock-excited gas. The [S III] lines are weak and there is no He II emission, but the [C I], [S II], [N I], and [Fe II] lines are unusually strong. The infrared spectrum is also very rich in molecular hydrogen lines. [See Latter *et al.* (1992) and Kelly *et al.* (1992) for a complete discussion of the λ=0.84–1.35 μm spectrum of AFGL 618].

3.2.2 HM Sge, V1016 Cyg

The symbiotic novae HM Sge and V1016 Cyg have evolved spectra with strong [S III], helium, and hydrogen lines. The low-ionization [S II] and [N I] lines are prominent in HM Sge, even though the central star is hot enough to excite He II emission. We compared our line strengths with the visible data of Schmid & Schild (1990) and Davidson *et al.* (1978) and with the infrared data of Thronson & Harvey (1981). The relative infrared and visible H I and [S II] line strengths are consistent with a reddening of A_V=1.0–1.3 mag (assuming no variability in the three years between observations). Thronson & Harvey found a reddening of A_V=12 mag from the Brackett line ratios, indicating that the primary H II emitting region is heavily obscured. As

discussed by Thronson & Harvey, the dust provides shielding that allows low ionization gas to survive in the outer parts of the nebula. From the [S II] and [S III] line ratios, we estimate an electron density of at least $n_e \approx 5 \times 10^5$ cm^{-3} in the forbidden line regions.

We compared our data on V1016 Cyg with the visible spectrum of Schmid & Schild (1990), the 0.46–1.3 μm data of Rudy et al. (1990), and the 2 μm data of Schild et al. (1992). From a comparison of visible and infrared H I, [S II], and He II lines, we adopt a reddening of $A_V = 1.15$ mag. This is similar to the value determined by Rudy et al., who derived the reddening separately for the H I, He I, and He II lines. Schmid & Schild found electron temperatures ranging from $T_e \approx 10^4$ to 4×10^4 K from a variety of line diagnostics. Our He I and [S II] line ratios are consistent with an electron temperature of $T_e \sim 10^4$ K. Nussbaumer & Schild (1981) found $n_e \approx 3 \times 10^6$ cm^{-3} from several sets of UV transitions. Our [S II] and [S III] line ratios indicate an electron density of at least 10^5 cm^{-3} and probably greater than 10^6 cm^{-3}. In addition, as discussed by Rudy et al., V1016 Cyg has strong, Lyβ-pumped O I fluorescence, which requires high densities in the H I–H II transition region.

There are several absorption features in the spectrum of V1016 Cyg, including H_2O at 0.938 μm and VO at 1.046 μm. As discussed by Rudy et al., these features and much of the continuum emission are produced by a late-M companion star. We have insufficient spectral coverage to improve upon Rudy et al.'s spectral classification of M6–M8.

3.2.3 Hubble 12

The planetary nebula Hubble 12 has a mostly low ionization spectrum with very prominent He I emission. The He I triplet/singlet line intensity ratio is about 3/1, as expected for recombination. The infrared [S II] lines are weak in Hubble 12, consistent with an electron density $n_e > 10^6$ cm^{-3}. In contrast, infrared [Fe II] line ratios indicate an electron density of only $n_e \approx 6 \times 10^4$ cm^{-3}, and the nebular lines of [S II] and [O II] indicate an even smaller density of $n_e \approx 3 \times 10^3$ cm^{-3} (Barker 1978; Aller & Czyzak 1983).

Hubble 12 has several features that are characteristic of a photon-dominated region (PDR). Among the PDR features are C I, Si I, and H_2 lines. The strongest H_2 lines are the (3–1) $S(1)$ line at 1.2327 μm and the 2–0 $Q(1)$ line at 1.2380 μm. The ratio of the H_2 lines is consistent with the fluorescent H_2 emission models of Black & van Dishoeck (1987; Dinerstein et al. 1988). Other detected H_2 lines are listed in Table 2, and additional H_2 identifications can be found in Kelly (1993). Fluorescence is also responsible for the O I emission from Hubble 12. The O I λ1.1287/λ1.3165 ratio is 0.3, consistent with UV continuum fluorescence with no significant resonance pumping by Lyβ. The lack of O I triplet line emission rules out recombination as the exciting mechanism for the O I.

3.2.4 NGC 6790

NGC 6790 is a strong source of He I emission. The He I triplet lines are very strong, indicating that the electron density is rather high, probably on the order of $n_e \approx 10^5$–10^6 cm^{-3}. We compared the infrared line strengths to the visible

line data of Kaler (1976). From the ratios of visible to infrared H I and [S II] lines, we derive $A_V = 2.2$ mag. [S II] and [S III] line ratios suggest $n_e \approx 10^5$ cm^{-3} for $T_e = 10^4$ K, or $n_e \approx 5 \times 10^5$ cm^{-3} for $T_e = 5 \times 10^3$ K. We analyzed He I line ratios using the collisional enhancement formulas of Clegg (1987), and we find the best agreement when we adopt $T_e < 10^4$ K. The weak forbidden lines in NGC 6790 provide further support for the high density, low temperature solution. This result contrasts with the electron densities determined from visible [S II], [O II], [Cl III], and [Ar IV] ratios by Stranghellini & Kaler (1989). They found densities ranging from $n_e \approx 5 \times 10^3$–$3 \times 10^4$ cm^{-3}. Thus, NGC 6790 is similar to Hubble 12 and AFGL 618 in having a variety of density and temperature regimes.

3.2.5 Vy 2–2

Vy 2–2 is also a strong source of He I emission. We compared our infrared spectrum to visible line data by Feibelman (1993) and Acker et al. (1989). From H I line ratios, we find extinction values ranging from $A_V \approx 3.1$–4.8 mag. We adopted a value of 3.4 mag for our analysis. Our [S II] and [S III] line ratios can be simultaneously fit for a temperature of $T_e = 1.5 \times 10^4$ K and a density of $n_e = 8 \times 10^4$ cm^{-3}, but we cannot rule out values differing from these by a factor of 2. No single density–temperature pair can account for all of the He I line ratios.

3.2.6 NGC 7027

The very hot PN NGC 7027 has a high ionization spectrum, with very strong He II and forbidden line emission and slightly weakened He I emission. The brightest He I lines are all triplet transitions, indicating high densities in the ionized regions. The infrared [S II] line ratios, which are excited outside the hydrogen Strömgren sphere, suggest an electron density of $n_e \lesssim 10^5$ cm^{-3}. There are a variety of PDR lines in the spectrum of NGC 7027, including [P II], C I, Si I, [C I], and perhaps H_2. Graham et al. (1993) showed from H_2 and CO kinematics and morphology that the H_2 1$\rightarrow$0 $S(1)$ line is excited by radiation, not by shocks. The presence of weak O I 1.3165 μm emission and the absence of the 1.1287 μm line and of any quintet transitions indicate that the O I emission is also excited by starlight fluorescence (Rudy et al. 1992).

4. DISCUSSION

There are few clear trends in the spectral characteristics of the objects in this survey. This is exacerbated by uncertainties in the evolutionary status of the individual objects. There are obvious trends, such as the evolution from the late-type stellar spectra of the AGB stars to the mixed spectra of the PPN and on to the emission line spectra of the PN. This evolution is not surprising, but details can be learned about the shaping of PN based on the distribution of lines at various evolutionary stages. For example, the great relative strength of the low ionization lines in the spectrum of AFGL 618 (see Table 2) is evidence for the importance of shocks. AFGL 618 and several of the PN have multiple density and temperature regimes, which is another characteristic of shock

excited gas. The presence of shock-heated gas in several of the PPN and PN indicates the general importance of shocks in the excitation and shaping of the nebulae. Multiple density and temperature regimes could also be the result of shielding by dense clumps. The presence of H_2 emission in the bipolar lobes of AFGL 618 is further evidence for shielding clumps (the H_2 would be rapidly dissociated if it were exposed to the full UV radiation field; see also Latter *et al.* 1992). Finally, H_2 emission from Hubble 12 and NGC 7027 shows that there is still an abundant supply of molecular material around young PN.

To understand the geometries of the emission line sources better, we worked backwards using line strengths to determine the filling factors of various ions. For permitted lines, we used the relationship

$$F_{i,n} = \frac{h\nu_{i,n}}{4\pi r^2} n_e n_{i+1} V \alpha_{i,n}^{\text{eff}}(i,T), \qquad (1)$$

where F is the dereddened line flux, r is the assumed distance, V is the volume of the emitting region, and α is the effective recombination coefficient for transition n of ion i. For forbidden lines we used the expression

$$F = \frac{h\nu}{16\pi} \frac{n_u A_{ul}}{r^2} V, \qquad (2)$$

where n_u is the population density of the upper state and A_{ul} is the transition probability in s^{-1}. Using densities and temperatures determined from line ratios, we assumed standard PN abundances from Aller & Czyzak (1983), assumed that the different ions of a given element are physically segregated, and solved for V. The resulting volumes are sensitive to the measured line fluxes and to the assumed extinction, distance, densities, temperatures, and abundances. When comparing ions, many of these factors cancel out and the relative volumes are accurate to within about a factor of two.

As expected, a progression can be seen in the relative sizes of the He^{++} and H^+ regions. V1016 Cyg and HM Sge have the largest He^{++}/H^+ volume ratios at 0.8, followed closely by NGC 7027 at 0.6. The He^{++}/H^+ ratio is much smaller in the other objects. The ratio is 0.02 in NGC 6790,

0.015 in Vy 2−2, and 0.003 in Hubble 12. He II was not detected in AFGL 618. The approach of using the He II $\lambda4686/H\beta$ ratio to determine stellar temperatures was first introduced by Ambartsumyan (1932). From Fig. 1 in Kaler & Jacoby (1989), we infer central star temperatures of $T_{\text{eff}} \approx 2.2 \times 10^5$ K for HM Sge, $T_{\text{eff}} \approx 1.9 \times 10^5$ K for V1016 Cyg and NGC 7027, and $T_{\text{eff}} \approx 8 \times 10^4$ K for NGC 6790.

A second and perhaps more interesting result concerns the size of the [C I], [O I], [N I], and [S II] emitting regions, all of which lie outside of the hydrogen Strömgren sphere. The gas in these regions can be excited by shocks or by absorption of photons with less than 13.6 eV. In V1016 Cyg, NGC 7027, NGC 6790, and Vy 2−2, this region is very thin—less than 1% the radius of the Strömgren sphere (R_{str}). The thickness is roughly 0.1 R_{str} in HM Sge, where dust shielding protects the low ionization species, 0.3 R_{str} in Hubble 12, and 6.6 R_{str} in AFGL 618. These numbers are partly influenced by the use of small apertures. Still, it is apparent that not very much PDR gas is excited in most planetary nebulae. The exceptions, Hubble 12 and AFGL 618, are very young. They have not had enough time to clear away much of the material that was ejected on the AGB, and their expanding nebulae are still sweeping through material that was ejected late on the AGB, while the mass loss rate was very high. Both have fluorescent H_2 transitions in their spectra.

In summary, the line ratios of an individual ion are determined by T_e and n_e, and we have determined these values for many of the objects. The relative ion strengths, on the other hand, depend on many parameters, including T_*, the evolution of the object, the excitation mechanisms, and the clumpiness of the gas. With our infrared data, we have been able to isolate each of these factors. We see that shocks are very important to the shaping and excitation of PN, clumps appear to be a common feature in PN envelopes, and young PN produce the strongest PDR emission because they have the largest reservoir of nearby molecular and low ionization gas.

REFERENCES

Acker, A., Köppen, J., Stenholm, B., & Jasniewicz, G. 1989, A&AS, 80, 201
Allard, F. 1992, personal communication
Aller, L. H., & Czyzak, S. J. 1983, ApJS, 51, 211
Ambartsumyan, V. A. 1932, Pulkovo Obs. Circ. Vol. 8, No. 4
Balick, B. 1987, AJ, 94, 671
Balick, B., Gonzalez, G., Frank, A., & Jacoby, G. 1992, ApJ, 392, 582
Balick, B., Rugers, M., Terzian, Y., & Chengalur, J. N. 1993, ApJ, 411, 778
Barker, T. 1978, ApJ, 219, 914
Becklin, E. E., Frogel, J. A., Hyland, A. R., Kristian, J., & Neugebauer, G. 1969, ApJ, 158, L133
Black, J. H., & van Dishoeck, E. F. 1987, ApJ, 322, 412
Clegg, R. E. S. 1987, MNRAS, 229, 31P
Cohen, M., *et al.* 1975, ApJ, 196, 179
Davidson, K., Humphreys, R. M., & Merrill, K. M. 1978, ApJ, 220, 239

Dinerstein, H. L., Lester, D. F., Carr, J. S., & Harvey, P. M. 1988, ApJ, 327, L27
Feibelman, W. A. 1993, PASP, 105, 595
Gehrz, R. D. 1988, ARA&A, 26, 377
Goebel, J. H., Bregman, J. D., Witteborn, F. C., Taylor, B. J., & Willner, S. P. 1981, ApJ, 246, 455
Graham, J. R., Serabyn, E., Herbst, T. M., Matthews, K., Neugebauer, G., Soifer, B. T., Wilson, T. D., & Beckwith, S. 1993, AJ, 105, 250
Hora, J. L., & Latter, W. B. 1994, ApJ, 437, 281
Hrivnak, B. J., Kwok, S., & Geballe, T. R. 1994, ApJ, 420, 783
Humphreys, R. M., Warner, J. W., & Gallagher, J. S. 1976, PASP, 88, 380
Jones, T. J., *et al.* 1993, ApJ, 411, 323
Jura, M. 1986, IAJ, 17, 322
Kaler, J. B. 1976, ApJS, 31, 517
Kaler, J. B., & Jacoby, G. H. 1989, ApJ, 345, 871

Kastner, J. H., Gatley, I. Merrill, K. M., Probst, R., & Weintraub, D. A. 1994, ApJ, 421, 600

Kelly, D. M. 1993, Ph.D. thesis, University of Arizona

Kelly, D. M., Latter, W. B., & Rieke, G. H. 1992, ApJ, 395, 174

Kirkpatrick, J. D., Kelly, D. M., Rieke, G. H., Liebert, J., Allard, F., & Wehrse, R. 1993, ApJ, 402, 643

Kwok, S. 1993, ARA&A, 31, 63

Kwok, S., Purton, C. R., & Fitzgerald, P. M. 1978, ApJ, 219, L125

Latter, W. B., Kelly, D. M., Hora, J. L., Deutsch, L. K., & Rieke, G. H. 1994, ApJ (submitted)

Latter, W. B., Hora, J. L., Kelly, D. M., Deutsch, L. K., & Maloney, P. R. 1993, AJ, 106, 260

Latter, W. B., Maloney, P. R., Kelly, D. M., Black, J. H., Rieke, G. H., & Rieke, M. J. 1992, ApJ, 389, 347

Le Bertre, T. 1988, A&A, 203, 85

Lockwood, G. W. 1969, ApJ, 157, 275

Lockwood, G. W. 1973, ApJ, 180, 845

Miller, J. S. 1970, ApJ, 161, L95

Nussbaumer, H., & Schild, H. 1981, A&A, 101, 118

O'Brien, G. T., & Lambert, D. L. 1986, ApJS, 62, 899

Oudmaijer, R. D., Geballe, T. R., Waters, L. B. F. M., & Sahu, K. C. 1994, A&A, 281, L33

Rix, H.-W., Carleton, N. P., Rieke, G., & Rieke, M. 1990, ApJ, 363, 480

Rudy, R. J., Rossano, G. S., & Puetter, R. C. 1989, ApJ, 346, 799

Rudy, R. J., Cohen, R. D., Rossano, G. S., & Puetter, R. C. 1990, ApJ, 362, 346

Rudy, R. J., Rossano, G. S., Erwin, P., & Peutter, R. C. 1991a, ApJ, 368, 468

Rudy, R. J., Cohen, R. D., Rossano, G. S., Erwin, P., Puetter, R. C., & Lynch, D. K. 1991b, ApJ, 380, 151

Rudy, R. J., Erwin, P., Rossano, G. S., & Puetter, R. C. 1992, ApJ, 384, 536

Rudy, R. J., Rossano, G. S., Erwin, P., Puetter, R. C., & Feibelman, W. A. 1993, AJ, 105, 1002

Schild, H., Boyle, S. J., & Schmid, H. M. 1992, MNRAS, 258, 95

Schmid, H., & Schild, H. 1990, MNRAS, 246, 84

Schönberner, D. 1987, in Planetary and Proto-Planetary Nebulae: From IRAS to ISO, edited by A. Preite Martinez (Reidel, Dordrecht), p. 113

Schwarz, H. E., Corradi, R. L. M., & Melnick, J. 1992, A&AS, 96, 23

Stranghellini, L., & Kaler, J. B. 1989, ApJ, 343, 811

Thompson, R. I., Schnopper, H. W., Mitchell, R. I., & Johnson, H. L. 1969a, ApJ, 158, L55

Thompson, R. I., Schnopper, H. W., Mitchell, R. I., & Johnson, H. L. 1969b, ApJ, 158, L117

Thronson, H. A. 1982, AJ, 87, 1207

Thronson, H. A. & Harvey, P. M. 1981, ApJ, 248, 584

Wing, R. F. 1967, Ph.D. thesis, University of California, Berkeley

Zirin, H. 1976, ApJ, 208, 414

A MID-INFRARED SEARCH FOR C$_{60}$ IN R CORONAE BOREALIS STARS AND IRC+10216

GEOFFREY C. CLAYTON[1]

Center for Astrophysics and Space Astronomy, Campus Box 389, University of Colorado, Boulder, Colorado 80309
Electronic mail: gclayton@fenway.colorado.edu

DOUGLAS M. KELLY[1] AND J. H. LACY[1]

Department of Astronomy, University of Texas, Austin, Texas 78712
Electronic mail: dkelly@danny.as.utexas.edu;lacy@astro.as.utexas.edu

IRENE R. LITTLE-MARENIN

Center for Astrophysics and Space Astronomy, Campus Box 389, University of Colorado, Boulder, Colorado 80309, and Whitin
Observatory, Wellesley College, Wellesley, Massachusetts 02181
Electronic mail: ilittle@casa.colorado.edu

P. A. FELDMAN

Herzberg Institute of Astrophysics, NRC, 100 Sussex Dr., Ottawa, K1A 0R6, Canada
Electronic mail: paf@hiaras.hia.nrc.ca

P. F. BERNATH

Department of Chemistry, University of Waterloo, Waterloo, ON, N2L 3G1, Canada
Electronic mail: bernath@watsci.uwaterloo.ca

Received 1994 December 12; revised 1995 January 26

ABSTRACT

Buckminsterfullerene (C$_{60}$) is suspected to be an important constituent of the Interstellar Medium but to date no certain detection of C$_{60}$ has been made in an astronomical context. Dust-forming material around R Coronae Borealis (RCB) stars may be ideal sites for the formation of C$_{60}$. The high-temperature, hydrogen-deficient, carbon-rich environment around RCB stars closely mimics the laboratory conditions under which C$_{60}$ forms. It is believed that dust is being formed continually in the atmospheres of the RCB stars during their pulsation cycles. The temperature at which this dust forms could be as high as 4000 K, and can occur in conditions far removed from thermodynamic equilibrium, as long as a mechanism exists to contain carbon atoms within a given volume. A likely form of carbon condensate is fullerenes such as C$_{60}$. Low Resolution Spectra from *IRAS* show the apparent presence of an emission feature near 8.6 μm in three RCB stars which could possibly be associated with C$_{60}$. However, the low resolution and poor S/N of these spectra do not permit identification of the features. Therefore, we obtained new observations using the Irshell mid-infrared spectrograph at the NASA Infrared Telescope Facility. We searched the 8.6 μm spectral region of the RCB stars, R CrB, RY Sgr, and V854 Cen. No narrow features were found at a level of 2% of the continuum. However, the carbon star, IRC+10216 did show a possible emission feature centered at 8.6 μm.

1. INTRODUCTION

It is expected that C$_{60}$, its various fullerene and fullerane complexed analogs,[2] and their ions may exist in significant amounts in the interstellar medium, in carbon-rich objects such as the R Coronae Borealis (RCB) stars, IRC+10216, and in the circumstellar envelopes of certain cool giants (Hecht 1991; Kroto & Jura 1992; Webster 1992; Whitney *et al.* 1993). The possibility that fullerene analogs might be the long-sought-after carriers of the diffuse interstellar bands

was first mentioned in the fullerene-discovery paper (Kroto *et al.* 1985), and the hypothesis has been developed further by Kroto & Jura (1992, and references therein). Fullerene and fullerane analogs have also been suggested as the causes of the unidentified emission features observed in the stellar outflow of the Red Rectangle (HD 44179), the unidentified infrared emission features found in such objects as NGC 7027, and the variable component of the interstellar extinction (Kroto & Jura 1992; Webster 1991, 1992, 1993). Several searches of astronomical objects for C$_{60}$ have been unsuccessful (Snow & Seab 1989; Somerville & Bellis 1989; Jeffery 1995). Recently, a possible detection of C$_{60}^+$ bands near 9600 Å was reported for interstellar lines of sight (Foing & Ehrenfreund 1994). The circumstellar shells of the RCB stars and IRC+10216 are sites of very complex carbon chemistry (e.g., Millar & Herbst 1994; Goeres & Sedlmayr 1992). Long carbon chains up to C$_5$ and HC$_{11}$N have been detected

---

[1]Visiting Astronomer at the Infrared Telescope Facility, which is operated by the University of Hawaii under contract from the National Aeronautics and Space Administration.

[2]Buckminsterfullerene or C$_{60}$, the soccerball molecule, is the best known fullerene. Fulleranes are formed by attaching hydrogen atoms and complexed analogs are formed by attaching other atoms or molecules.

in IRC+10216 (Bernath *et al.* 1989; Bell *et al.* 1982). The Swan bands of C_2 and the violet bands of CN have been seen in emission in several RCB stars (e.g., Whitney *et al.* 1992).

An ideal place to search for C_{60} may be the RCB stars. They are a small group of hydrogen-deficient carbon-rich supergiants which undergo very spectacular declines in brightness of up to eight magnitudes in the *V* band at apparently irregular intervals (Clayton 1995). A cloud of carbon-rich dust forms along the line of sight to the RCB star, eclipsing the photosphere, and producing a rich emission line spectrum. As the dust cloud disperses, the star returns to maximum light. Recent extensive ground- and space-based observations of R CrB, RY Sgr and V854 Cen have allowed us to put together a coherent empirical model of an RCB decline (Clayton *et al.* 1992; Whitney *et al.* 1993). The close connection of pulsational phase with the time of dust formation seen in RY Sgr and V854 Cen implies that the dust is forming near the star (Pugach 1977; Lawson *et al.* 1992). It is likely that dust is forming in close proximity ($< 2R_*$) to the RCB star photosphere, based on time scales for acceleration of the dust, eclipse of the chromospheric region, and dispersal of the dust.

While crystalline graphite can be formed under carefully controlled conditions at low temperatures, the more disordered amorphous graphite is produced in the laboratory from the pyrolysis of organic materials at temperatures of up to 3500 K (Rohlfing 1988). The important factors to consider seem to be whether condensation will occur under conditions of thermodynamic equilibrium and on what time scales the dust will be produced. In considering the case of dust formation in RCB stars, it is likely that the conditions of carbon nucleation will be rather different than that occurring in the outflows of mass-losing red giants for several reasons (Whitney *et al.* 1993). First, in most red-giant stars the observations are consistent with dust forming in a fairly symmetric fashion with mass loss occurring over the entire surface of the star (Danchi *et al.* 1994); while in RCB stars the mass loss seems to occur from particular areas of the surface. Second, in RCB stars the nucleation will proceed in the presence of much smaller amounts of hydrogen than in red giants where the hydrogen abundances are normal (Lambert 1986). Third, RCB stars have shocks propagating through the outer atmospheres, which cause local density enhancements, and certainly provide nonequilibrium conditions. Finally, nucleation of dust in RCB stars will most likely be from a plasma of atoms, compared with red giants in which the dust forms via the reaction of small molecular precursors such as acetylene, HCCH (Tielens 1990).

If we accept that the formation of fullerite dust in the laboratory (see Sec. 2) is a good model for the dust formation process in RCB stars, then we come to several conclusions. First, under such conditions carbon can nucleate to form dust at much higher temperatures than the canonical crystalline graphite temperature. It is likely that a high pressure plasma of carbon, perhaps produced by a shock or pulsation wave, could form a "puff" of carbon dust which is then ejected by radiation pressure. Second, as in the laboratory experiments, the dust produced will not be crystalline graphite but will be more amorphous in character. Finally,

and perhaps most intriguingly, since the closed carbon cage fullerenes are observed to form along with the dust during this process in the laboratory, then it seems that RCB stars are ideal sites for the formation of C_{60}. Goeres & Sedlmayr (1992) model RCB dust production and carbon gas chemistry. They find that the assumed temperatures and pressures make the production of large amounts of C_{60} unlikely but that it cannot be ruled out. They also suggest that C_{60} is most likely to be produced and therefore detected in emission at the beginning of an RCB star decline. If detected, C_{60} would be the long-sought-after spectroscopic signature of the RCB dust formation.

2. LABORATORY DATA CONCERNING C_{60}

The nucleation of carbon plasmas in the absence of other species such as hydrogen is interesting, because once atoms "stick" together to form clusters, they will start to form flat, graphitic networks consisting of six-membered rings. However, in such clusters, atoms present at the edges are not fully bonded. These are energetically unstable and can be reduced in number if the clusters incorporate five-membered rings into their networks. This leads to the formation of nonplanar networks which may close to form cages. These cages, called fullerenes, have been extensively studied in these experiments and have been isolated in macroscopic quantities (Krätschmer *et al.* 1990; Taylor *et al.* 1990). The mechanism that produces these fullerenes also produces fullerite dust— not crystalline graphite, but spheroidal material which appears to be made of spiraling layers of nonplanar carbon (Kroto & McKay 1988; Krätschmer & Huffman 1993).

The IR spectral bands of C_{60} have been measured in the laboratory at 7.5, 8.6, 17.5, and 19.0 μm (Frum *et al.* 1991; Nemes *et al.* 1994). Positions for two C_{60}^+ bands also have been measured (Fulara *et al.* 1993) at 7.1 and 7.5 μm. The position of the 8.6 μm line of C_{60} is expected to lie between 8.58 μm at 1000 K and 8.40 μm at 0 K (Nemes *et al.* 1994). The width of the possible C_{60} band is a combination of the rotational structure and the contributions of hot vibrational lines, and scales as the square root of the C_{60} gas temperature (Nemes *et al.* 1994). At 100 K, for example, it is expected to have a FWHM of about 0.04 μm. Or if the gas is much hotter (2000–4000 K), as is likely where the molecules are forming near an RCB star, bandwidths of 0.15–0.18 μm might be expected.

3. EXISTING OBSERVATIONS

Three RCB stars (R CrB, RY Sgr, and V854 Cen) and IRC+10216 were observed from 8–22 μm with the Low Resolution Spectrometer (LRS) on the Infrared Astronomical Satellite (*IRAS*) (Neugebauer *et al.* 1986). The published LRS spectra are averages of individual observations taken at "random" times during 1983. There are four spectra of R CrB and three each of RY Sgr, V854 Cen, and IRC+10216. We have extracted these individual LRS spectra. Table 1 gives the times of observation and *V* magnitude. We scaled the flux level of each individual spectrum to the Point Source

TABLE 1. LRS observations of RCB stars.

Star	IRAS	Time Tag [1]	JD(2400000+)	m_V
R CrB	15465+2818	820451171	45555.096	6.1
R CrB	15465+2818	831332186	45567.690	6.2
R CrB	15465+2818	848833137	45587.946	9.2
R CrB	15465+2818	852233876	45591.882	9.9
RY Sgr	19132-3336	716085102	45434.302	6.9
RY Sgr	19132-3336	722268340	45441.459	6.5
RY Sgr	19132-3336	880068194	45624.097	6.5
V854 Cen	14316-3920	821945275	45556.826	—
V854 Cen	14316-3920	831404944	45567.774	—
V854 Cen	14316-3920	846185343	45584.881	—
IRC +10216	09452+1330	744012786	45466.626	—
IRC +10216	09452+1330	752734021	45476.720	—
IRC +10216	09452+1330	902537806	45650.104	—

Note to TABLE 1

The time of observation of the individual PSC fluxes obtained from IPAC, measured in tenths of seconds from 1981 January 1.0 (*IRAS* Explanatory Supplement, p. X-15). The LRS usually references the time associated with the orbit- or day-confirmed observations. Hence the times associated with the LRS are usually later than those associated with the PSC observations by either ~103 minutes or ~12 h. The times listed are PSC time tags for R CrB, RY Sgr, and V854 Cen, and LRS time tags for IRC+10216.

Catalog (PSCII) 12 μm flux for each of the stars since the LRS spectra are not photometric. We have also corrected the spectra for the calibration problem associated with the short wavelength end of the spectrum (Volk & Cohen 1989).

Figure 1 shows the average LRS spectra for each of the four stars. The spectra have been averaged as described by Neugebauer *et al.* (1986). These spectra show blackbody continua due to dust emission plus some possible weak emission features. The dust around these stars will inevitably be a mixture of temperatures (e.g., Kelly & Latter 1995). However, a reasonable fit can generally be found to a single temperature in the mid-IR. A temperature can be derived by fitting a blackbody to the PSCII data from 12 to 100 μm. For the RCB stars, the typical dust temperatures are 650–900 K (Walker 1985). A blackbody fit to a single temperature has been made to each spectrum and then subtracted. The residual spectrum for each star is also plotted in Fig. 1. The best fits are R CrB (650 K), RY Sgr (800 K), V843 Cen (900 K), and IRC+10216 (450 K). Walker (1985, 1986) points out that the spectra are very smooth as would be expected from amorphous carbon dust. Small (10% of continuum) apparent features may be created due to uncertainties in the blackbody fit. However, some real emission features appear to be present. In particular, broad residual emission features appear to be present at 8.6 μm for all three RCB stars, and at 11.3 μm for V854 Cen, IRC+10216, and possibly RY Sgr. The LRS has very low resolution ($R=20-60$). Therefore, it samples the spectrum in the 8–9 μm region only every 0.17 μm, and the accuracy of measuring the peak wavelength of a

feature is of that order. The emission features were measured in the individual LRS spectra for each star and do not always show clearly in the average spectra plotted in Fig. 1.

Both RY Sgr and R CrB had declines in 1983. The LRS observations caught RY Sgr just coming out of a decline about half a magnitude below maximum light. The R CrB observations were fortuitously well timed to look for molecular emission related to dust formation. The first two spectra were obtained just before the decline began and the latter two were taken about three weeks later when the star was about three and four magnitudes below maximum light (see Table 1). Rao & Nandy (1986) mention that no significant variations in the broadband IR flux were seen in R CrB associated with its decline in 1983. This is typical of RCB declines (Feast 1979). There are no photometric observations for V854 Cen in 1983 although based on its behavior since 1985, there's a good chance it was in decline (Lawson *et al.* 1992).

We have analyzed the individual LRS spectra for the four stars. The LRS spectrum of R CrB at the beginning of its decline on JD 2445555 shows an emission feature at 8.6 μm, extending 15%–20% above a 650 K dust continuum. This feature is also seen by Buss *et al.* (1993) who measure a FWHM on the order of 1 μm. After JD 2445567, an emission excess shortward of 9 μm is seen, but a distinct emission feature is no longer visible. No other features can be identified unambiguously. On JD 2445555 and 2445567, a feature at 19 μm may be present at the 2σ level. No 17.5 μm feature is seen. If the 19 μm feature is real and due to C_{60} then the 17.5 μm feature must be less than half its intensity to remain undetected. All the LRS spectra of RY Sgr appear to indicate a very weak 11.3 μm emission feature, extending about 10% above an 800 K dust continuum. The first spectrum also appears to show a feature around 8.6 μm which becomes more difficult to distinguish in the latter two spectra since additional excess emission is present shortward of 9.5 μm. All V854 Cen spectra show the 11.3 μm feature at the 20%–30% level. An emission excess shortward of 9.5 μm is present, possibly showing an emission peak around 8.2 μm. It is possible that a weaker 8.6 μm feature is present within this excess emission. If the 8.6 μm feature is due to C_{60}, we should expect to see features at 17.5 and 19 μm. However, due to the lower S/N of all the spectra in this wavelength region, bands at the 15%–20% level cannot be identified in the LRS of the RCB stars. The three IRC+10216 spectra show no significant variations. They all show a steep rise in the emission shortward of about 8.6 μm, a broad 11.3 μm emission about 15% above the continuum and a depression at about 13.8 μm associated with C_2H_2+HCN (Little-Marenin *et al.* 1987). The 11.3 μm emission feature is atypical for carbon stars. The feature is double peaked at 11.1 and 11.7 μm with a FWHM of about 1 μm and looks similar to the "rectangular" feature identified by Cohen (1986) in the more heavily obscured carbon stars. This feature is usually associated with SiC and in most carbon stars has a maximum at 11.2 μm and a FWHM of 0.7 μm (Little-Marenin *et al.*
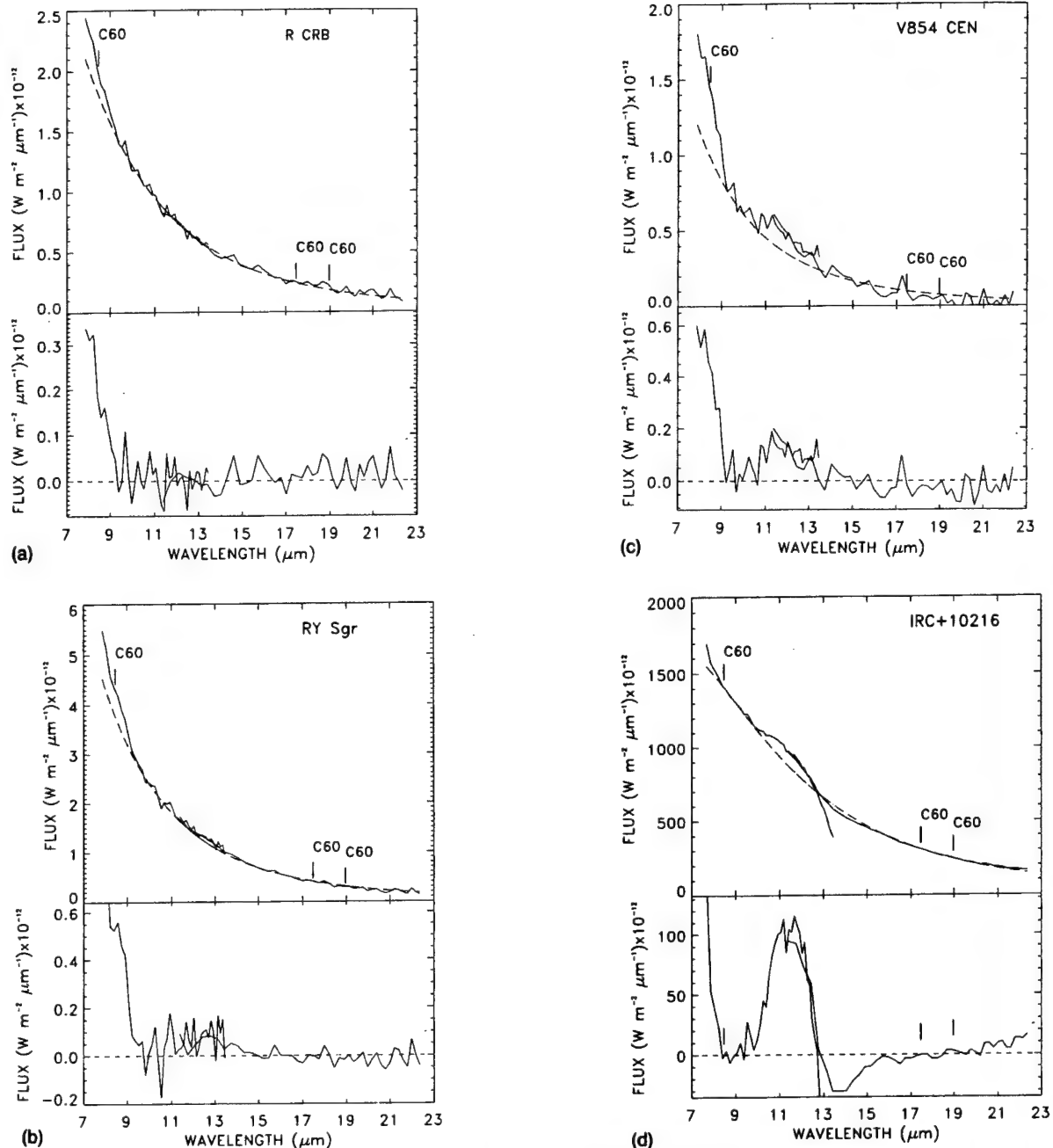
FIG. 1. Average LRS spectra (upper panel) and residual spectra (lower panel) after blackbody subtraction for (a) R CrB, (b) RY Sgr, (c) V854 Cen, and (d) IRC+10216 (see the text).

1987). It is possible that the feature in IRC+10216 is due to a combination of α and β SiC. The two forms of SiC have slightly different maxima and widths (Lorenz-Martins & Lefevre 1993; Blanco *et al.* 1994).

Another possible interpretation of the LRS spectra of RY Sgr and V854 Cen is that these stars show a 10 μm self-absorbed silicate feature. We argue against this interpretation since there is no evidence for a feature at 18 μm, either in emission or partly self-absorbed, as would be expected for silicate grains. Furthermore, for the 10 μm feature to be seen in absorption, we would have to assume a continuum temperature in this region in excess of 1000 K, which is too high to be applicable to a shell optically thick enough to produce self-absorbed features.

4. NEW OBSERVATIONS

The new observations were obtained with Irshell on the NASA Infrared Telescope Facility (IRTF) on Mauna Kea on 1994 June 2–3. Irshell is a mid-infrared (5–25 μm) spectrograph (Lacy *et al.* 1989). Irshell uses an 11×64 Si:As impurity band detector array to obtain 64 point spectra at 11 positions along the slit. The slit was 2″. We used Irshell with a low resolution ($R = 1000$) grating and a spectral coverage of about 3%. Telluric lines were used for wavelength calibration. For sources brighter than 10 Jy, Irshell is limited by systematic errors in correcting for instrumental and telluric features. We have found that we can reach a limiting sensitivity of 1% of the continuum by alternating between sources

and comparison stars, spending a total of two hours on each. The data were reduced using the SNOOPY program (Achtermann 1992). A dome-temperature blackbody, chopped against the sky, was used to flatfield, make atmospheric corrections, and calibrate intensity. Flux calibrations were made using β Her, τ Sgr, γ Leo, and σ Lib as comparison stars.

At the time of the observations, R CrB was at maximum light, RY Sgr was recovering from a decline at about 2 magnitudes below maximum, and V854 Cen was 4.4 magnitudes below maximum, also recovering from a decline. We observed R CrB, RY Sgr, V854 Cen, and IRC+10216 near 8.6 μm. The atmosphere has almost 100% transmission in this wavelength region, and numerous weak atmospheric lines are available for wavelength calibration. For R CrB, we repeated the observations with overlapping grating settings to be certain of the correction of systematic effects. The Irshell spectra are shown in Fig. 2. The grating setups used produced data between 8.3 and 8.8 μm. Three grating setups were used for R CrB and one each for RY Sgr, V854 Cen, and IRC+10216. The three observations of R CrB agree well within the errors, so they have been combined in Fig. 2. The spectra of R CrB and IRC+10216 approach the limiting sensitivity of 1% (1σ) but the spectra of RY Sgr and V854 Cen are noisier due to their shorter exposure times. The unsmoothed spectrum of V854 Cen, which had the least observing time, shows evidence of fringing in the detector which has not cancelled out perfectly. The spectra of the three RCB stars are very smooth and show no evidence for narrow (~ 0.2 μm) emission features at a level of a 2%. IRC+10216 does show a real structure including an apparent emission feature with a FWHM$\geqslant 0.2$ μm. The spectra plotted in Fig. 2 have been smoothed with a five point boxcar.

5. DISCUSSION

The IR emission features seen in carbon-rich objects are divided into two classes. Objects such as Planetary Nebulae and WC stars with large amounts of UV radiation tend to show the narrow (FWHM~ 0.2 μm) Polycyclic Aromatic Hydrocarbon (PAH) emission features at 3.3, 6.2, 7.7, 8.6, and 11.3 μm (Buss *et al.* 1993). Nonbinary carbon stars, on the other hand, tend to show broad (FWHM~ 1 μm) features at 8–9 μm and 11.3 μm (Buss *et al.* 1993). No PAH emission has been detected from a nonbinary carbon star (Jura 1993). The 11.3 μm feature is identified with SiC, or with carbonaceous microparticles with internal hydrogens (Balm & Kroto 1990). Buss *et al.* (1993) investigated the mid-IR (5–23 μm) emission features of a group of stars in transition from the Asymptotic Giant Branch to the Planetary Nebula stage. R CrB is included in this group. They find, in general, that the sources in this group show the narrow PAH emission features at 6.2, 7.7, and possibly 11.3 μm, as well as a very broad "plateau" at 6–9 μm. The 8.8 μm feature, seen in the transition objects, is broad like the feature seen in carbon stars and unlike the narrow PAH feature (Buss *et al.* 1993). Like the RCB stars, all the transition objects show emission features on top of a strong blackbody continuum due to dust. The emission features look quite different in R CrB than in the other transition objects (Buss *et al.* 1993). R CrB has a

feature at 6.3 μm rather than 6.2 μm plus emission from 7 to 9 μm that is unresolved. Unlike most of the other transition stars, there is no 3.3 μm feature in R CrB. The 3–3.5 μm spectrum is featureless (Nandy *et al.* 1986). The likely reason for the very different spectra seen in RCB stars is the near absence of hydrogen which will make molecules with hydrogen bonds rare or nonexistent (Whitney *et al.* 1993; Goebel *et al.* 1995). IRC+10216, like other carbon stars, shows no PAH emission at 3.3 μm (Witteborn *et al.* 1990).

There are LRS spectra for about 500 carbon stars. Most show the 11.3 μm SiC feature and many also show an emission feature between 8 and 9 μm (Little-Marenin & Clayton 1993). The relative strength of the 8–9 and 11.3 μm features varies strongly from star to star. In some carbon stars, the 8–9 μm feature is not present and in some it is stronger than the 11.3 μm feature. We have analyzed over 60 carbon stars with excess emission in the 8–9 μm region and find that a significant number (14) have a relatively strong feature that peaks around 8.6 μm (FWHM~ 1 μm). Most of the other carbon stars show emission features peaking at 9 μm or between 8.0 and 8.2 μm. However, many of these stars appear to have a contribution from a feature at 8.6 μm. The V854 Cen LRS spectra are similar to those of carbon stars, e.g., V781 Sgr (Little-Marenin & Clayton 1993). Perhaps the similarity of V854 Cen to the carbon stars is due to the fact that it has significantly more hydrogen than the other RCB stars. The strength of the 8.6 μm feature in carbon stars has been found to be slightly correlated to abundances determined by Lambert *et al.* (1986). Stars with larger C/O ratios (C/O>1.3) and greater $[(C+N+O)/H]$ deficiencies (< -0.70) tend to have stronger 8.6 μm features. The RCB stars satisfy the first criterion but not the second.

The LRS spectra of the RCB stars and possibly IRC+10216 show emission features close to the wavelength where at least one of the IR C_{60} bands is predicted to lie. The measured positions of the C_{60} bands are marked in Fig. 1. The low resolution of the LRS observations prevents positive identification of the emission features. All three RCB stars in our sample show strong 8.6 μm features. At the resolution of the LRS spectra it is not clear whether these broad (1 μm) features may be blends of narrower features. It seems unlikely that the 8.6 μm feature, seen in carbon stars and in our sample, is due to PAHs since the much stronger 7.7 μm feature appears to be absent. Also, the observed feature is much broader than the 8.6 μm PAH feature. One of the laboratory-measured C_{60} bands lies near 8.6 μm but these bands are also expected to be narrower. We have searched the LRS spectra for evidence of the 17.5 and 19.0 μm C_{60} bands but no unambiguous detection has been made. This is due in part to the low S/N typically present in this region of the LRS spectra. The 7.1 μm C_{60} line is at too short a wavelength to be detected by LRS.

Using Irshell, we searched the wavelength region 8.35 to 8.80 μm in R CrB, RY Sgr, V854 Cen and IRC+10216 covering the likely positions for this C_{60} feature. No broad or narrow features were found in the Irshell data at a level of 2% of the continuum in any of the three RCB stars. However, the carbon star, IRC+10216, did show a significant increase in flux from 8.5 to 8.7 μm. Although significant,
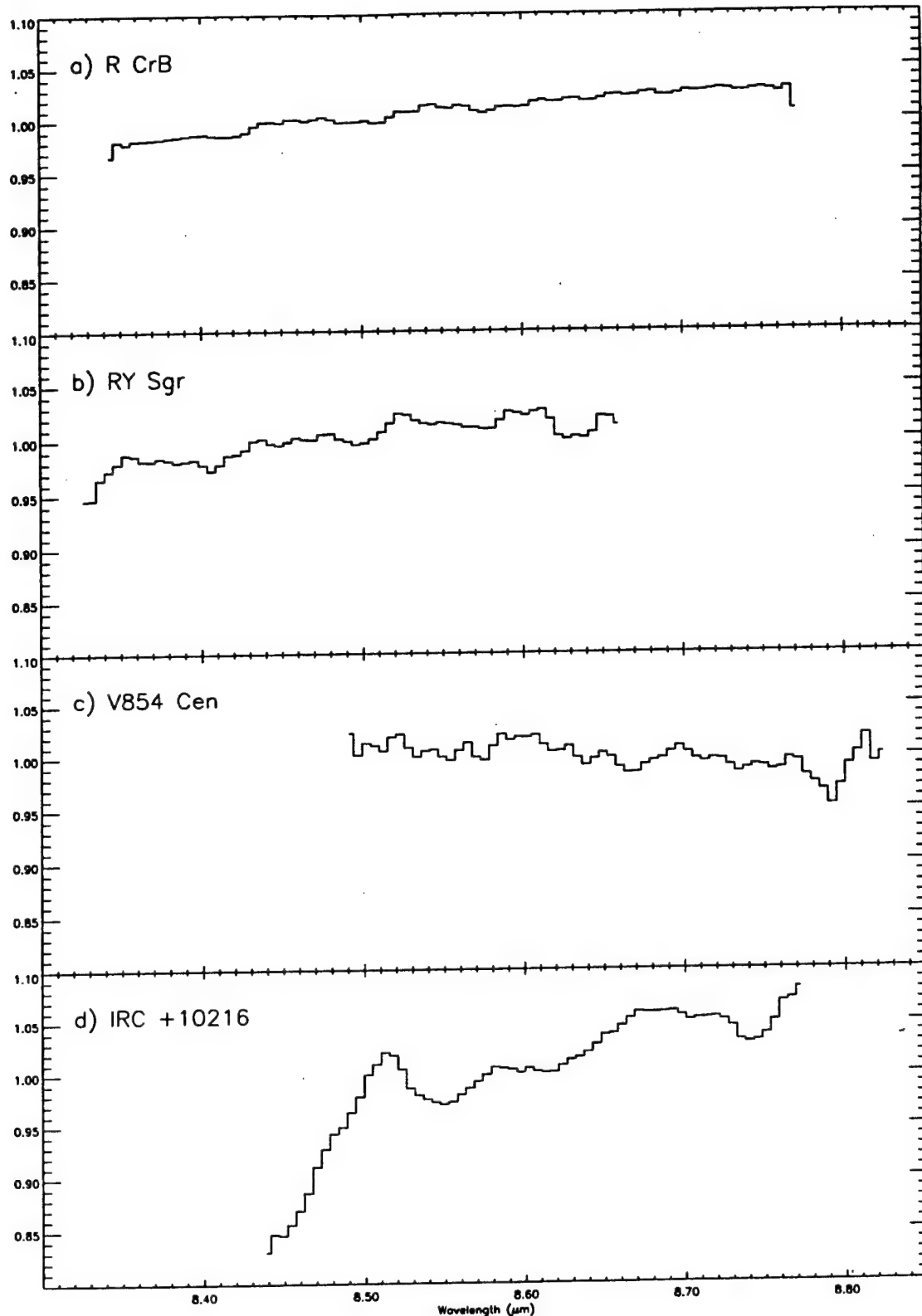
FIG. 2. Normalized Irshell spectra near 8.6 μm for (a) R CrB, (b) RY Sgr, (c) V854 Cen, and (d) IRC+10216.

this emission structure is too weak to have been identified with the LRS. Lacy *et al.* (1989) mapped out an 8.6 μm feature in the Red Rectangular with Irshell at similar resolution to our data. The Red Rectangular spectrum covers a larger wavelength range (8–9 μm) and shows a feature with a width of about 0.2 μm. The structure seen in Fig. 2 for

IRC+10216 is consistent with this feature. However, since the wavelength coverage of IRC+10216 with Irshell was less than 0.4 μm, the width and position of this possible feature are very uncertain. It is consistent with having a FWHM of $\geqslant$0.2 μm. The feature measured in the Red Rectangle is likely the PAH feature at 8.6 μm since, unlike IRC

46

+10216, its spectrum shows the other typical narrow PAH features.

The possible emission feature seen in Fig. 2 for IRC +10216 is also consistent with C_{60}. As a carbon star, IRC +10216 does not show any other narrow PAH feature, so the 8.6 μm PAH feature is not expected to be present. *However, unless another PAH or C_{60} feature in IRC+10216 is detected, a definitive identification is not possible.* The Irshell data for all four stars are only sensitive to narrow features such as those due to PAHs or C_{60} since none has wavelength coverage of more than 0.5 μm. The flat continua seen in the Irshell spectra of the RCB stars are probably part of the broad peak of the 1 μm wide 8.6 μm feature seen in the LRS spectra. The new much higher resolution Irshell data do not show any indication that this broad emission is a blend of narrow features.

We can make a rough estimate of the relative abundance of C_{60} to C_2. The swan bands of C_2 have been observed in emission in several RCB star declines, most recently in V854 Cen (Whitney *et al.* 1992). The integrated flux in the C_2 (0–0) 5165 Å band was measured to be 5.9×10^{-13} erg s^{-1} cm^{-2} when the star was in a deep decline at $\Delta V = 8.2$ mag. The gas is not likely to be in LTE since the time for collisional deexcitation is significantly larger than the radiative time (Goeres & Sedlmayr 1992). Therefore, a ratio of the C_{60} to C_2 abundances, assuming that every collisional excitation results in a radiative transition, is $\leqslant 0.03$. The numbers used in this estimate are very uncertain so this only places an order of magnitude upper limit on relative abundance of C_{60}.

The absence of detectable C_{60} emission around any of the RCB stars indicates that large amounts of C_{60} are not normally present around these stars. It has been suggested that Buckminsterfullerene in the interstellar medium is likely to be ionized and so may be present as C_{60}^+ (Kroto & Jura 1992). On the other hand, we might expect that C_{60} is only present for a short period of time around the beginning of a decline when carbon gas is condensing into dust (Goeres & Sedlmayr 1992; Whitney *et al.* 1993). There is weak evidence from the LRS spectra of R CrB that spectral variations in the 8.6 and 19 μm emission features took place around the time of the 1983 decline. RY Sgr and V854 Cen were both in decline when the Irshell data were obtained but there is no evidence that new dust was forming around these stars at that time. Also, without accurate photometry around the time of the observations we cannot determine whether the pulsation cycles of RY Sgr and V854 Cen were near the phase associated with dust formation. Since none of the RCB stars were in the early stages of a decline when these new observations were obtained, the possibility that C_{60} might be detected in the future in these stars has not been ruled out.

REFERENCES

Achtermann, J. M. 1992, in Astronomical Data Analysis Software, edited by D. M. Worrall, C. Biemesderfer, and J. Barnes, ASP Conf. Ser. 25, 451

Balm, S. P., & Kroto, H. W. 1990, MNRAS, 245, 193

Bell, M. B., Feldman, P. A., Kwok, S., & Matthews, H. E. 1982, Nature, 295, 389

Bernath, P. F., Hinkle, K. H., & Keady, J. J. 1989, Science, 244, 562

Blanco, A., Borghesi, A., Fonti, S., & Orofino, V. 1994, A&A, 283, 561

Buss, R. H., Tielens, A. G. G. M., Cohen, M., Werner, M. W., Bregman, J. D., & Witteborn, F. C. 1993, ApJ, 415, 250

Clayton, G. C. 1995, PASP, in preparation

Clayton, G. C., Whitney, B. A., Stanford, S. A., & Drilling, J. 1992, ApJ, 397, 652

Cohen, M. 1986, MNRAS, 206, 137

Danchi, W. C., Bester, M., Degiacomi, C. G., Greenhill, L. J., & Townes, C. H. 1994, AJ, 107, 1469

Feast, M. W. 1979, Changing Trends in Variable Star Research, IAU Colloquium No. 46, edited by F. M. Bateson, J. Smak, and I. M. Urch (University of Waikato, Hamilton), p. 246

Foing, B. H., & Ehrenfreund, P. 1994, Nature, 369, 296

Frum, C. I., Engleman, R., Jr., Hedderich, H. G., Bernath, P. F., Lamb, L. D., & Huffman, D. R. 1991, Chem. Phys. Lett. 176, 504

Fulara, J., Jakobi, M., & Maier, J. P. 1993, Chem. Phys. Lett., 211, 227

Goebel, J. H., Cheeseman, P., & Gerbault, F. 1995, ApJ (in press)

Goeres, A., & Sedlmayr E. 1992, ApJ, 265, 216

Hecht, J. H. 1991, ApJ, 367, 635

Jeffery, C. S. 1995, A&A (in press)

Jura, M. 1993, Philos. Trans. R. Soc. Lond. A, 343, 63

Kelly, D. M., & Latter, W. B. 1995, AJ, 109, 1320

Krätschmer, W., & Huffman, D. R. 1993, Phil. Trans. R. Soc. London, A, 343, 33

Krätschmer, W., Lamb, L. D., Fostiropoulos, K., & Huffman, D. R. 1990, Nature, 347, 354

Kroto, H. W., & Jura, M. 1992, A&A, 263, 275

Kroto, H. W., & McKay, K. 1988, Nature, 331, 328

Kroto, H. W., Heath, J. R., O'Brien, S. C., Curl, R. F., & Smalley, R. E. 1985, Nature, 318, 162

Lacy, J. H., Achtermann, J. M., Bruce, D. E., & Lester, D. F. 1989, PASP, 101, 1166

Lambert, D. L. 1986, in Hydrogen Deficient Stars and Related Objects, edited by K. Hunger (Reidel, Dordrecht), p. 217

Lambert, D. L., Gustafsson, B., Eriksson, K., & Hinkle, K. H. 1986, ApJS, 62, 373

Lawson, W. A., Cottrell, P. L., Gilmore, A. C., & Kilmartin, P. M. 1992, MNRAS, 256, 339

Little-Marenin, I. R. & Clayton, G. C. 1993, BAAS, 25, 743

Little-Marenin, I. R., Ramsay, M. E., Stephenson, C. B., Little, S. J., & Price, S. D. 1987, AJ, 93, 663

Lorenz-Martins, S., & Lefevre, J. 1993, A&A, 280, 567

Millar, T. J., & Herbst, E. 1994, A&A, 288, 561

Nandy, K., Rao, N. K., & Morgan, D. H. 1986, in Hydrogen Deficient Stars and Related Objects, edited by K. Hunger (Reidel, Dordrecht), p. 203

Nemes, L., Ram, R. S., Bernath, P. F., Tinker, F. A., Zumwalt, M. C., Lamb, L. D., & Huffman, D. R. 1994, Chem. Phys. Lett. 218, 295

Neugebauer, G., *et al.* 1986, A&AS, 65, 607

Pugach, A. F. 1977, Inf. Bull. Variable Stars, No. 1277

Rao, N. K., & Nandy, K. 1986, MNRAS, 222, 357

Rohlfing, E. A. 1988, J. Chem. Phys., 89, 6103

Snow, T. P., & Seab, C. G. 1989, A&A, 213, 291

Somerville, W. B., & Bellis, J. G. 1989, MNRAS, 240, 41P

Taylor, R., Hare, J. P., Abdul-Sada, A. K., & Kroto, H. W. 1990, J. Chem. Soc. Chem. Commun. 1423

Tielens, A. G. G. M. 1990, Carbon in the Galaxy: Studies from Earth & Space, edited by J. C. Tarter, S. Chang, and D. J. DeFrees (NASA Conf. Publ. 3061, Washington, DC), p. 59

Volk, K., & Cohen, M. 1989, AJ, 98, 1918

Walker, H. J. 1985, A&A, 152, 58

Walker, H. J. 1986, in Hydrogen Deficient Stars and Related Objects, edited by K. Hunger (Reidel, Dordrecht), p. 407

Webster, A. S. 1991, Nature, 352, 412

Webster, A. S. 1992, A&A, 257, 750

Webster, A. S. 1993, MNRAS, 264, L1

Whitney, B. A., Clayton, G. C., Schulte-Ladbeck, R., & Meade, M. R. 1992, AJ, 103, 1652

Whitney, B. A., Balm, S. P., & Clayton, G. C. 1993, Luminous High-Latitude Stars, ASP Conf. Ser. No. 45, edited by D. Sasselov, p. 115

Witteborn, F. C., Strecker, D. W., Erickson, E. F., Smith, S. M., Goebel, J. H., & Taylor, B. J. 1990, ApJ, 238, 577

ACCURATE WAVENUMBERS FOR MID-INFRARED FINE-STRUCTURE LINES

Douglas M. Kelly[1,2] and John H. Lacy[1]
Department of Astronomy, University of Texas, Austin, TX 78712

ABSTRACT

We present accurate new wavenumbers for a set of 13 mid-infrared fine-structure lines. The wavenumbers were determined from observations of the planetary nebula NGC 7027 and of the red supergiant α Scorpii. Most of the new wavenumbers are good to within 0.0025%, or 8 km s^{-1}. We provide details on the measurements and present an analysis of the errors. In addition, we present the first observations of hyperfine splitting in the [Na IV] 1106 cm^{-1} line.
Subject headings: atomic data — infrared: ISM: lines and bands — planetary nebulae: individual (NGC 7027)

1. INTRODUCTION

The strongest features in the mid-infrared spectra of gaseous nebulae are the fine-structure lines of [Ne II], [S III], [S IV], and [Ar III] and the series of unidentified polycyclic aromatic hydrocarbon (PAH) or carbon grain features. This set of atomic and solid state features has been the center of attention for most mid-infrared galaxy studies to date, and it represents the general limit of what can be detected in galaxies from the ground with 4 m class telescopes (e.g., Roche et al. 1991; Kelly et al. 1995). However, with the impending launch of the *Infrared Space Observatory* (*ISO*) and with the development of 8 m class, infrared-optimized telescopes, new opportunities are unfolding in the field of mid-infrared spectroscopy.

ISO will be capable of observing a large number of lines in bright galaxies, including many lines that have never been detected before except in novae. In most galaxies, however, the number of detectable lines will be relatively small, so obtaining complete spectral coverage would be inefficient. It is therefore essential to have accurate wavenumbers for the lines of interest. In the course of this study, we have found that predicted wavenumbers can be in error by as much as several tenths of a percent. Thus, in support of the *ISO* mission and of our own ground-based programs, we have undertaken a project to determine accurate new wavenumbers for fine-structure lines in the mid-infrared.

Our target for most of these observations has been the hot, young planetary nebula NGC 7027. This planetary nebula is unusual in that the central star has a temperature of roughly 2×10^5 K (Kaler & Jacoby 1989), but it is still surrounded by a neutral, molecular cloud (see Graham et al. 1993). The kinematics and morphologies of the various ions in NGC 7027 could be quite different from each other, and the extended, complicated nature of NGC 7027 is the major source of our wavenumber uncertainties.

2. OBSERVATIONS

We measured a variety of fine-structure lines in the mid-infrared spectrum of NGC 7027 during observing runs at the NASA Infrared Telescope Facility (IRTF) in 1992 August,

1993 June, and 1994 October. The observations were made using Irshell, a mid-infrared grating spectrometer (Lacy et al. 1989; Achtermann 1994). Irshell has an 11×64 pixel Si : As array, with 11 rows in the spatial direction and 64 columns in the spectral direction. We used a low-dispersion grating in 1992 August to measure the entire 8–13 μm spectrum of NGC 7027 at a resolution of $\lambda/\Delta\lambda \approx 1000$. We switched to an echelle grating to measure individual lines during the 1993 June and 1994 October runs. The dispersion of the echelle observations ranged from 16,000 to 25,000 (depending on the grating angle), and, with a 2 pixel slit width (2″ on the 3 m IRTF), the resulting resolution ranged from 8000 to 12,500. A dome-temperature card, chopped against the sky, was used for flat-fielding, atmospheric correction, and fluxing (Lacy et al. 1989). For the 1994 October run, we installed a test-grade Hughes 20×64 pixel Si : As array. The 20×64 array has slightly smaller pixels, and the 1994 October data were measured through a 2 pixel (1″6) wide slit at a resolution of 9500–15,000. We used the bright star μ Cephei (spectral type M2 Ia; Hoffleit & Jaschek 1982) for flat-fielding, atmospheric correction, and fluxing of our 1994 October data.

The ideal approach to this project would be to make spectral maps of each of the lines, and we made such a map for the [S III] line in 1993 June (see Fig. 1). With these data cubes, we could register the spatial and spectral positions of the line emission, which would give us the best chance at determining the rest-frame wavenumber of the emission. As a bonus, we would also get line intensities and kinematic information. However, since time was limited, we had to make a number of compromises. First, we observed at only one slit position for each line. Since we did not cover the entire source, our information on line strengths was limited to one-dimensional line intensity profiles. Second, we did not have the time to be precise in our pointing. Our usual practice was to move our north-south slit back and forth a few arcseconds east-west across the western emission lobe until we found the maximum signal. Our pointing varied because of guiding and tracking errors and because the morphologies of the various ions are not identical. Third, we rarely measured calibration star spectra. The card calibration is adequate in most cases, but a star spectrum is helpful for removing strong telluric features. Fourth, we speeded up our observations by opening the slit to 2″ even though we could have improved our resolution by using a slightly narrower slit. Fifth, we did not make long observations. We spent 2–5 minutes on each of the strong lines
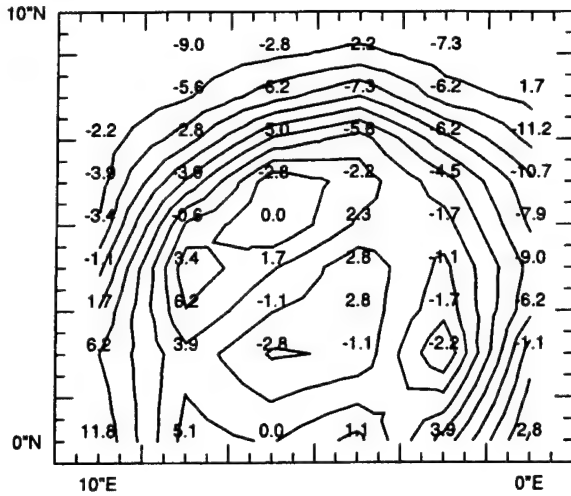

FIG. 1.—Intensity map for the continuum-subtracted [S III] emission in NGC 7027. The contour interval is 0.172 ergs s^{-1} cm^{-2} (cm^{-1})$^{-1}$ sr^{-1}. The two contour lines in the center of the nebula denote a low-flux region. North is roughly 6° west of vertical in this plot. Velocities are indicated for each of the points. The velocity uncertainties are 4 km s^{-1}.

TABLE 2

NONDETECTION SUMMARY

Target Line	Wavenumber Coverage (cm^{-1})	Nondetections
[Fe II]	406.25–408.60	⋯
[Ne v]	410.75–413.30	[Ca vi] 411.5[a]
[S iii]	533.8–535.1	⋯
[Fe ii]	556.75–558.50	⋯
[Mg v]	735.22–741.1	[Fe iii] 739.1
[F v]	742.75–746.99	[F v] 746.3
[Ar v]	759.66–767.12	[S v] 767.5[a]
[Ne ii]	778.9–781.6	⋯
[S iii]	831.70–835.18	[S iii] 832.5[b]
[Cl iv]	848.93–853.94	[Cl iv] 849.6
[Al vi]	1095.25–1099.78	[Al vi] 1097.0
[Na iv] + [Mg vii] + [Ar iii]	1104.7–1113.0	⋯
[K vi]	1129.9–1133.4	⋯
[Na vi]	1159.33–1165.20	[Na vi] 1161.4, [Mg ix] 1162.3,[a] [Cl vi] 1165.4[a]
[Ar v]	1263.4–1266.0 1268.07–1270.81	⋯ ⋯

[a] Line is from an excited term and so is expected to be very weak.
[b] Electric quadrupole transition is expected to be very weak.

and no more than 15 minutes on the fainter lines. In § 3, we discuss the effects of these compromises on the accuracy of our wavenumbers.

The most important results from this Letter are the vacuum rest wavenumbers of the lines. These values are presented in Table 1, along with estimated 1 σ uncertainties (see § 3) and relative intensities. Of particular note are the three hyperfine components of [Na iv] at 1106 cm^{-1} (see § 6). The reasonable agreement between the observational wavenumbers and the wavenumbers predicted by Kaufman & Sugar (1986) and Wiese, Smith, & Glennon (1966) gives us confidence in our line identifications. We present a summary of our wavenumber coverage and nondetections in Table 2. Spectra for the lines detected in NGC 7027 are presented in Figure 2. The spectra are usually set to zero in regions of very poor atmospheric transmission (<15%). All data were reduced using the Snoopy data reduction program (Achtermann 1994).

3. UNCERTAINTIES IN WAVENUMBER MEASUREMENTS

The main sources of error in our wavenumber measurements are summarized below. These contributions were summed in quadrature to determine the uncertainties listed with the wavenumbers in Table 1. For convenience, we quote errors in km s^{-1}, i.e., as fractions of the wavenumber.

1. The wavenumber calibration and, when possible, the dispersion of the mid-infrared spectra were determined from the atmospheric lines. We determined the centroids of the atmospheric features from our off-position nod frames, and we were able to determine the centroids to within 0.5–2 km s^{-1}. The errors introduced by our dispersion solution were always less than 1 km s^{-1}.

2. We obtained wavenumbers for the atmospheric lines from the AFGL line list (McClatchey et al. 1973), and the wavenumbers are good to well under 1 km s^{-1}. However, the atmospheric lines are often blended, and their relative

TABLE 1

FINE-STRUCTURE LINE MEASUREMENTS

Ion	Transition	Observation Date	Wavenumber (cm^{-1})	Peak Intensity[a] (ergs s^{-1} cm^{-2} sr^{-1})	χ_{lower} (eV)	χ_{upper} (eV)
[Fe ii]	$a^4F_{5/2}-a^4F_{7/2}$	1993 Jun 6–8	407.84 ± 0.02	⋯	7.87	16.18
[Ne v]	$^3P_0-^3P_1$	1993 Jun 6	411.256 ± 0.006	1.3 (−11)	97.11	126.21
[S iii]	$^3P_1-^3P_2$	1993 June 4	534.387 ± 0.005	2.6 (−12)	23.33	34.83
[Fe ii]	$a^4F_{7/2}-a^4F_{9/2}$	1993 Jun 6–8	557.50 ± 0.02	⋯	7.87	16.18
[Mg v]	$^3P_1-^3P_0$	1993 Jun 9	739.581 ± 0.012	1.5 (−12)	109.24	141.27
[Ar v]	$^3P_0-^3P_1$	1992 Aug 20	763.23 ± 0.05	1.3 (−12)	59.81	75.02
[Ne ii]	$^2P_{3/2}-^2P_{1/2}$	1993 Jun 4	780.4238 ± 0.001[b]	2.5 (−12)	21.56	40.96
[Na iv]	$^3P_{2(F=7/2)}-^3P_1$	1993 Jun 10	1105.88 ± 0.02	3 (−13)	71.64	98.91
	$^3P_{2(F=5/2)}-^3P_1$	1993 Jun 10	1106.12 ± 0.02	2 (−13)	71.64	98.91
	$^3P_{2(F=3/2)}-^3P_1$	1993 Jun 10	1106.30 ± 0.03	1 (−13)	71.64	98.91
	$^3P_{2(F=1/2)}-^3P_1$	1993 Jun 10	⋯	⋯	71.64	98.91
[Mg vii]	$^3P_0-^3P_1$	1993 Jun 10	1110.00 ± 0.05	8 (−14)	186.51	224.95
[Ar iii]	$^3P_2-^3P_1$	1993 Jun 10	1112.176 ± 0.015	5.1 (−12)	27.63	40.74
[K vi]	$^3P_0-^3P_1$	1993 Jun 10	1132.52 ± 0.03	1.0 (−13)	82.66	99.89
[Ar v]	$^3P_1-^3P_2$	1994 Oct 24	1265.57 ± 0.04	1.9 (−12)	59.81	75.02

[a] Not corrected for extinction; uncertainties can be large (see § 5).
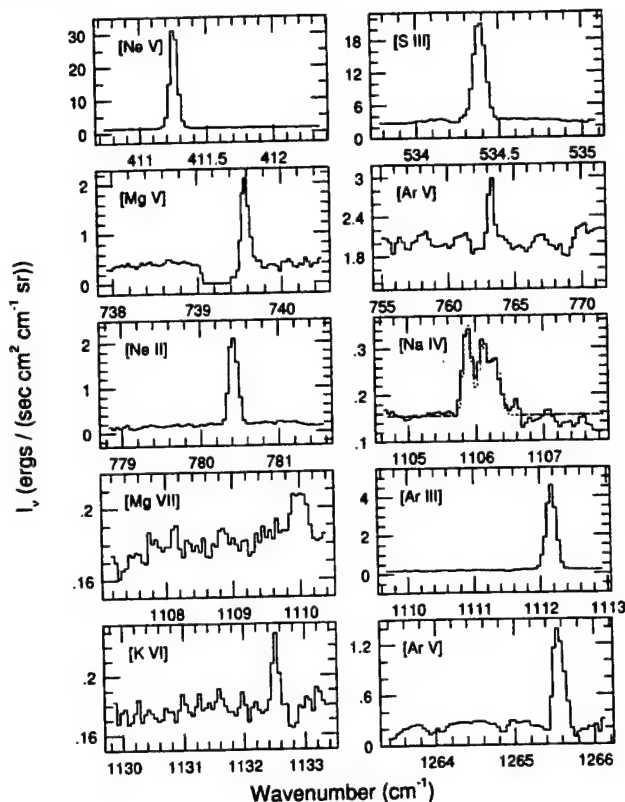[b] Wavenumber determined from laboratory measurements by Yamada et al. 1985.

FIG. 2.—Dereddened spectra for the 12 emission lines detected in NGC 7027. Wavenumbers are presented in Table 1, and uncertainties are discussed in § 3. The dotted line in the [Na IV] plot denotes our model fit for the hyperfine splitting. The [Na IV] energy splittings were determined by scaling from the hyperfine measurements of [^{17}O I] by Harvey (1965) and from the fine-structure splittings of [O I] and [Na IV]. Relative line intensities were calculated using the formulae of Townes & Schawlow (1955). The spectrum has been convolved to have the same resolution as the [Na IV] data.

strengths depend on atmospheric conditions, so there is some uncertainty in the effective wavenumbers determined from atmospheric models. When we had to calibrate our wavenumber scale from a blend of atmospheric features, our uncertainties ranged up to 4 km s^{-1}.

3. Photon noise led to scatter in the measured wavenumbers of the individual emission lines. It is almost impossible to determine the magnitude of this effect because of the velocity structure of NGC 7027, but we estimate that the errors are negligible for the strong lines and up to 4 km s^{-1} for the weaker lines. Since most line measurements involve the averaging of detections at several positions along the slit, the photon noise is reduced and is expected to contribute no more than 2 km s^{-1} to the wavenumber uncertainties.

4. The lines in NGC 7027 do not have simple line profiles. There is often emission at more than one velocity from a given position in the nebula. We had limited success at deconvolving the line profiles, so we instead determined centroids for the lines. We were able to measure line centroids that were accurate to 0.5–1 km s^{-1}. In some cases, bad flat-fielding could altered the line profiles. In these cases our line centroids could be off by as much as 5 km s^{-1}. The trio of lines at 1106 cm^{-1} was severely blended, leading to 3–6 km s^{-1} of uncertainty in the line positions.

5. We hinge our velocity reference frame on the [S III] line. The 3 km s^{-1} uncertainty in the [S III] wavenumber is propa-

gated into the error estimate for all of the other lines. The previous best measurements of the [S III] wavenumber were by Baluteau et al. (1976), who found a wavenumber of 534.39 ± 0.01 cm^{-1} based on measurements of the Orion Nebula, and by Greenberg, Dyal, & Geballe (1977), who found a wavenumber of 534.41 ± 0.03 cm^{-1} from observations of three planetary nebulae, including NGC 7027. We used three methods to estimate the [S III] wavenumber. First, by measuring the mean wavenumber over the [S III] map and correcting for the heliocentric velocity of 8.8 ± 0.6 km s^{-1} given by Schneider et al. (1983), we determine an average wavenumber of 534.388 ± 0.004 cm^{-1}. Second, by comparing the intensity and velocity profiles of the [S III] and [Ne II] emission, we find the best match if the [S III] wavenumber is 534.388 ± 0.005 cm^{-1}. The rest wavenumber for [Ne II] was measured in the laboratory by Yamada, Kanamori, & Hirota (1985) and is 780.424 ± 0.001 cm^{-1}. Third, by comparing the velocities of the bright ridges in our [S III] map to those in the H76α velocity map by Roelfsema et al. (1991), we determine a wavenumber of 534.387 ± 0.005 cm^{-1}. These three values combine to form our new [S III] wavenumber estimate of 534.387 ± 0.005 cm^{-1}. The two [S III] slit positions that pass through the center of the nebula have flux-weighted average velocity shifts of roughly −1 km s^{-1} relative to the nebular mean.

6. Telescope tracking errors and pointing uncertainties could have a strong influence on our line profiles and measured wavenumbers. We see velocity gradients of as large as 6 km s^{-1} arcsec^{-1} along the slit, with a total shift of 15–20 km s^{-1} in the line centroids from one end of the slit to the other. In the east-west direction, we see a shift of over 10 km s^{-1} to the red in the flux-weighted mean wavenumber along the slit as the slit is moved from west to east across the nebula, with most of the shift taking place in the faint outskirts of the nebula. We determined our north-south and east-west positions for each line by comparing the intensity and velocity profiles along the slit to the [S III] intensity and velocity map presented in Figure 1. These comparisons allowed us to determine the slit positions to within 2″, which allowed us to remove the velocity offsets relative to the [S III] frame with 2 km s^{-1} uncertainty. On the basis of these comparisons, we estimate that the velocity uncertainties due to internal motions in NGC 7027 are 2–4 km s^{-1}. In cases in which there was not enough flux to determine the profile of the line emission along the slit, we estimate our uncertainties to be 4–6 km s^{-1}.

4. [Fe II] MEASUREMENTS IN ALPHA SCORPII

We observed two [Fe II] lines in the mid-infrared spectrum of the red supergiant α Scorpii. These observations will be discussed by Haas, Werner, & Becklin (1996). The wavenumbers were reduced to the rest frame using the heliocentric velocity of −5.0 ± 0.6 km s^{-1} determined by Brooke, Lambert, & Barnes (1974) for low-excitation metals in the spectrum of α Scorpii. The wavenumber uncertainties are dominated by uncertainties in the effective wavenumbers of blended atmospheric lines. The [Fe II] wavenumbers are listed in Table 1.

5. LINE INTENSITIES

Our slit measurements provide us with intensity measurements for the mid-infrared lines in NGC 7027. As can be seen from the [S III] map in Figure 1, the brightest emission for the low-ionization lines comes from the bright ridges to either side

of the nebula center (see also Aitken & Roche 1983). Our slit profiles for the higher ionization lines are consistent with their having similar spatial distributions. Since most of our line measurements were made with our north-south slit crossing one or both lobes, we have reasonable estimates for the peak intensities of the lines. These peak intensities are listed in Table 1. It should be emphasized that these intensities do not all refer to identical spatial positions, and there is a factor of 2 variation in the continuum levels for the various lines. No corrections have been made for extinction. These intensities are provided only as a general guideline to the strengths of mid-infrared lines in photoionized gas. Line ratios using these numbers could easily be off by a factor of 2.

6. HYPERFINE SPLITTING OF THE [Na IV] LINE

Since the dominant isotope of sodium, ^{23}Na, has nuclear spin, we suspect that the group of lines at 1106 cm^{-1} are the hyperfine components of the [Na IV] $^3P_2$–$^3P_1$ transition, which is predicted to lie near this wavenumber. To test this hypothesis, we calculated the expected hyperfine splitting and relative line intensities. The hyperfine energy splittings are due mainly to the interaction between the magnetic dipole moment of the nucleus and the magnetic field at the nucleus due to the orbital and spin motion of the electrons. There is a secondary contribution due to the interaction between the quadrupole electric field of the nucleus and the electrons. Hyperfine splitting has not previously been observed in [^{23}Na IV] but was observed by Harvey (1965) in the isoelectronic atom [^{17}O I]. To calculate the [Na IV] hyperfine splittings, we used the fact that both fine-structure and hyperfine structure splittings are proportional to $\langle r^{-3} \rangle$ to scale from the hyperfine splitting mea-

surements of [^{17}O I] and the fine-structure splittings of [O I] and [Na IV], taking into account the differing nuclear magnetic dipole and electric quadrupole moments and the fact that the fine-structure splittings are also proportional to Z_i. We calculated the expected line intensities using the formulae presented in Townes & Schawlow (1955). There are eight hyperfine components in four closely spaced groups, from the four hyperfine sublevels of the $J = 2$ fine-structure level. Of these, the two highest wavenumber groups are blended at our resolution, leaving three resolved lines. The resulting spectrum (shown as a dotted curve in the [Na IV] spectrum of Fig. 2) agrees remarkably well with the data, confirming our identification of this multiplet of lines.

We note that ^{25}Mg, ^{39}K, and ^{41}K also have nuclear spin, but the observed $^3P_0$–$^3P_1$ transitions should have unresolvably small hyperfine splittings. However, the hyperfine splitting of the strong $^3P_2$–$^3P_1$ (5.6 μm) line of [^{25}Mg V] should be resolvable, allowing a determination of the ^{25}Mg/^{24}Mg abundance ratio. Several isotopic K and Cl fine-structure lines may also have resolvable hyperfine structure.

REFERENCES

Achtermann, J. M. 1994, PASP, 106, 173
Aitken, D. K., & Roche, P. F. 1983, MNRAS, 202, 1233
Baluteau, J. P., Bussoletti, E., Anderegg, M., Moorwood, A. F. M., & Coron, N. 1976, ApJ, 210, L45
Brooke, A. L., Lambert, D. L., & Barnes, T. G. 1974, PASP, 86, 419
Graham, J. R., Serabyn, E., Herbst, T. M., Matthews, K., Neugebauer, G., Soifer, B. T., Wilson, T. D., & Beckwith, S. 1993, AJ, 105, 250
Greenberg, L. T., Dyal, P., & Geballe, T. R. 1977, ApJ, 213, L71
Haas, M. R., Werner, M. W., & Becklin, E. E. 1996, in preparation
Harvey, J. S. M. 1965, Proc. R. Soc. London A, 285, 581
Hoffleit, D., & Jaschek, C. 1982, Bright Star Catalogue (4th rev. ed.; New Haven: Yale Univ. Obs.)
Kaler, J. B., & Jacoby, G. H. 1989, ApJ, 345, 871
Kaufman, V., & Sugar, J. 1986, J. Phys. Chem. Ref. Data, 15, 321
Kelly, D. M., van der Hulst, J. M., Lacy, J. H., & Achtermann, J. M. 1995, in preparation
Lacy, J. H., Achtermann, J. M., Bruce, D. E., Lester, D. F., Arens, J. F., Peck, M. C., & Gaalema, S. D. 1989, PASP, 101, 1166

McClatchey, R. A., Benedict, W. S., Clough, S. A., Burch, D. E., Calfee, R. F., Fox, K., Rothman, L. S., & Garing, J. S. 1973, AFCRL Atmospheric Absorption Line Parameters Compilation (AFCRL-TR-73-0096) (Bedford, MA: AFCRL)
Roche, P. F., Aitken, D. K., Smith, C. H., & Ward, M. J. 1991, MNRAS, 248, 606
Roelfsema, P. R., Goss, W. M., Pottasch, S. R., & Zijlstra, A. 1991, A&A, 251, 611
Schneider, S. E., Terzian, Y., Purgathofer, A., & Perinotto, M. 1983, ApJS, 52, 399
Townes, C. H., & Schawlow, A. L. 1955, Microwave Spectroscopy (New York: McGraw-Hill)
Wiese, W. L., Smith, M. W., & Glennon, B. M. 1966, Atomic Transition Probabilities (Washington: NBS)
Yamada, C., Kanamori, H., & Hirota, E. 1985, J. Chem. Phys., 83, 552

THE CENTRAL STAR CLUSTER OF THE STAR-FORMING DWARF GALAXY NGC 5253

S. C. BECK

School of Physics and Astronomy of the Sackler Faculty of Exact Sciences and Wise Observatory,[1]
Tel Aviv University, 69978 Ramat Aviv, Israel

J. L. TURNER

Department of Physics and Astronomy, UCLA, Los Angeles, CA 90095-1562

P. T. P. HO

Harvard-Smithsonian Center for Astrophysics, Cambridge, MA 02138

AND

J. H. LACY AND D. M. KELLY

Astronomy Department, University of Texas, Austin, TX 78712
Received 1995 March 27; accepted 1995 July 6

ABSTRACT

We have observed the star-forming dwarf galaxy NGC 5253 at optical, radio, and infrared wavelengths. Our data, combined with other observations from the literature, indicate that star formation in this galaxy has proceeded from the outer parts inward and that the center of NGC 5253 is now the site of an obscured, concentrated, and extremely young burst of star formation. The centimeter-wavelength radio continuum spectrum is very flat, which indicates that the radio emission is almost entirely due to thermal emission from H II regions. There is no evidence for synchrotron emission from supernova remnants, which is most unusual for a starburst galaxy. The observed radio continuum flux is consistent with infrared recombination-line observations, with $N_{Lyc} \sim 3 \times 10^{52}$ s^{-1}. The infrared spectrum resembles II Zw 40 and no other star-forming galaxy in that it has strong [S IV] 10.5 μm emission. We analyze the infrared spectrum with a grid of model H II regions and conclude that the young star cluster is dominated by stars of 42,000–45,000 K. The star cluster is probably a few Myr, and in any case less than 10 Myr, old, and the stellar density in the starburst is 0.5–1 O stars pc^{-3}.

Subject headings: galaxies: individual (NGC 5253) — galaxies: starburst — galaxies: star clusters — H II regions — radio continuum: galaxies — stars: formation

1. INTRODUCTION

NGC 5253 is a dwarf galaxy with an elliptical underlying structure but with bright, amorphous H II regions in the core, extensive ionized filaments, and over 100 young star clusters in the halo (Van den Bergh 1980; Caldwell & Phillips 1989). It is known to be a site of active star formation, and the starburst typically is estimated to be no older than 10 Myr. Its optical and ultraviolet spectra show the presence of hot young stars, including Wolf-Rayet stars (Walsh & Roy 1987, 1989), and it has strong Brγ emission and weak CO band-head absorption, which lead Rieke, Lebofsky, & Walker (1988) to call it the youngest starburst known. NGC 5253 is only 114′ (93 kpc at 2.8 Mpc) from the large barred spiral M83, which is also undergoing a starburst, and it has been suggested that tidal interaction of the two systems has triggered their activity, although there is no direct evidence for such interaction (Rogstad, Lockhart, & Wright 1974).

The star-formation process in NGC 5253 is clearly unusual and extreme. We set out to study how star formation manifests itself at long wavelengths in this galaxy. Starbursts in large–spiral-galaxy nuclei have been well studied in the infrared, millimeter, and radio regions, and their observational signatures are more or less understood; the long-wavelength appearance of starbursts in dwarfs is much less well known. Since the interstellar medium, dust content, and metal content

of dwarf galaxies may differ strongly from spirals, their behavior may be quite different. We have therefore obtained VLA radio continuum data at 2 cm and high-resolution spectra of several lines in the 8–13 μm region, which we combine with published data and a new grid of H II–region models to analyze the present stellar population of the burst and predict its future development. We have also obtained lower frequency VLA continuum data and 3 mm continuum and CO molecular-line data, which will be published separately (Turner, Ho, & Beck 1995b; Turner, Beck, & Hurt 1995a).

2. OBSERVATIONS

Hα images of NGC 5253 were obtained at the 1 m telescope of the Wise Observatory in Mitzpe Ramon, with the use of a 50 Å–wide filter centered at the rest frequency (the heliocentric velocity of NGC 5253 is 360 km s^{-1}) and a 512 × 512 CCD with spatial resolution of 0″.8 pixel^{-1}. An Hα image with the R-band continuum emission removed is shown in Figure 1. Astrometry was done on the full image using the Hubble Guide Star Catalog: absolute positions on the Hα image are accurate to ~1″–2″. The image resembles the Hα contour map in Walsh & Roy (1989) in having a concentrated peak and a weak extension to the south, which Caldwell & Phillips (1989) call the Hα "fork." The bright H II region in the center coincides with the compact infrared and radio emission; we will refer to it as the nucleus since "nucleus" in a star-forming dwarf is not very well defined. There is diffuse Hα emission over at least 40″ that is much weaker than the peak.
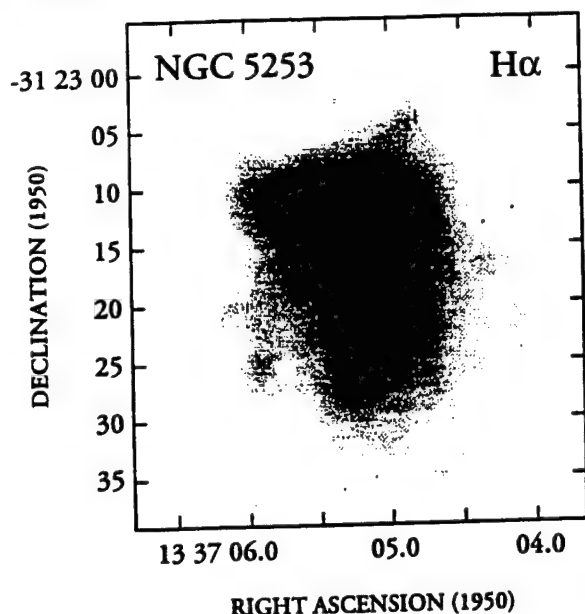
FIG. 1.—Central region of NGC 5253, in continuum-free Hα emission. Absolute positions are accurate to 1″–2″.

High-resolution radio continuum maps were made at the Very Large Array.[2] The 2 cm observations were made 1992 February 11 with the array in BC configuration. The 2 cm absolute flux is accurate to better than 5%, and the absolute positional accuracy is 0″.05. The synthesized beam size is 1″.9 × 1″.5, FWHM, p.a. 32°. The 2 cm map is shown in Figure 2 (left) and is also shown overlaid on the Hα gray-scale image (right). The registration accuracy of the latter is limited by the uncertainty in the astrometry of the Hα image, which is ~1″–2″. The radio results, along with those at longer wavelengths from the literature, are shown in Table 1.

Published infrared data on NGC 5253 include IRAS fluxes, a spectrum by the Low Resolution Spectrometer on IRAS, which did not see any clear features, near-infrared photometry by Moorwood & Glass (1982), measurements of the 2.17 and 4.05 μm Brγ and Brα lines by Kawara, Nishida, & Phillips (1989), searches for H_2 emission by Mouri et al. (1989), and a moderate-resolution 8–13 μm spectrum by Aitken et al. (1982). We obtained a spectrum with high spatial (1″.6) and spectral (30 km s^{-1}) resolution of lines in the 8–13 μm region by use of a cryogenic spectrometer, Irshell (Lacy et al. 1989), on the 3.6 m ESO telescope at La Silla, Chile. Wavelength regions equivalent to 900 km s^{-1} in velocity centered on each of the [Ne II] 12.8 μm, [Ar III] 8.99 μm, and [S IV] 10.5 μm lines were measured. The [S IV] line was observed in three positions separated by 1″.6 north-south and the [Ar III] in three positions separated by 1″ north-south. Fluxes and limits for spectral features in the infrared are shown in Table 1. A typical measurement of the [S IV] line is displayed in Figure 3.

3. RESULTS AND DISCUSSION

3.1. Spatial Structure; Extinction

The different long-wavelength measurements result in slightly different sizes for the central source, but all indicate that it is

TABLE 1

NGC 5253

Right Ascension (2 cm peak) 13^{h}37^{m}5^s.124
Declination (2 cm peak) −31°23′13″.23
Distance 2.8 Mpc

Feature	θ_s	Flux	Reference
$S_{21\,cm}$	<1′	90 ± 40 mJy	1
$S_{20\,cm}$	20″ × 40″	55 mJy[a]	2
$S_{6\,cm}$	<2″.5	64 ± 10 mJy	3
$S_{6\,cm}$	20″ × 40″	49 mJy[a]	2
$S_{2\,cm}$	6″	35 ± 3 mJy	4
$S_{2\,cm}$	20″ × 40″	54 mJy[a]	4
[Ne II] 12.8 μm	1″.6	<10^{-13} ergs s^{-1} cm^{-2}	4
[S IV] 10.5 μm	1″.6	3.9 × 10^{-12} ergs s^{-1} cm^{-2}	4
[Ar III] 8.99 μm	1″.6	3.6 × 10^{-13} ergs s^{-1} cm^{-2}	4

[a] Fluxes measured from interferometer maps: there may be unresolved flux for size scales larger than 15″–20″ for the 6 and 2 cm maps, and larger than 45″–60″ for the 20 cm map. See text.

REFERENCES.—(1) Lequeux 1971; (2) Turner et al. 1995b; (3) Whiteoak 1970; (4) this paper.

very small—less than 6″ in the 10 μm continuum (Telesco, Dressel, & Wolstencroft 1993). It is not pointlike: the central radio source, which contains nearly half the flux of the central 30″ region, can be fit by a Gaussian of peak intensity S = 23 mJy beam^{-1} and size 0″.8–0″.9, FWHM. The position of the radio peak is α = 13^{h}37^{m}05^s.124, δ = −31°23′13″.23. This central source is surrounded by bright emission that covers ~6″ in diameter, or 80–90 pc. The [S IV] emission extends over 2″–4″, which is significantly larger than the point-spread function. For the adopted distance to NGC 5253, the characteristic size of the infrared source is less than 100 pc, which is a factor of ~5 smaller than the area over which optical emission lines are seen. However, although it is compact, the source is very unlikely to be a Seyfert or other active galactic nucleus (AGN) because of the low velocity width of the [S IV] line (displayed in Fig. 3). It is almost certainly a cluster of very young stars. We discuss in the following sections the stellar contents of this cluster, its age, and how it fits into the overall processes of star formation and evolution in NGC 5253.

Figure 2 (right) shows the relative locations of the 2 cm emission and Hα emission in the starburst. Because the 2 cm emission is nearly all thermal bremsstrahlung emisson (§ 3.2), the 2 cm emission and the Hα emission both trace ionized gas. However, the morphologies of these tracers are similar, but not identical, in NGC 5253. The 2 cm and Hα peaks are not coincident, although the offset is small enough, ~2″, that it conceivably could be caused by uncertainties in the optical astrometry. Extinction is also a possibility. The Hα is slightly more extended overall than the 2 cm emission, although this may be due to undersampling of the extended emission by the interferometer, on size scales greater than 15″. The patchy features around the edges of the continuum source (Fig. 2, left) suggest that this is the case.

In star-formation regions, only a fraction of the total activity is typically visible at short wavelengths, and although dwarf galaxies have less obscuration than do spiral nuclei, the extinction can still be substantial on small size scales. Walsh & Roy (1989) found A_v = 1 ± 1 mag from the Hα/Hβ ratio in the central part of the galaxy. We estimate the extinction through the star-forming region from the Brackett lines, which may be expected to probe deeper into the galaxy and find greater total obscuration. If we assume T_e = 12,500 K, similar to the
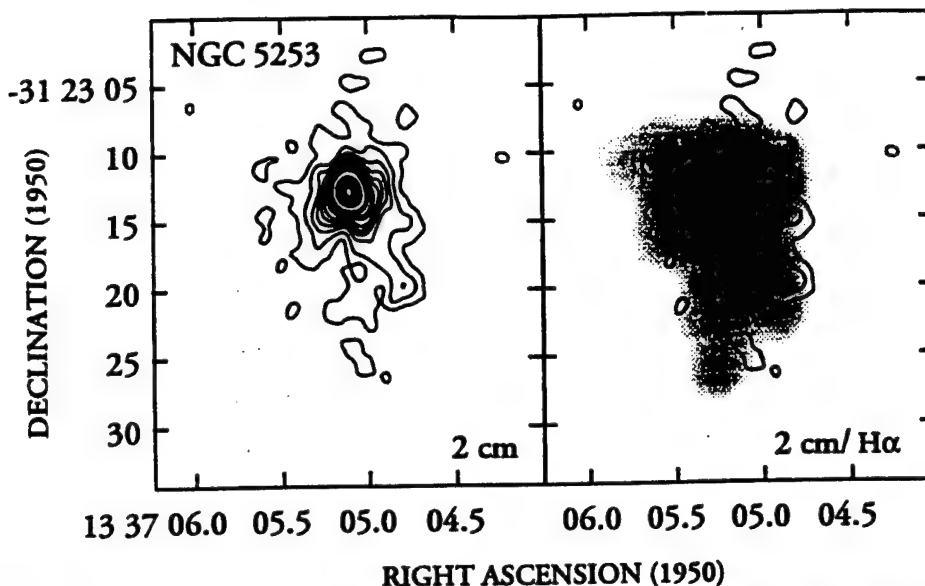
FIG. 2.—The 2 cm emission from the central region of NGC 5253 (*left*). The beam size is 1″9 × 1″5, p.a. 32°. Contour levels are multiples of 0.2 mJy beam⁻¹ up to 1.2 mJy beam⁻¹, then 1.6, 2.0, 3.0, and multiples of 4 mJy beam⁻¹ thereafter. The peak flux density is 22 mJy beam⁻¹. The 2 cm contours are also shown overlaid on the Hα image (*right*). Registration uncertainties are ~1″–2″, limited by the optical astrometry.

11,000–13,000 K temperatures derived by Walsh & Roy, the intrinsic value of Brα/Brγ is 2.77 (Ho, Beck, & Turner 1990), and the Brackett-line measurements of Kawara et al. (1989) indicate that there are 0.56 mag of relative extinction between 2.17 and 4.05 μm. This implies A_v of 12 mag if extinction varies as λ^{-2} or 7 mag for a $\lambda^{-1.5}$ extinction law. These values of A_v are consistent with what Kawara et al. found from the depth of the 10 μm feature and are close to the obscuration in typical spiral-galaxy nuclei but are significantly larger than the Hα/Hβ result. That there is extinction of less than 1 mag at 4.05 μm implies that it is unlikely for there to be a very obscured component that is not sampled even in the infrared.

The extinction and spatial structure show that the infrared and radio emission come from a compact region that is so obscured it cannot reliably be studied in the optical or ultraviolet. This cluster is embedded in the extended ionized gas excited by the less obscured young stars seen at optical and shorter wavelengths.
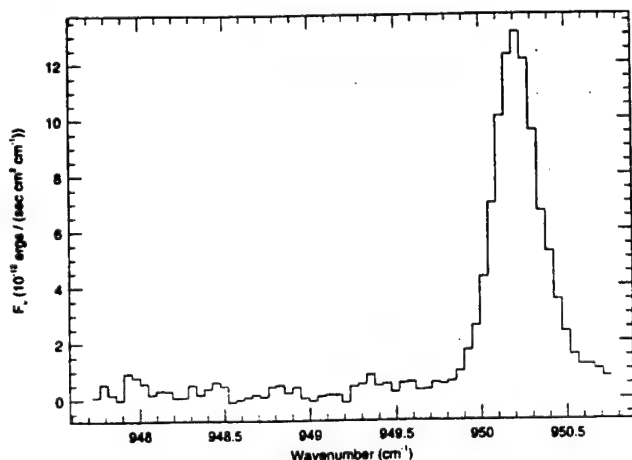

FIG. 3.—[S IV] line observed with Irshell with a 1″6 slit

3.2. Radio Spectrum

The plasmas ionized by recently formed OB stars are sources of radio continuum emission as well as Brackett lines. In almost all normal galaxies, the radio spectrum is a mixture of optically thin, thermal free-free emission, with a $\nu^{-0.1}$ spectrum, and nonthermal synchrotron emission, which has a significantly steeper slope. The shorter radio wavelengths will therefore see more thermal and less nonthermal emission, which was our motivation for obtaining 2 cm data on NGC 5253. Analysis of the radio spectrum of NGC 5253 is made difficult by the heterogeneity of the data: the 21 cm and 6 cm measurements of Lequeux (1971) and Whiteoak (1970) were made with single-dish telescopes of differing beam size, and although Lequeux determined that the 21 cm source size was less than 1′, these fluxes cannot be simply compared to the high-resolution 2 cm map. The maximum extent of the mapped 2 cm emission is 20″ × 40″, or 270 pc × 540 pc. The total flux in this map, 54 mJy, is nearly twice that in the central 6″, which is 35 mJy. There is evidence that the 2 cm flux is resolved out by the interferometer on size scales greater than 15″, although comparison with the single-dish 6 cm flux of Whiteoak indicates that this "missing" flux represents less than 15%–20% of the total. However, the central 15″–20″ region is well sampled by the 2 cm map.

The most striking result of the radio data is the flatness of the spectrum. The radio data can be described by a single power law of spectral index ~0 to −0.09—that is, completely thermal. There is no sign of the steeper component of spectral index −0.7 that dominates the continuum emission for wavelengths of 6 cm or longer in starburst galaxies (Turner & Ho 1994). Nor is there a break in the spectrum as is common in extragalactic radio sources (Deeg et al. 1993). While it is possible in theory to reproduce such a flat spectrum from an optically thick synchrotron source, such as the core sources of AGNs, the extended nature of the radio emission rules out this possibility. The simplest and most natural explanation of the spectrum is that NGC 5253 has almost entirely thermal radio

emission. We estimate that no more than 10% of the 6 cm flux is nonthermal, and less than 5% at 2 cm. NGC 5253 is comparable to II Zw 40, which is remarkable for its flat spectrum (Deeg et al. 1993), but NGC 5253 is actually flatter, with a slope of -0.1 ± 0.01, compared to -0.21 ± 0.03 for II Zw 40.

How does the radio flux of NGC 5253 compare to the visible and infrared recombination lines of hydrogen? The radio continuum flux expected from Brackett line fluxes may be found from $S_{6 \, cm}(mJy)/S_{Br\alpha}(10^{-12} \, ergs \, s^{-1} \, cm^{-2}) \approx 40$, which is appropriate for a $T_e = 12,500$ K H II region. From the observed Brackett line fluxes in NGC 5253 (Kawara et al. 1989), we would then predict radio fluxes of ~ 40 mJy at 6 cm and 35 mJy at 2 cm for the $10'' \times 20''$ region corresponding to the Brackett measurement (we have assumed 0.35 mag extinction at Brα). The observed 2 cm flux in the same region is 45 mJy. The predicted 2 cm flux is therefore 75%–80% of the observed flux. Given that the total radio fluxes of Table 1 indicate that most of the radio emission is thermal, it is likely that the discrepancy between the Brackett prediction and the observed radio flux is due to extinction in the near-infrared, although peculiar nebular conditions (including temperature variations) or a small amount of nonthermal radio emission are also possibilities. It is more difficult to compare the radio and infrared line fluxes to the Hα and Hβ measurements; while the radio continuum and infrared lines are likely to arise in the same volume and are relatively unaffected by extinction, the optical lines are much more susceptible to obscuration and may be dominated by the low-density, unobscured ionized regions that are less important at longer wavelengths. We conclude that the discrepancy between the 20 mJy of 6 cm flux that would be predicted from Osmer, Smith, & Weedman's (1974) measurement of Hβ in a 38'' aperture and the observed value of 51 mJy in the same region (Turner et al. 1995b) is best explained by extinction, the alternative explanation of a major nonthermal contribution to the radio being ruled out by the flat radio spectrum and the basic agreement of the radio and Brackett line fluxes.

The Brackett lines and the radio spectrum of NGC 5253 thus imply that the galaxy contains a large population of OB stars responsible for ionizing the gas, but the absence of a significant nonthermal radio component means the number of supernovae must be very small. Standard supernovae and SNRs have a wide range of radio luminosity, so we cannot calculate an exact upper limit on their number in NGC 5253. Given that the nonthermal fraction in NGC 5253 is less than 5% at 2 cm, or 2–3 mJy, and that the typical Galactic SNR has a spectral luminosity at 2 cm of $L_2 = 2 \times 10^{17}$ W Hz^{-1}, we estimate that we could have detected 10 SNRs. Bright SNRs or radio supernovae (RSNs; Weiler & Sramek 1988) are even harder to hide—we could have detected fewer than half a dozen Cas A's, for example, or a single RSN. This is most unusual for a starburst. For comparison, the starburst in the nucleus of NGC 253 has a nonthermal fraction of 80% at 2 cm (Turner & Ho 1983), and contains the energetic equivalent of hundreds of SNRs, yet has a Lyman continuum rate only twice that of NGC 5253.

The simplest explanation for the lack of radio SNRs in NGC 5253 is that the nuclear starburst is very young [less than $(1–2) \times 10^7$ yr] and that star formation in the cluster was coeval to a very high degree. This would be consistent with the lack of CO band-head absorption (Rieke et al. 1988). That there are two optically detected supernovae in the last century more than 30'' from the nucleus agrees with the model that star

formation in NGC 5253 started in the outer regions well before it started in the center (Caldwell & Phillips 1989). Our maps show no sign of radio emission from the neighborhood of SN 1895b, 32'' northeast of the nucleus, and do not include the region of SN 1972e, 102'' south of the nucleus; the large-beam radio maps were made before SN 1972e and after SN 1895b had faded. The absence of supernovae in the nucleus argues that the unusual [Fe II] and [Fe III] emission observed by Lumsden, Puxley, & Doherty (1994) is more likely to be due to their first suggested mechanism (H II regions with low iron depletion) than to their second (many young supernovae). Similarly, the soft X-ray emission (Martin & Kennicutt 1995) and filamentary morphology (Marlowe et al. 1995) are more likely to be the result of stellar winds or some other mechanism than SNRs.

There are other possible, although far less likely, explanations for the lack of radio SNRs in NGC 5253. Radio synchrotron emission in SNRs is produced by cosmic rays accelerated in the turbulent regions behind supernova shocks. This process is of course very dependent on the circumstellar environment, which probably explains the difference between the bright and short-lived RSNs and the longer lived, standard SNRs. Low-metallicity stars will have low mass-loss rates, so the circumstellar environment in this starburst may not be sufficiently extensive to favor the formation of either RSNs or SNRs. However, these stars are so young that there must be gas left over from the star-formation process that would generate radio emission. Other improbable explanations for the lack of radio SNRs include the lack of a magnetic field, which seems unlikely given the presence of ionized gas and likely turbulence, or an unusually swift evolution of the SNRs into the radiative phase, which would have no obvious cause in NGC 5253, and which would not explain why it is different from other starbursts in this regard. Yet another possibility, even more speculative, is that the highest mass stars may not become supernovae, in which case a top-heavy initial mass function (IMF) could be the reason for the lack of SNRs.

3.3. Stellar Population

The current stellar population in the obscured nucleus can be deduced from the mid-infrared spectrum. However, this technique, which has been widely used for Galactic sources, must be applied with care to extragalactic objects, the metallicities of which may differ drastically from solar. The [S IV] line in particular is not a reliable stellar temperature diagnostic unless the metallicity and the details of the nebular structure are known and accounted for. Beck & Sutherland (1995) have shown that the [S IV] line can be enhanced strongly by low metallicity and suppressed by high density. The lines of argon and neon are less affected by nebular structure and metallicity, but only [Ar III] was seen in NGC 5253, so it is necessary to use [S IV] and a more realistic model grid that will take account of the metallicity and nebular parameters if we are to derive the stellar temperature. We have used the program MAPPINGS II (Sutherland & Dopita 1993) to calculate line strengths of isobaric spherical H II regions with nebular characteristics typical of infrared star-formation sources: log $nt = 8$ or density $\sim 10^4$ and ionization parameters log $Q = 8.5$ (where log $Q = $ log $U + $ log c). The input ionizing spectra were R. L. Kurucz (1992, private communication) models with solar or 0.1 solar metal abundances (these models are, strictly speaking, applicable only to single sources, and the ionizing spectrum of a group of stars may differ from that of a single star, so these

results should be taken as approximate). The correction for relative extinction between the [Ar III] and [S IV] wavelengths is negligible.

We found that the [S IV]/[Ar III] ratio observed in NGC 5253 cannot be produced by any solar-abundance model, even one excited by 50,000 K stars. The $Z = 0.1 Z_\odot$ models, which are closest to the Z of 0.15–0.25 $Z_\odot$ found from optical measurements of Walsh & Roy (1989), indicate that stars between 40,000 and 45,000 K with the above nebular parameters will have [S IV]/[Ar III] and [S IV]/[Ne II] ratios consistent with those seen in NGC 5253. (Aitken et al. 1982, using simple models with solar abundances, deduced that the exciting stars in NGC 5253 must be well over 50,000 K for the [S IV] 10.5 μm line to be so strong. Our much less extreme result reflects the enhancement of [S IV] for a star of a given temperature at low metallicity.) This result is not very sensitive to small (less than a factor of 3) changes in the metallicity or to the presence of a reasonable amount of dust. A main-sequence star of the deduced temperature would have 35–40 $M_\odot$ and a main-sequence lifetime at that temperature of $(1.5–2) \times 10^6$ yr (Schaller et al. 1993).

The above assumes that the star cluster is very young and coevally formed, which, as discussed above, is the simplest explanation for the lack of supernovae. If we admit one of the more speculative possibilities mentioned above to explain the absence of SNRs, the small [S IV]–emitting cluster may contain more massive stars that have cooled down or entered the W-R stage. Preliminary calculations of the ionizing spectra of clusters (Sutherland, Shull, & Beck 1995) indicate that a coevally formed cluster with this effective temperature would be no older than 2×10^6 yr. If star formation took place in a Gaussian burst in which the star-formation rate is peaked at 5×10^6 yr with a spread of 2×10^6 yr, the cluster could be this hot at ages as advanced as 9×10^6 yr (4×10^6 yr after the peak). If Wolf-Rayet stars form in the cluster and dominate the ionization at late times, when it would otherwise be too cool to produce the observed infrared spectrum, it could be 1.5×10^7 yr old (this possibility is open to speculation, as the behavior and appearance of Wolf-Rayet stars in dense, obscured clusters are neither observationally nor theoretically known). Approximate as these numbers are, they do agree with the thermal radio spectrum, the lack of supernovae, and the absence of supergiants (Moorwood & Glass 1982) in suggesting that the central starburst is no more than 10^7 yr old and probably much younger.

We can estimate the stellar population needed to account for the radio, infrared, and line emission from the total ionization rate. Using Ho et al.'s (1990) calculations relating radio and Brackett line fluxes to ionizing flux and Lacy, Beck, & Geballe's (1982) work on the emission measure from ionic fine-structure lines, we find that the Brackett line fluxes require an ionizing rate of 2.7×10^{52} s^{-1}, the 2 cm radio continuum (in the same area as the Brackett lines) needs 3.2×10^{52} s^{-1}, and the [S IV] flux requires 2.2×10^{52} s^{-1}. The last differs from Aitken et al.'s (1982) result for several reasons. First, the flux we measured is only 65% of theirs, which may be related to the higher spectral resolution. Second, they used 4 Mpc for the distance and we used 2.8 Mpc. Third, they assumed solar abundances and we assumed 0.25 solar abundance for sulfur, which is what is seen in the optical emission region of NGC 5253, and that the fraction of sulfur in S^{+3} was 0.5, which the models indicate is a plausible ionic fraction for 45,000 K stars and 0.1–0.2 $Z_\odot$.

Because of the uncertainties in the sulfur abundance and the difference between the Brackett and radio emission described above, we adopt 3×10^{52} s^{-1} for the ionization rate. From Panagia's (1973) results, this ionizing flux could be produced by $\sim 2 \times 10^3$ O6 stars at 42,000 K or $\sim 1 \times 10^3$ O5.5 stars at 44,500 K. Vacca (1994) showed that the ionizing flux from a star at a fixed temperature increases as the metallicity decreases, to the extent that stars of these temperatures will produce roughly twice as much ionizing flux if they are of 0.05 solar metallicity as compared to solar-metallicity stars. For the moderate metallicity of NGC 5253, the effect will be less; we estimate a 25% increase in the ionization per star. Another complication is that the ionization rate of a physical cluster of mixed stellar types will differ from that of simplified model used here. Even with all these uncertainties, it is still apparent that the small obscured star cluster in NGC 5253 contains from several hundred to several thousand early O stars.

Of particular interest is the very compact 2 cm emission core, which has a size of 11–12 pc. The 2 cm flux in this core is 23 mJy, which is about half the total flux. We would therefore expect that this region contains ~ 500–1000 O stars. If these are all in the $\sim 0\overset{''}{.}8$–$0\overset{''}{.}9$ area of the radio core, the stellar density will be 0.5–1 O stars pc^{-3}. The total stellar density may be estimated from the number of O stars if we assume an IMF. If we choose an IMF $\propto M^{-3.2}$ for stars larger than 10 $M_\odot$ and flatter for smaller stars, we find for every 35–40 $M_\odot$ star ~ 40 stars of masses 10–35 $M_\odot$ and 20–90 stars, depending on the exponent chosen in the low-mass region, of 1–10 $M_\odot$. This would lead to a total stellar density of 30–130 stars pc^{-3} in the central star cluster. This high stellar density is uncharacteristic of Galactic star-forming regions and instead is more what one would expect for the central regions of a globular cluster.

4. CONCLUSIONS

Our infrared and radio observations of the obscured nucleus of NGC 5253 show that it contains a dense cluster of a few thousand massive and very young stars. From the high [S IV]/[Ar III] ratio we deduce that the cluster ionization is dominated by metal-poor stars of 40,000–45,000 K; the deduced age of the cluster is no more than 10^7 yr and more likely a few times 10^6 yr. This young age is probably the reason the radio continuum emission is entirely thermal; in fact, this requires that the cluster be not only young but coeval. The youth of the nuclear star cluster agrees with the picture that star formation has proceeded from the outskirts toward the nucleus in this galaxy. We may expect in the near (astronomically speaking) future to see supernovae in this star cluster and, possibly, changes in the ionization as Wolf-Rayet stars develop.

While the youth of the NGC 5253 starburst and its progress through the galaxy are well established, there are still important, unanswered questions about this object. First, the starburst started so recently that the triggering mechanism should still be obvious, but there is no candidate for a trigger except the hypothesized interaction with M83. What started the starburst? Second, what will happen to the dense central star cluster? What are its dynamics? Finally, are the characteristics of NGC 5253 that now appear so unusual—the thermal radio spectrum and the concentrated cluster of coevally formed hot stars—actually common among dwarf-galaxy starbursts?

REFERENCES

Aitken, D. K., Roche, P. F., Allen, M. C., & Phillips, M., M. 1982, MNRAS, 199, 31P
Beck, S. C., & Sutherland. R. S. 1995, in preparation
Caldwell, N., & Phillips, M. M. 1989, ApJ, 338, 789
Deeg, H.-J., Brinks, E., Duric, N., Klein, U., & Skillman. E. 1993, ApJ, 410, 626
Ho, P. T. P., Beck, S. C., & Turner, J. 1990, ApJ, 349, 57
Kawara, K., Nishida, M., & Phillips, M. M. 1989, ApJ, 337, 230
Lacy, J. H., Achtermann, J. M., Bruce, D. E., Lester, D. F., Peck, M. C., & Gaalema, S. D. 1989, PASP, 101, 1166
Lacy, J. H., Beck, S. C., & Geballe, T. R. 1982, ApJ, 255, 510
Lequeux, J. 1971, A&A, 15, 30
Lumsden, G. L., Puxley, P. J., & Doherty, R. M. 1994, MNRAS, 268, 821
Marlowe, A. T., Heckman, T. M., Wyse, R. F. G., & Schommer, R. 1995, ApJ, 438, 563
Martin, C. L., & Kennicutt, R. C., Jr. 1995, preprint
Moorwood, A. F. M., & Glass, I. S. 1982, A&A, 115, 84
Mouri, H., Taniguchi, Y., Kawara, K., & Nishida, M. 1989, ApJ, 346, L73
Osmer, P. S., Smith, M. G., & Weedman, D. W. 1974, ApJ, 192, 279
Panagia, N. 1973, AJ, 78, 929
Rieke, G. H., Lebofsky, M. J., & Walker, C. E. 1988, ApJ, 325, 679
Rogstad, D. H., Lockhart, I. A., & Wright, M. C. H. 1974, ApJ, 193, 309
Schaller, P. G., Schaerer, D., Meynet, G., & Maeder, A. 1993, A&AS, 96, 269
Sutherland, R. S., & Dopita, M. A. 1993, ApJS, 88, 253
Sutherland, R. S., Shull, M., & Beck, S. C. 1995, in preparation
Telesco, C. M., Dressel, L. L., & Wolstencroft, R. D. 1993, ApJ, 414, 120
Turner, J. L., Beck, S. C., & Hurt, R. L. 1995a, in preparation
Turner, J. L., & Ho, P. T. P. 1983, ApJ, 268, L79
———. 1994, ApJ, 421, 122
Turner, J. L., Ho, P. T. P., & Beck, S. C. 1995b, in preparation
Vacca, W. D. 1994, ApJ, 421, 140
Van den Bergh, S. 1980, PASP, 92, 122
Walsh, J. R., & Roy, J.-R. 1987, ApJ, 319, L57
———. 1989, MNRAS, 239, 297
Weiler, K., & Sramek, R. 1988, ARA&A, 26, 295
Whiteoak, J. B. 1970, Astrophys. Lett., 5, 29

SPECTROSCOPY OF EVOLVED STARS IN THE NEAR INFRARED: EXPLORATIONS BEYOND THE AGB

DOUGLAS M. KELLY

Department of Astronomy, University of Texas, Austin, Texas 78712
Electronic mail: dkelly@astro.as.utexas.edu

WILLIAM B. LATTER

National Radio Astronomy Observatory,[1] 949 N. Cherry Avenue, Campus Building 65, Tucson, Arizona 85721
Electronic mail: wlatter@nrao.edu

ABSTRACT

We present spectra taken between $\lambda = 0.9-1.3$ μm for a sample of evolved stars ranging from Mira variable stars to planetary nebulae. An evolution can be seen from the absorption spectra of the late-type stars to the emission line spectra of the planetary nebulae. We compare emission line strengths for objects ranging from $T_{eff} = 30\,000$ to $200\,000$ K, and we use infrared and visible line ratios to determine densities and temperatures in the emission line regions. We examine the four factors that are most important to determining relative ion strengths—stellar temperature, evolutionary status, excitation mechanism, and clumpiness. It is found that clumps appear to be common, and that shocks are very important to the excitation and shaping of planetary nebulae. We also find that the strength of the low ionization and molecular emission lines decreases with age, and we use a filling factor analysis to show that this evolution is caused by a decrease in the amount of low ionization material close to the star.

1. INTRODUCTION

Recent imaging studies are providing important insights into the formation and evolution of planetary nebulae (PN; e.g., Schwarz *et al.* 1992; Balick *et al.* 1992, 1993; Graham *et al.* 1993; Latter *et al.* 1993; Kastner *et al.* 1994; Latter *et al.* 1994). Stars with initial masses of roughly $\mathscr{M}_* \sim 1-8$ $\mathscr{M}_\odot$ build up a carbon–oxygen degenerate core while on the asymptotic giant branch (AGB). Mass is driven from the surface by a combination of pulsations and radiation pressure (Jura 1986). When the core mass approaches $0.6\mathscr{M}_\odot$, the efficiency of radiation-driven mass loss increases rapidly and most of the remaining envelope material is ejected during a $\tau \approx 1000-10\,000$ yr period. Since the density in the stellar atmosphere is high and the temperature is low, the ejected material is predominantly molecular. When the envelope mass drops to $\mathscr{M}_{env} \approx 0.01 \mathscr{M}_\odot$, the pulsations cease, the mass loss rate drops by a factor of 100, and the star evolves off the AGB (Schönberner 1987). As the envelope of the star contracts and rises in temperature, the luminosity of the star remains nearly constant. The momentum of the wind is undiminished and the low mass wind is accelerated to very high velocities ($v \sim 1500$ km s^{-1}). This fast wind plows into the slower red giant wind and sweeps the material into shells (see Kwok *et al.* 1978). As the central star and nebula evolve, a photodissociation front moves through the gas and the circumstellar envelope changes from molecular to atomic to ionized. The gross morphology of the nebula depends mainly on its age and on the isotropy of mass loss on the AGB (see Balick 1987). By studying details of the morphology and spectra of PN and protoplanetary nebulae (PPN), we can learn more about the nature of AGB mass loss and the shaping and excitation of PN envelopes.

In this paper, we investigate the origin and evolution of planetary nebulae by tracing the evolution of their $\lambda = 0.9-1.3$ μm spectra. Our study begins with AGB stars and other highly evolved stars (WX Ser, IRC+10°420, IRC+10°216, AFGL 915). We also observed four of the PPN candidates identified by Kwok (1993) (IRAS 04296+3429, IRAS 23304+6147, AFGL 618, AFGL 2688), two symbiotic stars (HM Sge, V1016 Cyg), as well as several young and more evolved PN (Hubble 12, NGC 6790, Vy 2−2, NGC 7027). The Orion Nebula is presented as a comparison object.

The $\lambda = 0.9-1.3$ μm region has several attributes that make it a good choice for this study. It offers low attenuation, numerous molecular features, including high vibrational transitions of H_2, and good sensitivity to blackbody sources as cool as $T = 2000$ K. It also contains electronic transitions for many ions, including the Paschen series of hydrogen. We searched for new lines and species in our target objects and traced their atomic, molecular, and continuum emission. As we discuss in later sections, these observations give us a better understanding of the distribution and excitation of gas in PN.

A number of papers have been written over the last three decades about the infrared spectra of post-main sequence stars. The reader is referred to the following references for $\lambda = 0.9-1.35$ μm spectra of giants, supergiants, and oxygen- and carbon-rich AGB stars. Wing (1967) compared the $\lambda = 0.75-1.1$ μm spectra of dwarfs, giants, and supergiants of various spectral types. He found that TiO and ZrO are the dominant features in the spectra of oxygen-rich post-main sequence stars, with VO becoming important for late-M

TABLE 1. Log of observations.

Object	Obs. Date	Ref. Star	Sp. Type
WX Ser	4/9/90	HR 5659	G5 V
IRC+10°420	6/9/90	HR 7354	F6 V
IRC+10°216	5/12-15/90	HR 3998	F7 V
AFGL 915	10/27/90	HR 2313	F8 V
IRAS 04296+3429	10/27-28/90	HR 1489	G0 V
IRAS 23304+6147	10/27/90	HR 8853	F8 V
AFGL 2688	10/27-28/90	HR 8170	F8 V
	11/4/90		
V1016 Cyg	11/5/90	HR 7550	F4 V
HM Sge	11/3/90	HR 7560	F8 V
Hubble 12	10/27-28/90	HR 8853	F7 V
	11/3-5/90		
NGC 6790	10/27/90	HR 7354	F6 V
Vy 2-2	10/28/90	HR 7354	F6 V
	11/4/90		
NGC 7027	11/14/89	HR 8170	F8 V
Orion Neb.	11/14-16/89	HR 2007	G4 V
	10/28/90		
	11/3/90		

stars. He also found that CN bands are the dominant features in carbon-rich stars. Lockwood (1969) measured the 0.96–1.08 μm spectra of oxygen-rich Mira variables and found a relationship between TiO band strength and temperature. Thompson et al. (1969a,b) detected ^{13}CO in the λ=1.2–4.2 μm spectra of carbon-rich stars and presented evidence that the Δv=2 and Δv=3 bands of ^{12}CO are saturated in these

stars. Miller (1970) observed the CN bands in the λ=0.7–1.1 μm spectrum of IRC+10°216. Lockwood (1973) made improved measurements of TiO and VO band strengths in the λ=0.96–1.04 μm spectra of M-type stars. Finally, Goebel et al. (1981) confirmed that CN bands are the dominant features in the λ=0.7–1.5 μm spectra of carbon-rich stars and showed that more complex molecules such as HCN and C_2H_2 are the dominant features in the λ=1.5–8.0 μm region.

There have been several recent studies of the infrared spectra of PN and PPN. The λ=0.84–1.35 μm spectrum of the bipolar PPN AFGL 618 is discussed by Latter et al. (1992) and Kelly et al. (1992). They found that the infrared spectrum is dominated by low-ionization, shock-heated lines, including strong H_2 emission. The $T_{eff} \sim 30\,000$ K central star excites fluorescent O I and H_2 lines in the λ=1.11–1.23 μm spectrum of that region. Rudy and collaborators presented a series of papers on the λ=0.8–1.3 μm spectra of PN, including IC 4997 (Rudy et al. 1989), V1016 Cyg (Rudy et al. 1990), NGC 6572 (Rudy et al. 1991a), BD+30°3639 (Rudy et al. 1991b), NGC 7027 (Rudy et al. 1992), and Hubble 12 (Rudy et al. 1993). They found that the infrared O I lines are excited by Lyβ fluorescence in IC 4997 and V1016 Cyg and by UV continuum fluorescence in the other sources. They devised a method for removing the nebular

TABLE 2. Line identifications and relative fluxes.

ID	λ(μm)	GL618	V1016Cyg	HMSge	Hbl2	N6790	Vy 2-2	N7027	Orion
Fe II?	0.8930	-	.030	.023	-	-	-	-	-
?	0.8975	.025	-	-	-	-	-	-	-
He I	0.8997	-	-	.015	.0082	-	.020	-	-
Pa 10	0.9015	.106	.072	.145	.106	.052	.145	.121	.079
[FeII]	0.9034	.088	-	-	-	-	-	-	-
[S III]	0.9069	.106	.15	.77	.81	.53	1.88	1.68	1.32
C I	0.9112	.34	-	x	x	x	x	.176	.128
Pa 9	0.9229	.136	x	x	x	x	x	-	-
[Fe II]	0.9345	-	x	x	x	x	x	.055	-
He II	0.9362	-	x	x	x	x	x	.008	-
?	0.9449	-	-	-	-	-	.025	-	-
?	0.9464	-	-	-	.023	.028	.042	.012	.017
He I	0.9495	-	-	.013	-	-	-	•	•
?	0.9516	-	-	-	-	.14	-	-	-
?	0.9531	.66	.32	1.97	3.16	1.48	4.37	5.29	7.02
[S III]	0.9546	.14	.064	.29	.23	.27	-	-	.029
Pa 8	0.9604	-	x	x	x	x	x	-	.008
He I	0.9703	-	x	x	x	x	x	.003	-
He I	0.9756	-	x	x	x	x	x	.006	-
[Fe II]	0.9770	-	x	x	x	x	x	.010	.006
?	0.9824	.91	x	x	x	x	x	.035	.020
[C I]	0.9850	2.6	x	x	x	x	x	.011	.006
[C I]	0.9904	-	x	x	x	x	x	-	.0059
C II	1.0014	-	-	-	-	x	x	•	.027
?	1.0031	.022	-	-	-	x	x	.35	.38
He I	1.0049	.28	.19	.28	x	x	x	-	.0030
Pa 7	1.0109	.12	-	.35	.83	x	x	x	.82
N I	1.0124	-	.35	.0088	x	x	x	-	-
He II	1.0212	-	-	-	.011	.015	.026	.072	.097
?	1.0286	.34	.015	.15	-	-	-	-	-
[S II]	1.0311	-	-	-	.0053	-	-	.105	.137
He I	1.0320	.47	.024	.20	.015	.029	.035	.079	.109
[S II]	1.0336	.34	.019	.13	.0096	.021	.020	.036	.053
[S II]	1.0370	.16	.013	.088	.0035	.0077	.011	.029	.016
[N I]	1.0398	1.69	.020	.18	.011	.0059	.012	.024	.0072
[N I]	1.0408	1.16	.015	.14	.0068	.0053	.011	.015	-
He II	1.0420	-	-	.046	-	-	-	-	-
?	1.0447	-	-	-	-	-	-	-	.007
?	1.0519	-	x	x	.003	x	x	.006	.013
C I	1.0685	.06	x	x	-	x	x	.015	.005
C I	1.0754	-	x	x	-	x	x	-	-
He I	1.0830	.75	3.01	6.48	6.30	9.11	7.67	8.10	4.98
H2	1.0848	.34	-	-	-	-	-	-	-
?	1.0858	-	.065	-	-	-	-	-	-

ID	λ(μm)	GL618	V1016Cyg	HMSge	Hbl2	N6790	Vy 2-2	N7027	Orion
He I	1.0913	.084	.036	.059	.045	.077	.063	.030	.011
Paγ	1.0938	.375	.351	.527	.411	.507	.729	.566	.495
H2	1.0997	.13	-	-	.0011	-	-	-	-
H2	1.1172	.27	-	x	-	x	-	-	-
H2	1.1201	.059	-	x	-	x	-	-	-
H2	1.1208	.062	-	x	-	x	-	-	-
O I	1.1287	.059	.17	x	.0081	x	.017	-	.011
H2	1.1301	.066	-	x	-	x	-	-	.0091
C I	1.1330	-	-	x	-	x	-	-	-
?	1.1344	-	-	x	-	x	x	.016	.006
[P II]	1.1468	.075	-	x	-	x	x	-	-
H2	1.1619	.23	x	x	.001	x	x	-	-
He II	1.1626	-	x	x	-	x	x	.182	-
He II	1.1673	-	x	x	-	x	x	.025	-
C I	1.1754	.022	x	x	.001	x	x	.002	.015
[Fe II]	1.1831	.025	x	x	.001	x	x	-	-
H2	1.1854	.16	x	x	.002	x	x	.051	.012
[Fe II]	1.1882	.21	x	x	.001	x	x	-	-
[P II]									
H2	1.1892	.081	-	x	.0015	x	x	.013	-
C I	1.1894	-	x	x	.015	x	x	.012	.015
He I	1.1969	-	x	x	.002	x	x	.002	.004
?	1.2292	-	x	x	.002	x	x	.011	.003
H2	1.2327	.14	x	x	.002	x	x	.001	.002
H2	1.2380	.19	x	x	-	x	x	.003	-
H2	1.2416	.088	x	x	.027	x	x	.014	.021
He I	1.2528	-	x	x	.010	x	x	.007	.014
[Fe II]	1.2567	.72	x	x	.055	.073	.079	.033	.030
He I	1.2785	.138	-	.035	-	-	-	-	-
Paβ	1.2818	1.00	1.00	1.00	1.00	1.00	1.00	1.00	1.00
H2	1.2870	.072	-	-	.012	-	-	-	-
?	1.2893	-	-	-	-	-	-	.005	-
He II	1.2914	-	-	-	-	-	-	-	-
H2	1.2929	.034	-	-	.0022	-	.0042	.0022	.0047
[Fe II]	1.2943	.100	-	-	-	-	-	-	-
C I	1.2950	.012	-	-	.0037	.0050	-	.0033	.0044
He I	1.2968	-	-	-	.0046	x	x	.0027	.0036
He I	1.2985	-	-	-	.024	x	x	.003	.038
O I	1.3165	.13	x	x	.0035	x	x	.0026	.0089
[Fe II]	1.3205	.22	x	x	.0012	x	x	.0011	.0063
[Fe II]	1.3278	.062	x	x	-	-	-	-	-

Notes to Table 2

- observed, line not clearly detected
x spectra do not include this wavelength
• line probably present but cannot be deblended from adjacent features
: highly uncertain line flux due to uncertain continuum level and fluxing
All line ratios are listed relative to Paβ and have been dereddened. The uncorrected Paβ fluxes (erg s⁻¹ cm⁻²) and Av (mag) values are as follows: AFGL 618 – 1.9 × 10⁻¹³, 2.1; V1016 Cyg – 3.45 × 10⁻¹¹, 1.15; HM Sge – 1.16 × 10⁻¹¹, 1.3; Hubble 12 – 1.8 × 10⁻¹¹, 2.0; NGC 6790 – 1.09 × 10⁻¹¹, 2.2; Vy 2-2 – 6.6 × 10⁻¹², 3.4; NGC 7027 – 3.6 × 10⁻¹¹, 2.5; Orion – 6.3 × 10⁻¹³, 1.0.
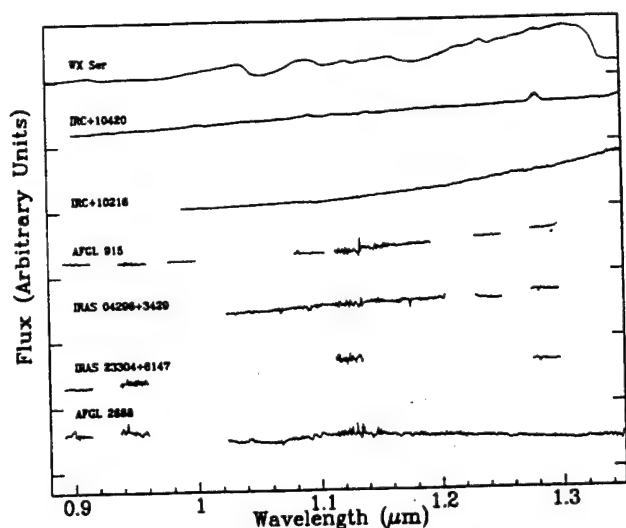
FIG. 1. The $\lambda=0.9-1.35$ μm spectra of continuum dominated sources. These data were acquired with the Steward Observatory 2.3 m telescope and a germanium diode spectrometer. See Sec. 3.1.

FIG. 2. The $\lambda=0.9-1.35$ μm spectra of emission line objects, acquired with the Steward Observatory 2.3 m telescope and a germanium diode spectrometer. See Sec. 3.2. Identifications for many of the prominent lines can be found in Fig. 3.

continuum emission from a spectrum and used this technique to isolate the spectra of the central stars. They determined densities and temperatures in the emitting regions of the nebulae, and derived new abundances for several of the objects.

2. OBSERVATIONS AND DATA REDUCTION

The spectra presented in this paper were measured at the Steward Observatory 2.3 m telescope on Kitt Peak, Arizona using the GeSpec, a $\lambda=0.9-1.6$ μm spectrometer with a 2×32 pixel germanium photodiode array. The twin apertures of the GeSpec are 6″ in diameter and are separated by 1′. With the 600 l/mm grating the resolution is $\lambda/\Delta\lambda\approx1000$ and the spectral coverage of each segment is $\Delta\lambda\approx0.022$ μm. With the 150 l/mm grating (used for WX Ser and IRC +10°420), the resolution is $\lambda/\Delta\lambda\approx300$ and the spectral coverage of each segment is $\Delta\lambda\approx0.1$ μm. F and G dwarf stars were used to remove telluric absorption features and to provide flux calibration. Observing and data reduction procedures are discussed by Rix et al. (1990). All sources were centered in the 6″ apertures, and up to 20% intensity variations resulted from pointing and guiding fluctuations. Since the data collection was very time consuming, we only made complete spectral scans of the spectroscopically most interesting objects. For the others, we observed the hydrogen recombination lines and several other diagnostic lines. The observations are summarized in Table 1; line identifications of the emission line objects are included in Table 2, and the resulting spectra are presented in Figs. 1 and 2. A more detailed version of the Orion Nebula spectrum is shown in Fig. 3. Only 5σ and better detections are listed in Table 2. See Kelly (1993) for additional (less certain) line identifications in the spectra of Hubble 12, NGC 7027, and the Orion Nebula.

3. COMMENTS ON INDIVIDUAL SOURCES

3.1 Absorption Spectra

3.1.1 WX Serpentis

WX Serpentis is a Mira variable star with spectral type M8.5. Its infrared spectral features are similar to but stronger than those found in late M dwarfs (see Kirkpatrick et al. 1993). The strong VO absorption bands at $\lambda=1.06$ and 1.18 μm and the deep H_2O feature at 1.34 μm are especially noticeable in the spectrum of WX Ser.

3.1.2 IRC +10°420

IRC+10°420 is an OH/IR star (spectral type F8 Ia), but it appears to be a high mass supergiant rather than a late-AGB star (Jones et al. 1993). It has an infrared spectrum similar to
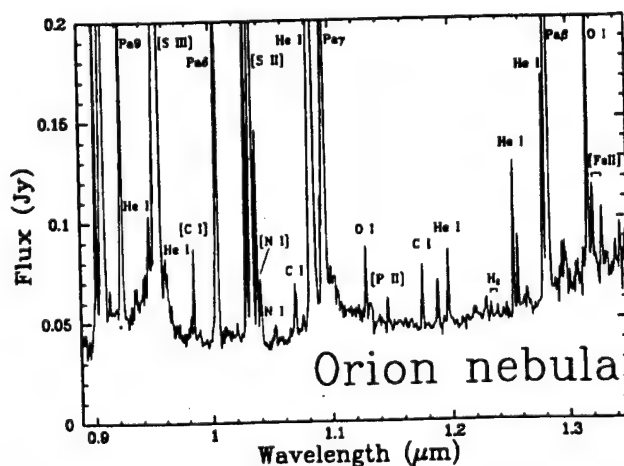

FIG. 3. The $\lambda=0.89-1.35$ μm spectrum of the Orion Nebula, acquired with the Steward Observatory 2.3 m telescope and a germanium diode spectrometer. This spectrum is shown for comparison and line identifications only. There is no analysis of the Orion Nebula in the text.

most of the early M dwarfs. Of the stars studied by Kirkpatrick *et al.* (1993), IRC+10°420 is most similar to the unpublished M1 dwarf GL 15A. IRC+10°420 has weaker FeH 0.99 μm absorption than GL 15A, as expected because of the lower density atmosphere (Allard 1992), and it has stronger ZrO (0.93–0.94, 1.166, 1.177, 1.187 μm) and VO (1.05 μm) bands. IRC+10°420 also produces weak Paβ emission. Oudmaijer *et al.* (1994) presented slightly blueshifted line profiles for Brγ, Brα, and Pfγ and a double-peaked profile for Hα, and they argued that the H I lines come from a bipolar outflow that developed in the past ten years.

3.1.3 IRC +10°216

The 1.0–1.5 μm spectrum of the carbon star IRC −10°216 has few easily discernable features other than shallow CN absorption at 1.1 μm. Among the numerous faint absorption features, there are acetylene (C_2H_2) bands at 1.04 and 1.17 μm, CN bands at 1.0926, 1.0968, 1.0996, and 1.1244 μm, and dozens of what appear to be molecular absorption features scattered throughout the spectrum. The $\lambda = 1.0–1.5$ μm spectrum is dominated by thermal dust emission and is well fit by a $T_c \approx 900$ K blackbody. Miller (1970) reported that the $\lambda = 0.7–1.1$ μm spectrum has the energy distribution of a $T_c \approx 1250$ K blackbody, Becklin *et al.* (1969) fit the 1–5 μm spectrum with a $T_c \approx 650$ K blackbody, and Le Bertre (1988) matched 0.55–25 μm photometry with blackbodies in the temperature range $T_c \approx 530–670$ K, depending on the phase of pulsation. From Le Bertre's work, it is clear that the large range in dust temperatures cannot be accounted for by pulsations alone. Instead, one can fit the broadband photometry and our data simultaneously by invoking a two component model composed primarily of $T_d \approx 650$ K dust but with 0.055% of the dust having a temperature $T_d \approx 1185$ K. The maximum dust temperature is probably closer to the $T_d \approx 1250$ K determined from the $\lambda = 0.7–1.1$ μm spectra of Miller (1970). This value is similar to the continuum temperatures of $T_c \approx 1000–1200$ K found at the onset of dust emission in carbon-rich novae (Gehrz 1988).

3.1.4 AFGL 915

The protoplanetary nebula AFGL 915 (the "Red Rectangle") has an interesting near-infrared spectrum. Our 6″ beam captured both the binary exciting star HD 44179 and some of the surrounding nebulosity. The blue end of our infrared spectrum is dominated by the photosphere of HD 44179, including weak absorption lines of H I, He I, C I, and N I. HD 44179 has been classified as a B9 to A0 III (Cohen *et al.* 1975), but the strong helium absorption lines near 0.9 μm indicate a spectral type of A1 III. Cool dust contributes to the emission from AFGL 915 starting at about 0.7 μm (Cohen *et al.* 1975), and it veils most of the atmospheric features longward of 1 μm. Brγ (Thronson 1982) and Paβ are completely obscured, and Paγ appears only weakly in absorption.

The most interesting feature in the infrared spectrum of AFGL 915 is He I at 1.0830 μm, which appears prominently in emission. Cohen *et al.* (1975) also found narrow Hα and Na D emission lines. The presence of He I recombination

emission normally indicates a central star temperature of at least $T_{\rm eff} \approx 20\ 000$ K, but given the cool photospheric temperature of AFGL 915, an alternative excitation mechanism such as chromospheric or coronal emission is required. Such activity is common in mid-F through late-K stars, but it is unexpected in an early-A star (Zirin 1976; O'Brien & Lambert 1986).

3.1.5 IRAS 04296+3429, IRAS 23304+6147, AFGL 2688

IRAS 04296+3429, IRAS 23304+6147, and AFGL 2688 (the "Egg Nebula") are carbon-rich PPN and have similar near-IR spectra. Their near-infrared spectra include a large number of absorption features, mostly from C I and CN. Other possible absorbers are Si I and He I. In addition, there is H I absorption in the spectrum of IRAS 04296+3429, consistent with the results of Hrivnak *et al.* (1994). The lack of emission lines in these spectra might be due in part to our large aperture size. With a narrow slit, Hora & Latter (1994) find CN and C_2 emission in a fairly isolated region of AFGL 2688, and C_2 Swan band emission is prominent in the visible spectrum of this object (Humphreys *et al.* 1976).

3.2 Emission Line Sources

The line strengths for the emission line sources are presented in Table 2, with all fluxes dereddened and listed relative to the Paβ flux. Paβ fluxes and visual extinctions are listed in the footnotes. Line fluxes from a bright knot in the Orion Nebula are presented for comparison. In examining Table 2, the reader should be aware of uncertainties in reddening corrections in addition to the ~20% uncertainty in line flux measurements. Still, it is easy to see that there are significant differences in the relative line strengths of the various objects.

3.2.1 AFGL 618

The PPN AFGL 618 has an emission line spectrum dominated by low ionization, predominantly shock-excited gas. The [S III] lines are weak and there is no He II emission, but the [C I], [S II], [N I], and [Fe II] lines are unusually strong. The infrared spectrum is also very rich in molecular hydrogen lines. [See Latter *et al.* (1992) and Kelly *et al.* (1992) for a complete discussion of the $\lambda = 0.84–1.35$ μm spectrum of AFGL 618].

3.2.2 HM Sge, V1016 Cyg

The symbiotic novae HM Sge and V1016 Cyg have evolved spectra with strong [S III], helium, and hydrogen lines. The low-ionization [S II] and [N I] lines are prominent in HM Sge, even though the central star is hot enough to excite He II emission. We compared our line strengths with the visible data of Schmid & Schild (1990) and Davidson *et al.* (1978) and with the infrared data of Thronson & Harvey (1981). The relative infrared and visible H I and [S II] line strengths are consistent with a reddening of $A_V = 1.0–1.3$ mag (assuming no variability in the three years between observations). Thronson & Harvey found a reddening of $A_V = 12$ mag from the Brackett line ratios, indicating that the primary H II emitting region is heavily obscured. As

discussed by Thronson & Harvey, the dust provides shielding that allows low ionization gas to survive in the outer parts of the nebula. From the [S II] and [S III] line ratios, we estimate an electron density of at least $n_e \sim 5 \times 10^5$ cm^{-3} in the forbidden line regions.

We compared our data on V1016 Cyg with the visible spectrum of Schmid & Schild (1990), the 0.46–1.3 μm data of Rudy et al. (1990), and the 2 μm data of Schild et al. (1992). From a comparison of visible and infrared H I, [S II], and He II lines, we adopt a reddening of $A_V = 1.15$ mag. This is similar to the value determined by Rudy et al., who derived the reddening separately for the H I, He I, and He II lines. Schmid & Schild found electron temperatures ranging from $T_e \sim 10^4$ to 4×10^4 K from a variety of line diagnostics. Our He I and [S II] line ratios are consistent with an electron temperature of $T_e \sim 10^4$ K. Nussbaumer & Schild (1981) found $n_e \sim 3 \times 10^6$ cm^{-3} from several sets of UV transitions. Our [S II] and [S III] line ratios indicate an electron density of at least 10^5 cm^{-3} and probably greater than 10^6 cm^{-3}. In addition, as discussed by Rudy et al., V1016 Cyg has strong, Lyβ-pumped O I fluorescence, which requires high densities in the H I–H II transition region.

There are several absorption features in the spectrum of V1016 Cyg, including H_2O at 0.938 μm and VO at 1.046 μm. As discussed by Rudy et al., these features and much of the continuum emission are produced by a late-M companion star. We have insufficient spectral coverage to improve upon Rudy et al.'s spectral classification of M6–M8.

3.2.3 Hubble 12

The planetary nebula Hubble 12 has a mostly low ionization spectrum with very prominent He I emission. The He I triplet/singlet line intensity ratio is about 3/1, as expected for recombination. The infrared [S II] lines are weak in Hubble 12, consistent with an electron density $n_e > 10^6$ cm^{-3}. In contrast, infrared [Fe II] line ratios indicate an electron density of only $n_e \sim 6 \times 10^4$ cm^{-3}, and the nebular lines of [S II] and [O II] indicate an even smaller density of $n_e \sim 3 \times 10^3$ cm^{-3} (Barker 1978; Aller & Czyzak 1983).

Hubble 12 has several features that are characteristic of a photon-dominated region (PDR). Among the PDR features are C I, Si I, and H_2 lines. The strongest H_2 lines are the (3–1) $S(1)$ line at 1.2327 μm and the 2–0 $Q(1)$ line at 1.2380 μm. The ratio of the H_2 lines is consistent with the fluorescent H_2 emission models of Black & van Dishoeck (1987; Dinerstein et al. 1988). Other detected H_2 lines are listed in Table 2, and additional H_2 identifications can be found in Kelly (1993). Fluorescence is also responsible for the O I emission from Hubble 12. The O I λ1.1287/λ1.3165 ratio is 0.3, consistent with UV continuum fluorescence with no significant resonance pumping by Lyβ. The lack of O I triplet line emission rules out recombination as the exciting mechanism for the O I.

3.2.4 NGC 6790

NGC 6790 is a strong source of He I emission. The He I triplet lines are very strong, indicating that the electron density is rather high, probably on the order of $n_e \sim 10^5$–10^6 cm^{-3}. We compared the infrared line strengths to the visible

line data of Kaler (1976). From the ratios of visible to infrared H I and [S II] lines, we derive $A_V = 2.2$ mag. [S II] and [S III] line ratios suggest $n_e \sim 10^5$ cm^{-3} for $T_e = 10^4$ K, or $n_e \sim 5 \times 10^5$ cm^{-3} for $T_e = 5 \times 10^3$ K. We analyzed He I line ratios using the collisional enhancement formulas of Clegg (1987), and we find the best agreement when we adopt $T_e < 10^4$ K. The weak forbidden lines in NGC 6790 provide further support for the high density, low temperature solution. This result contrasts with the electron densities determined from visible [S II], [O II], [Cl III], and [Ar IV] ratios by Stranghellini & Kaler (1989). They found densities ranging from $n_e \sim 5 \times 10^3$–3×10^4 cm^{-3}. Thus, NGC 6790 is similar to Hubble 12 and AFGL 618 in having a variety of density and temperature regimes.

3.2.5 Vy 2–2

Vy 2–2 is also a strong source of He I emission. We compared our infrared spectrum to visible line data by Feibelman (1993) and Acker et al. (1989). From H I line ratios, we find extinction values ranging from $A_V \sim 3.1$–4.8 mag. We adopted a value of 3.4 mag for our analysis. Our [S II] and [S III] line ratios can be simultaneously fit for a temperature of $T_e = 1.5 \times 10^4$ K and a density of $n_e = 8 \times 10^4$ cm^{-3}, but we cannot rule out values differing from these by a factor of 2. No single density–temperature pair can account for all of the He I line ratios.

3.2.6 NGC 7027

The very hot PN NGC 7027 has a high ionization spectrum, with very strong He II and forbidden line emission and slightly weakened He I emission. The brightest He I lines are all triplet transitions, indicating high densities in the ionized regions. The infrared [S II] line ratios, which are excited outside the hydrogen Strömgren sphere, suggest an electron density of $n_e \lesssim 10^5$ cm^{-3}. There are a variety of PDR lines in the spectrum of NGC 7027, including [P II], C I, Si I, [C I], and perhaps H_2. Graham et al. (1993) showed from H_2 and CO kinematics and morphology that the H_2 1$\rightarrow$0 $S(1)$ line is excited by radiation, not by shocks. The presence of weak O I 1.3165 μm emission and the absence of the 1.1287 μm line and of any quintet transitions indicate that the O I emission is also excited by starlight fluorescence (Rudy et al. 1992).

4. DISCUSSION

There are few clear trends in the spectral characteristics of the objects in this survey. This is exacerbated by uncertainties in the evolutionary status of the individual objects. There are obvious trends, such as the evolution from the late-type stellar spectra of the AGB stars to the mixed spectra of the PPN and on to the emission line spectra of the PN. This evolution is not surprising, but details can be learned about the shaping of PN based on the distribution of lines at various evolutionary stages. For example, the great relative strength of the low ionization lines in the spectrum of AFGL 618 (see Table 2) is evidence for the importance of shocks. AFGL 618 and several of the PN have multiple density and temperature regimes, which is another characteristic of shock

excited gas. The presence of shock-heated gas in several of the PPN and PN indicates the general importance of shocks in the excitation and shaping of the nebulae. Multiple density and temperature regimes could also be the result of shielding by dense clumps. The presence of H_2 emission in the bipolar lobes of AFGL 618 is further evidence for shielding clumps (the H_2 would be rapidly dissociated if it were exposed to the full UV radiation field; see also Latter et al. 1992). Finally, H_2 emission from Hubble 12 and NGC 7027 shows that there is still an abundant supply of molecular material around young PN.

To understand the geometries of the emission line sources better, we worked backwards using line strengths to determine the filling factors of various ions. For permitted lines, we used the relationship

$$F_{i,n} = \frac{h\nu_{i,n}}{4\pi r^2} n_e n_{i+1} V \alpha_{i,n}^{\text{eff}}(i,T), \tag{1}$$

where F is the dereddened line flux, r is the assumed distance, V is the volume of the emitting region, and α is the effective recombination coefficient for transition n of ion i. For forbidden lines we used the expression

$$F = \frac{h\nu}{16\pi} \frac{n_u A_{ul}}{r^2} V, \tag{2}$$

where n_u is the population density of the upper state and A_{ul} is the transition probability in s^{-1}. Using densities and temperatures determined from line ratios, we assumed standard PN abundances from Aller & Czyzak (1983), assumed that the different ions of a given element are physically segregated, and solved for V. The resulting volumes are sensitive to the measured line fluxes and to the assumed extinction, distance, densities, temperatures, and abundances. When comparing ions, many of these factors cancel out and the relative volumes are accurate to within about a factor of two.

As expected, a progression can be seen in the relative sizes of the He^{++} and H^+ regions. V1016 Cyg and HM Sge have the largest He^{++}/H^+ volume ratios at 0.8, followed closely by NGC 7027 at 0.6. The He^{++}/H^+ ratio is much smaller in the other objects. The ratio is 0.02 in NGC 6790,

0.015 in Vy 2−2, and 0.003 in Hubble 12. He II was not detected in AFGL 618. The approach of using the He II $\lambda4686/H\beta$ ratio to determine stellar temperatures was first introduced by Ambartsumyan (1932). From Fig. 1 in Kaler & Jacoby (1989), we infer central star temperatures of $T_{\text{eff}} \approx 2.2 \times 10^5$ K for HM Sge, $T_{\text{eff}} \approx 1.9 \times 10^5$ K for V1016 Cyg and NGC 7027, and $T_{\text{eff}} \approx 8 \times 10^4$ K for NGC 6790.

A second and perhaps more interesting result concerns the size of the [C I], [O I], [N I], and [S II] emitting regions, all of which lie outside of the hydrogen Strömgren sphere. The gas in these regions can be excited by shocks or by absorption of photons with less than 13.6 eV. In V1016 Cyg, NGC 7027, NGC 6790, and Vy 2−2, this region is very thin—less than 1% the radius of the Strömgren sphere (R_{str}). The thickness is roughly 0.1 R_{str} in HM Sge, where dust shielding protects the low ionization species, 0.3 R_{str} in Hubble 12, and 6.6 R_{str} in AFGL 618. These numbers are partly influenced by the use of small apertures. Still, it is apparent that not very much PDR gas is excited in most planetary nebulae. The exceptions, Hubble 12 and AFGL 618, are very young. They have not had enough time to clear away much of the material that was ejected on the AGB, and their expanding nebulae are still sweeping through material that was ejected late on the AGB, while the mass loss rate was very high. Both have fluorescent H_2 transitions in their spectra.

In summary, the line ratios of an individual ion are determined by T_e and n_e, and we have determined these values for many of the objects. The relative ion strengths, on the other hand, depend on many parameters, including T_*, the evolution of the object, the excitation mechanisms, and the clumpiness of the gas. With our infrared data, we have been able to isolate each of these factors. We see that shocks are very important to the shaping and excitation of PN, clumps appear to be a common feature in PN envelopes, and young PN produce the strongest PDR emission because they have the largest reservoir of nearby molecular and low ionization gas.

REFERENCES

Acker, A., Köppen, J., Stenholm, B., & Jasniewicz, G. 1989, A&AS, 80, 201
Allard, F. 1992, personal communication
Aller, L. H., & Czyzak, S. J. 1983, ApJS, 51, 211
Ambartsumyan, V. A. 1932, Pulkovo Obs. Circ. Vol. 8, No. 4
Balick, B. 1987, AJ, 94, 671
Balick, B., Gonzalez, G., Frank, A., & Jacoby, G. 1992, ApJ, 392, 582
Balick, B., Rugers, M., Terzian, Y., & Chengalur, J. N. 1993, ApJ, 411, 778
Barker, T. 1978, ApJ, 219, 914
Becklin, E. E., Frogel, J. A., Hyland, A. R., Kristian, J., & Neugebauer, G. 1969, ApJ, 158, L133
Black, J. H., & van Dishoeck, E. F. 1987, ApJ, 322, 412
Clegg, R. E. S. 1987, MNRAS, 229, 31P
Cohen, M., et al. 1975, ApJ, 196, 179
Davidson, K., Humphreys, R. M., & Merrill, K. M. 1978, ApJ, 220, 239

Dinerstein, H. L., Lester, D. F., Carr, J. S., & Harvey, P. M. 1988, ApJ, 327, L27
Feibelman, W. A. 1993, PASP, 105, 595
Gehrz, R. D. 1988, ARA&A, 26, 377
Goebel, J. H., Bregman, J. D., Witteborn, F. C., Taylor, B. J., & Willner, S. P. 1981, ApJ, 246, 455
Graham, J. R., Serabyn, E., Herbst, T. M., Matthews, K., Neugebauer, G., Soifer, B. T., Wilson, T. D., & Beckwith, S. 1993, AJ, 105, 250
Hora, J. L., & Latter, W. B. 1994, ApJ, 437, 281
Hrivnak, B. J., Kwok, S., & Geballe, T. R. 1994, ApJ, 420, 783
Humphreys, R. M., Warner, J. W., & Gallagher, J. S. 1976, PASP, 88, 380
Jones, T. J., et al. 1993, ApJ, 411, 323
Jura, M. 1986, IAJ, 17, 322
Kaler, J. B. 1976, ApJS, 31, 517
Kaler, J. B., & Jacoby, G. H. 1989, ApJ, 345, 871

Kastner, J. H., Gatley, I. Merrill, K. M., Probst, R., & Weintraub, D. A. 1994, ApJ, 421, 600

Kelly, D. M. 1993, Ph.D. thesis, University of Arizona

Kelly, D. M., Latter, W. B., & Rieke, G. H. 1992, ApJ, 395, 174

Kirkpatrick, J. D., Kelly, D. M., Rieke, G. H., Liebert, J., Allard, F., & Wehrse, R. 1993, ApJ, 402, 643

Kwok, S. 1993, ARA&A, 31, 63

Kwok, S., Purton, C. R., & Fitzgerald, P. M. 1978, ApJ, 219, L125

Latter, W. B., Kelly, D. M., Hora, J. L., Deutsch, L. K., & Rieke, G. H. 1994, ApJ (submitted)

Latter, W. B., Hora, J. L., Kelly, D. M., Deutsch, L. K., & Maloney, P. R. 1993, AJ, 106, 260

Latter, W. B., Maloney, P. R., Kelly, D. M., Black, J. H., Rieke, G. H., & Rieke, M. J. 1992, ApJ, 389, 347

Le Bertre, T. 1988, A&A, 203, 85

Lockwood, G. W. 1969, ApJ, 157, 275

Lockwood, G. W. 1973, ApJ, 180, 845

Miller, J. S. 1970, ApJ, 161, L95

Nussbaumer, H., & Schild, H. 1981, A&A, 101, 118

O'Brien, G. T., & Lambert, D. L. 1986, ApJS, 62, 899

Oudmaijer, R. D., Geballe, T. R., Waters, L. B. F. M., & Sahu, K. C. 1994, A&A, 281, L33

Rix, H.-W., Carleton, N. P., Rieke, G., & Rieke, M. 1990, ApJ, 363, 480

Rudy, R. J., Rossano, G. S., & Puetter, R. C. 1989, ApJ, 346, 799

Rudy, R. J., Cohen, R. D., Rossano, G. S., & Puetter, R. C. 1990, ApJ, 362, 346

Rudy, R. J., Rossano, G. S., Erwin, P., & Peutter, R. C. 1991a, ApJ, 368, 468

Rudy, R. J., Cohen, R. D., Rossano, G. S., Erwin, P., Puetter, R. C. & Lynch, D. K. 1991b, ApJ, 380, 151

Rudy, R. J., Erwin, P., Rossano, G. S., & Puetter, R. C. 1992, ApJ, 384, 536

Rudy, R. J., Rossano, G. S., Erwin, P., Puetter, R. C., & Feibelman, W. A 1993, AJ, 105, 1002

Schild, H., Boyle, S. J., & Schmid, H. M. 1992, MNRAS, 258, 95

Schmid, H., & Schild, H. 1990, MNRAS, 246, 84

Schönberner, D. 1987, in Planetary and Proto-Planetary Nebulae: From IRAS to ISO, edited by A. Preite Martinez (Reidel, Dordrecht), p. 113

Schwarz, H. E., Corradi, R. L. M., & Melnick, J. 1992, A&AS, 96, 23

Stranghellini, L., & Kaler, J. B. 1989, ApJ, 343, 811

Thompson, R. I., Schnopper, H. W., Mitchell, R. I., & Johnson, H. L. 1969a, ApJ, 158, L55

Thompson, R. I., Schnopper, H. W., Mitchell, R. I., & Johnson, H. L. 1969b, ApJ, 158, L117

Thronson, H. A. 1982, AJ, 87, 1207

Thronson, H. A. & Harvey, P. M. 1981, ApJ, 248, 584

Wing, R. F. 1967, Ph.D. thesis, University of California, Berkeley

Zirin, H. 1976, ApJ, 208, 414

High resolution mid-infrared spectroscopy of interstellar ices

John H. Lacy   Dept. of Astronomy, University of Texas at Austin

Hassan Faraji   Dept. of Physics, University of Texas at Austin

Observations

Spectra were measured between 7 and 13 μm with Irshell (Lacy et al. 1989) on the NASA IRTF of the embedded infrared sources W33 A, NGC 7538 IRS 1, NGC 7538 IRS 9, and W3 IRS 5. A low resolution grating and a coarse image scale were used to obtain a spectral resolution of $\Delta\lambda \approx 0.01$ μm. The 10×64 pixel detector array covered $\sim 24'' \times 0.25$ μm at each grating setting. To cover the entire 7-13 μm spectral region, the grating angle was stepped so that each pixel independently sampled the spectrum. The overlap between scans by the different pixels were then used to measure and correct for flux variations caused by guiding and seeing. Telluric absorption was corrected by division by similarly measured spectra of Vega and Capella. Optical depths were derived from the measured fluxes by dividing by black body spectra passing through points at the ends of the observed spectral regions. By doing this, we assumed that the interstellar extinction is zero near 7 and 13 μm and that the underlying sources are black bodies. Neither assumption is correct, but the errors introduced should not affect seriously the relatively narrow features of interest. Additional details of the data reduction are given by Lacy et al (1991) and Faraji (1994).

Solid-State Absorption Features

The spectra of all observed sources are dominated by the 10 μm silicate absorption feature. Two procedures were used to try to remove this feature to allow weaker features to be seen. First, a polynomial fit was made to the derived optical depths near a suspected feature. This procedure appeared to be successful in the 1250-1350 cm^{-1} (7.4-8.0 μm) region where several relatively narrow features were seen, but was less clearly valid for broader features nearer the center of the silicate absorption. Consequently, a second procedure involving subtraction of optical depth curves of different sources, scaled to make their silicate features match, was also used.

Six additional features were seen, at 825 cm^{-1} (12.1 μm), 885 cm^{-1} (11.3 μm), 1125 cm^{-1} (8.9 μm), 1300 cm^{-1} (7.7 μm), 1320 cm^{-1} (7.6 μm), and 1350 cm^{-1} (7.4 μm). The observed widths and optical depths of these features in each source are given in Table 1, along with possible identifications. All of the observed interstellar features coincide with absorption bands of molecules that have been observed in the laboratory, with multiple identifications possible for many of the features.

Identifications with Molecular Ices

Of the possible identifications listed in Table 1, CH$_3$OH and NH$_3$ have most frequently been discussed as likely grain-mantle constituents. CH$_3$OH has been thought to be abundant, based on its identification with the strong 6.85 μm feature. However, several authors have questioned this identification, or at least the large abundance derived from it, because of the weakness of other CH$_3$OH features (Grim et al. 1991; Schutte et al. 1991; Skinner et al. 1992). CH$_3$OH has two features in the region we observed, at 1026 and 1128 cm^{-1} (Schutte et al.). The former is at the center of the silicate feature and the telluric O$_3$ absorption, but probably should have been detectable at least in NGC 7538/9, if present. The latter wavenumber matches that at which a feature was observed toward W33 A and NGC 7538/9, but the laboratory absorption is only 35 cm^{-1} wide and relatively unaffected by solid environment. In addition, laboratory spectra show the 1026 cm^{-1} absorption to be $\sim$10 times as deep as the 1128 cm^{-1} feature, a ratio which is ruled out for NGC 7538/9 (1026 cm^{-1} was unobservable toward W33 A). NH$_3$ also has a feature near

9 μm wavelength (and no others in our spectral region). Crystalline NH_3 absorbs at 1050 cm^{-1} with a FWHM of only 14 cm^{-1}, whereas amorphous NH_3 absorbs at 1065 cm^{-1} with a FWHM of 65 cm^{-1} (Moore et al. 1994). Neither matches our observed feature at 1125 cm^{-1}, but Moore et al. found a metastable phase of NH_3 to form on annealing amorphous NH_3 at 110K, which has a peak absorption at 1097 cm^{-1} and FWHM of 20 cm^{-1}. NH_3 may contribute at least part of the interstellar feature.

CH_4 is also thought to be present in grain mantles, and in fact is likely to form there (Brown et al. 1988). Lacy et al. (1991) identified the 1300 cm^{-1} absorption toward NGC 7538/1 and 7538/9 and possibly the broader feature toward W33 A with CH_4. CH_4 has no other features in the region observed, so we cannot test this identification, but we note that several molecules discussed below also absorb near this frequency.

Three other molecules appear as possible identifications of observed features in Table 1. The NO_3^- ion absorbs at 820 and 1337 cm^{-1} in our spectral region (Grim et al. 1989). The former matches our observed 825 cm^{-1} feature, and the latter falls near our 1350 cm^{-1} feature, both of which are seen toward W33 A. We know of no other identifications of these features, but hesitate to consider this a detection. The $HCOO^-$ ion absorbs at 887, 1263, and 1304 cm^{-1} (Grim et al.). The first and third of these match observed features toward W33 A, NGC 7538/1, and NGC 7538/9, although the second was not seen. Finally, N_2H_2 has bands at 1300 and 1306 cm^{-1} (Grim et al; 1290 and 1315 cm^{-1} according to Hagen 1982), in close agreement with our 7.7 and 7.6 μm features, and providing another alternative to the identification of CH_4.

Table 1: Observed Features, Optical Depths, and Identifications

ν_0(cm^{-1})	FWHM	W33 A	NGC7538/1	NGC7538/9	W3/5	IDs
825	20	0.2	—	—	—	NO_3^-
885	30	0.4	0.1	0.1	n.o.	$HCOO^-$
1125	55	1.2	—	0.5	—	CH_3OH, NH_3
1300	10	0.33[1]	0.11	0.10	n.o.	CH_4, $HCOO^-$, N_2H_2
1320	10		0.09	—	n.o.	NO_3^-, N_2H_2
1350	15	0.14	0.05	n.o.	n.o.	NO_3^-

—: not detected; optical depth <.05 cm^{-1}.

n.o.: wavelength not observed.

[1]: a single broad feature centered at 1310 cm^{-1}.

References

Brown, P. D., Charnley, S. B., & Millar, T. J. 1988, MNRAS, 231, 409

Grim, R. J. A., Baas, F., Geballe, T. R., Greenberg, J. M., & Schutte, W. 1991, A&A, 243, 473

Grim, R. J. A., Greenberg, J. M., de Groot, M. S., Baas, F., Schutte, W. A., & Schmitt, B. 1989, A&AS, 78, 161

Faraji, H. 1994, M. S. Thesis, University of Texas, Austin

Lacy, J. H., Achtermann, J. M., Bruce, D. E., Lester, D. F., Arens, J. F., Peck, M. C., & Gaalema, S. D. 1989, PASP, 101, 1166

Lacy, J. H., Carr, J. S., Evans, N. J., Baas, F., Achtermann, J. M., & Arens, J. F. 1991, ApJ, 376, 556

Moore, M. H., Ferrante, R. F., Hudson, R. L., Nuth, J. A., & Donn, B. 1994, ApJ, 428, L81

Schutte, W. A., Tielens, A. G. G. M., & Sandford, S. A. 1991, ApJ 382, 523

Skinner, C. J., Tielens, A. G. G. M., Barlow, M. J., & Justtanont, K. 1992, ApJ, 399, L79

159   **B14**

A search for interstellar gas-phase CO_2[*]

Gas: solid state abundance ratios

E.F. van Dishoeck[1], F.P. Helmich[1], Th. de Graauw[2,4], J.H. Black[3], A.C.A. Boogert[4], P. Ehrenfreund[1], P.A. Gerakines[5], J.H. Lacy[6], T.J. Millar[7], W.A. Schutte[1], A.G.G.M. Tielens[8], D.C.B. Whittet[5], D.R. Boxhoorn[2,9], D.J.M. Kester[2], K. Leech[9], P.R. Roelfsema[2,9], A. Salama[9], and B. Vandenbussche[9,10]

[1] Leiden Observatory, P.O. Box 9513, 2300 RA Leiden, The Netherlands
[2] SRON, P.O. Box 800, 9700 AV Groningen, The Netherlands
[3] Onsala Space Observatory, Chalmers University of Technology, S-43992 Onsala, Sweden
[4] Kapteyn Astronomical Institute, P.O. Box 800, 9700 AV Groningen, The Netherlands
[5] Department of Physics, Applied Physics & Astronomy, Rensselaer Polytechnic Institute, Troy, NY 12180, USA
[6] Department of Astronomy, University of Texas at Austin, Austin, TX 78712-1083, USA
[7] Department of Physics, UMIST, P.O. Box 88, Manchester M60 1QD, UK
[8] NASA-Ames Research Center, MS 245-3, Moffett Field, CA 94035, USA
[9] ISO Science Operation Center, Astrophysics Dvision of ESA, P.O. Box 50727, E-28080 Villafranca/Madrid, Spain
[10] Instituut voor Sterrenkunde, K.U. Leuven, Celestijnenlaan 200B, B-3001 Heverlee, Belgium

Abstract. We present searches for gas–phase CO_2 features in the ISO–SWS infrared spectra of four deeply embedded massive young stars, which all show strong solid CO_2 absorption. The abundance of gas–phase CO_2 is at most $2. \, 10^{-7}$ with respect to H_2, and is less than 5% of that in the solid phase. This is in strong contrast to CO, which is a factor of 10–100 more abundant in the gas than in solid form in these objects. The gas/solid state ratios of CO_2, CO and H_2O are discussed in terms of the physical and chemical state of the clouds.

Key words: ISM: abundances; ISM: molecules; ISM: individual: AFGL 2591, AFGL 4176, AFGL 2136, NGC 7538 IRS9

1. Introduction

Although more than 100 different molecules have been identified in the interstellar gas, some of the simplest species have remained elusive. Either their presence in the Earth's atmosphere has blocked astronomical observations, or they have no strong millimeter transitions because of their symmetry. CO_2 suffers from both problems, so that up to now only indirect searches of the chemically related $HOCO^+$ ion have been possible from

the ground (Thaddeus et al. 1981; Minh et al. 1988, 1991). The *Short Wavelength Spectrometer* (SWS) (de Graauw et al. 1996a) on board the *Infrared Space Observatory* (ISO) (Kessler et al. 1996) opens up the possibility to search for the infrared–active asymmetric stretch and bending modes of gas–phase CO_2 around 4.3 and 15.0 μm along the line of sight toward bright infrared sources.

CO_2 is predicted to be one of the more abundant carbon– and oxygen–bearing molecules in the gas phase (e.g., Herbst & Leung 1989; Millar et al. 1991), and as such forms a significant test case of the chemical networks. Moreover, the detection of abundant solid CO_2 in interstellar clouds by d'Hendecourt & de Muizon (1989) and de Graauw et al. (1996b) suggests that CO_2 could be a particularly sensitive probe of gas–grain interactions. The observed abundance of solid CO_2 with respect to hydrogen of about $\sim (1-5) \, 10^{-6}$ is a factor of 10 larger than that predicted by cold gas–phase models. Thus, large amounts of gas–phase CO_2 could be produced by the evaporation or destruction of icy grain mantles. Comparison of the observed gas/solid CO_2 ratios with those of other species known to be abundant in icy mantles, especially H_2O and CO, will allow us to address the formation route of CO_2.

We present here searches for gas–phase CO_2 in the spectra of four deeply embedded young stellar objects. Mitchell et al. (1989, 1990) have measured near–infrared absorption lines of gas–phase ^{12}CO and ^{13}CO for three of these objects (GL 2591, GL 2136, NGC 7538 IRS9) at high spectral resolution from the ground, which indicate the presence of both cold, $T_{kin} = 15 - 60$ K, and warm, $T_{kin} = 120 - 1000$ K, gas along the lines of

sight. We use these data, together with the new ISO data on solid CO$_2$ of de Graauw et al. (1996b) and on gaseous H$_2$O by van Dishoeck & Helmich (1996), to constrain the gas/solid abundance ratios for these objects.

2. Search for gas–phase CO$_2$

We searched for gas–phase CO$_2$ in the ISO–SWS spectra through its fundamental ro–vibrational ν_3 and ν_2 transitions at 4.257 and 14.984 μm, respectively. The observational data are the same as those used by de Graauw et al. (1996b) to investigate solid CO$_2$, and were taken with AOT06. At 15 μm, systematic instrumental noise was removed with a Fourier transform method.

Gas–phase molecules can be distinguished from solid state features at the resolving power $\lambda/\Delta\lambda \approx 2000$ of the SWS grating by their characteristic ro–vibrational structure. This is clearly illustrated in Figure 1, which contains the 4.1-4.7 μm spectrum of GL 2591. It shows the complete R–branch and part of the P–branch of the $v = 1-0$ band of gas–phase CO centered at 4.67 μm, together with the strong, broad single absorption feature due to solid CO$_2$. The lack of individual P– and R–lines due to gas–phase CO$_2$, together with the absence of any broad absorption feature due to solid CO, indicates a very different chemical behavior for the two species: most of the CO is in the gas phase, whereas most of the CO$_2$ is in solid form.

2.1. ν_3 band

In order to constrain the amount of gas–phase CO$_2$, simulated spectra have been made following the method of Helmich (1996). The frequencies and intensities of the lines in the ν_3 $\Sigma - \Sigma$ asymmetric stretch were taken from the HITRAN data base (Rothman et al. 1992a; see also Rothman et al. 1992b for the molecular parameters). All levels up $J''=90$ (corresponding to 4585 K above ground) were taken into account in the model. CO$_2$ is a symmetric molecule with zero nuclear spin so that all odd–numbered rotational levels are missing. The adopted Doppler parameters b and excitation temperatures are based on infrared absorption line observations of warm gaseous CO (Mitchell et al. 1990) (see Table 1). The CO$_2$ rotational excitation can also be affected by pumping by infrared radiation at 15 μm, but is likely to be thermalized at densities of $10^3 - 10^5$ cm^{-3} except in regions where the temperature characterizing the radiation field at 15 μm exceeds 75 K.

Figure 1 includes a simulated spectrum of gas–phase CO$_2$ for a column density of 5. 10^{16} cm^{-2}, b=7.5 km s^{-1}, and T_{ex}=250 K. The position of the gas–phase CO$_2$ ν_3 stretch is not shifted significantly from that of solid CO$_2$, so that the P– and R–branch structure will be superposed on the solid feature. Since such structure is not seen, 5. 10^{16} cm^{-2} is the maximum column density that could be hidden under the solid CO$_2$ feature. The inferred limit on the gas–phase CO$_2$ changes by at most a factor of 2 if b is varied from 5 to 12 km s^{-1} and T_{ex} from 100 to 500 K. No useful limits can be obtained on the amount of CO$_2$ in cold gas with small b-values (< 2 km s^{-1}) from the ν_3-band data.
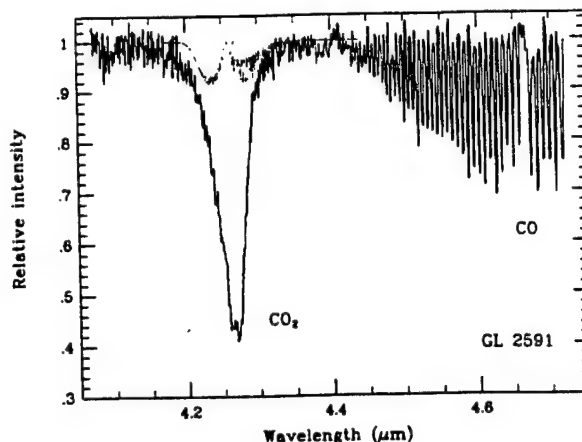

Fig. 1. ISO–SWS grating spectrum toward the embedded young stellar object GL 2591 in the 4.1–4.7 μm region. Broad absorption due to solid CO$_2$ is seen at 4.26 μm, as well as a forest of R– and P–branch lines between 4.4 and 4.7 μm due to warm, gas–phase CO. The light (dotted) line indicates the model absorption spectrum of gas–phase CO$_2$ using a column density of 5. 10^{16} cm^{-2}, b=7.5 km s^{-1} and T_{ex}=250 K.

Similar limits are obtained toward GL 4176 and GL 2136 (see Table 1). The ν_3 solid CO$_2$ feature toward NGC 7538 IRS9 is so strong and broad (see de Graauw et al. 1996b) that no useful limits can be obtained.

2.2. ν_2 band

More stringent constraints on the gas–phase CO$_2$ can be deduced from the ν_2 bending mode data. This transition is of $\Pi - \Sigma$ type and has a Q–branch in addition to the P– and R–branch lines. Because all Q–branch lines coalesce into a single feature at the resolving power of the ISO–SWS grating, the Q–branch produces stronger absorption, even though the ν_2 band is intrinsically a factor of 10 weaker than the ν_3 band. Moreover, the gas–phase ν_2 band is shifted by at least 0.2 μm to the blue compared with the solid CO$_2$ bending mode, and can therefore be more easily detected on the shoulder of the solid state feature. Finally, the continuum is stronger at 15 μm than at 4 μm in these objects, so that higher S/N can be achieved.

Figure 2 shows the ISO–SWS spectra of the four sources around 15 μm, with model CO$_2$ spectra included. The line frequencies have been calculated using the constants of Paso et al. (1980), whereas the band strength of Reichle & Young (1972) is adopted. These values agree well with those given in HITRAN. Two cases are considered. First, the same b–values and high excitation temperatures as for the ν_3 model spectra have been used. The resulting spectra for $N(CO_2)$=1. 10^{16} cm^{-2} are shown in Figure 2 for GL 2591 and GL 4176. Second, limits on the CO$_2$ in the cold, quiescent gas have been studied. For GL 2136 and NGC 7538 IRS9, T_{ex}=25 K and b=1.5 km s^{-1} are adopted. As Table 1 and Figure 2 show, the ν_2 band data are equally sensitive to the warm and the cold gas.

It is seen that in all four sources, a 3–4σ absorption feature is present at the position of the CO$_2$ ν_2 Q–branch. The corresponding CO$_2$ column densities are comfortably below the up-

Table 1. Inferred gas–phase CO_2 column densities and abundances

Object	ν_3 band cm^{-2}	ν_2 band^a cm^{-2}	$x(CO_2)^a$	T_{ex} K	b km s^{-1}
N7538 I9	...	$8.\,10^{15}$	$1.6\,10^{-7}$	200	5.0
	...	$8.\,10^{15}$	$1.6\,10^{-7}$	25	1.5
GL 2136	$< 5.\,10^{16}$	$1.\,10^{16}$	$9.0\,10^{-8}$	250	5.0
	...	$1.\,10^{16}$	$9.0\,10^{-8}$	25	1.5
GL 2591	$< 5.\,10^{16}$	$1.\,10^{16}$	$1.0\,10^{-7}$	250	7.5
GL 4176	$< 2.\,10^{16}$	$5.\,10^{15}$	$6.7\,10^{-8}$	250	5.0

^{a} Tentative values

Table 2. Gas/solid state abundance ratios^a

Object	CO	CO_2	H_2O
NGC 7538 IRS9	10	0.01	<0.04
GL 2136	200	0.02	0.4
GL 2591	>400	0.04	1.1
GL 4176	>400	0.04	2.2

^{a} Based on gas–phase CO from Mitchell et al. (1990), solid CO from Tielens et al. (1991) and Ehrenfreund et al. (1996, in preparation, GL 4176), solid CO_2 and solid H_2O from de Graauw et al. (1996b), and gas–phase H_2O from Helmich et al. (1996) and van Dishoeck & Helmich (1996)

per limits derived from the ν_3 band data. The Q–branch data are highly suggestive of the presence of gas–phase CO_2, especially toward GL 2136 and NGC 7538 IRS9. The major problem with the identification is the limited S/N of the data. The presence of gas–phase CO_2 could be confirmed through high S/N, high resolution Fabry–Perot data. The feasibility of such observations is currently uncertain, but until better data are obtained the column densities listed in Table 1 should be regarded as tentative.

2.3. Gas–phase CO_2 abundance

The column densities of $\sim 10^{16}$ cm^{-2} derived above correspond to gas–phase CO_2 abundances with respect to total H_2 of $\sim 10^{-7}$ (see van Dishoeck & Helmich 1996 for the adopted H_2 column densities). These abundances are more than an order of magnitude smaller than the limits of $< 2.\,10^{-6}$ (or $CO_2/CO<0.01$) derived from HOCO$^+$ by Minh et al. (1988) for several clouds, including NGC 7538. HOCO$^+$ has been detected in Galactic Center clouds, with an inferred CO_2 abundance of $\sim 10^{-5}$.

Pure gas–phase models predict steady–state CO_2 abundances of $3.6\,10^{-7}$ (Millar et al. 1991) and $(1.3 - 4.4)\,10^{-7}$ (Herbst & Leung 1989) using dark cloud parameters. At higher temperatures, $\sim 7.\,10^{-7}$ is found (Helmich 1996). Thus, the observed CO_2 abundances are even lower than expected from pure gas–phase chemistry. The primary production route is through $CO + OH \rightarrow CO_2 + H$, whereas destruction in cold clouds occurs by cosmic ray induced photons, and reactions with ions such as H_3^+, H^+, He^+, C^+ and N_2H^+.

3. Gas/solid state abundance ratios

The derived column densities of gas–phase CO_2 of at most 10^{16} cm^{-2} are significantly lower than the observed column densities of solid CO_2 of $10^{17} - 10^{18}$ cm^{-2} for the same lines of sight (de Graauw et al. 1996b). Thus, typically less than 5% of the CO_2 is in the gas phase. This is in strong contrast with CO and H_2O. Table 2 lists the gas/solid state abundance ratios for the three species for the four sources. It is seen that in all four sources, CO is principally in the gas phase, whereas the gas/solid state H_2O ratio varies from less than 4% for NGC 7539 IRS9 to unity for GL 2591 and GL 4176.

It is tempting to ascribe the latter variation to an increase in the amount of high temperature gas and dust. The CO data of Mitchell et al. indicate that less than 2% of the gas is at $T_{kin} >100$

K in NGC 7538 IRS9, whereas this fraction is 50-70% for GL 2591 and GL 2136. The H_2O icy mantles start to evaporate when the dust temperature is 90 K or higher. Alternatively, shocks associated with the outflows could have removed the ice mantles and created high–temperature conditions in which H_2O is rapidly produced through neutral–neutral gas–phase reactions. All three sources are known to have massive outflows, but in GL 2591 and GL 2136 the outflows have apparently affected a larger volume of the surrounding cloud than in NGC 7538 IRS9. If this is an evolutionary effect, it would indicate that NGC 7538 IRS9 is at an earlier state than the other two sources. Less information is available for GL 4176, but the fact that it has the smallest abundance of solid CO_2 and H_2O of the sources studied here and no solid CO absorption suggests a large fraction of high temperature gas.

The large fraction of CO in the gas phase is not surprising, because solid CO readily evaporates at dust temperatures above 20 K. The real mystery is why the gas to solid ratio of H_2O is so much larger than that of CO_2 in three of the sources. If evaporation of icy mantles were the main production mechanism, the CO_2 gas/solid state ratio would be expected to be comparable to or larger than that of H_2O, because its sublimation temperature of $\sim45-72$ K is lower than that of H_2O (Sandford & Allamandola 1990).

There are at least four possible explanations for this dilemma. The first, unlikely possibility is that solid CO_2 is trapped in a matrix or clathrate which only allows evaporation at much higher temperatures than H_2O. Second, one can speculate that, perhaps due to the chemistry involved, solid CO_2 is characteristic for ices in dark clouds and not for (high density) regions which collapse and form stars. In that case, CO_2–containing ices may never be heated to the sublimation temperature of CO_2.

Third, CO_2 could be destroyed on short time scales ($< 10^4$ yr) in the hot, dense gas following evaporation. Most reactions of CO_2 with abundant species (H, O, N, C, ...) have huge activation energies. However, there are some species for which the rates are larger. For example, Si atoms react with CO_2 to form SiO and CO with a rate coefficient of $1.1\,10^{-11}$ cm^3 s^{-1} at 300 K (Husain & Norris 1978). This could be an effective destruction path if Si atoms were present with an abundance of 10^{-7} or more. Alternatively, CO_2 could be effectively destroyed in the vibrationally excited state.
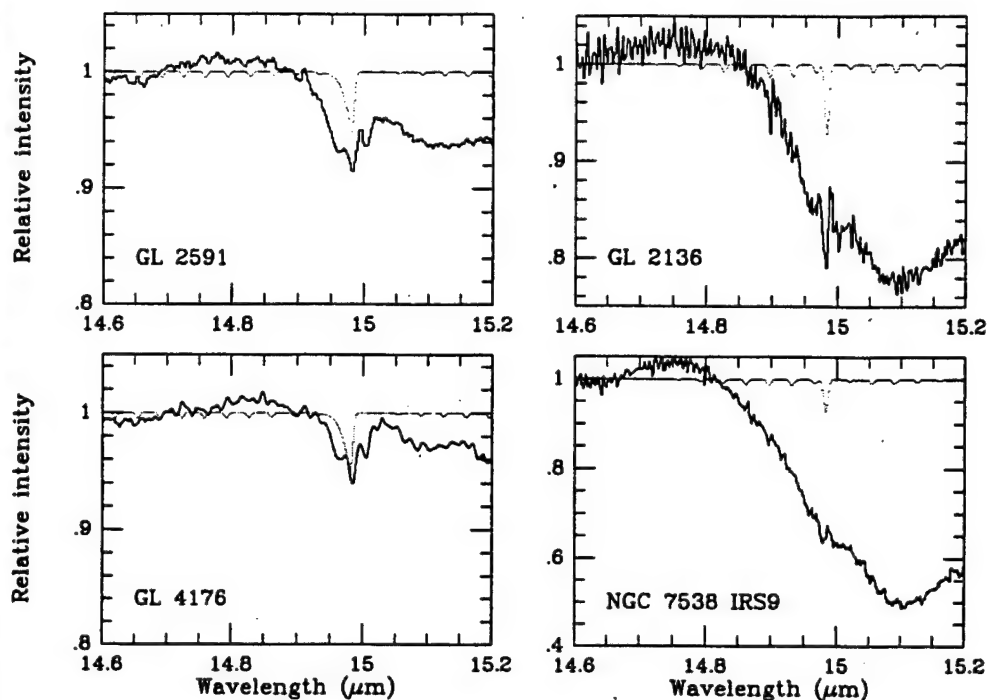
Fig. 2. Normalized ISO–SWS grating spectra toward four embedded young stellar objects around $15\mu m$. The broad absorption feature starting around $14.8\ \mu m$ is due to solid CO_2. The light (dotted) lines indicate the model absorption spectra of gas–phase CO_2 for $N(CO_2)=1.\ 10^{16}\ cm^{-2}$. For GL 2591 and GL 4176, the same b and T_{ex} as for the ν_3 band are used. For GL 2136 and NGC 7538 IRS9, $b=1.5\ km\ s^{-1}$ and $T_{ex}=25$ K are adopted, resulting in a narrower Q–branch feature.

The final, perhaps most plausible explanation is that a large fraction of the observed gas–phase H_2O does not originate from icy mantles but from high–temperature gas–phase reactions in shocks or radiatively heated gas. This scenario can be tested by observations once a larger data set is available (van Dishoeck & Helmich 1996). Also, comparison with the gas/solid state ratios of other species such as CH_4, C_2H_2 and HCN, which are not readily produced by high temperature reactions, should provide insight (Carr et al. 1995, Boogert et al. 1996). Observations of the HDO/H_2O ratio could test this scenario as well.

In summary, the ISO–SWS observations demonstrate that gas–phase CO_2 is not abundant in interstellar clouds, in spite of the ubiquitous presence of solid CO_2. Further searches for gas–phase CO_2 and other species in a larger variety of sources are warranted to test the different explanations. This study also demonstrates the potential of ISO to obtain reliable gas to solid state abundance ratios, which should provide insight into the physical and chemical evolution during star formation.

References

Boogert, A.C.A., et al. 1996, this volume
Carr, J., Evans, N.J., Lacy, J.H., Zhou. S. 1995, ApJ 450, 667
de Graauw, Th., et al. 1996a, this volume
de Graauw, Th., et al., 1996b, this volume

d'Hendecourt, L., Jourdain de Muizon, M. 1989, A&A 223, L5
Helmich, F.P., 1996, PhD thesis, University of Leiden
Helmich, F.P., et al. 1996, this volume
Herbst, E., Leung, C.M., 1989, ApJS 69, 271
Husain, D., Norris, P.E., 1978, J. Chem. Soc. Far. Trans. 74, 106
Kessler, M.F. et al. 1996, this volume
Millar, T.J., Rawlings, J.M.C., Bennett, A., Brown, P.D., Charnley, S.B., 1991, A&AS 87, 585
Minh, Y.C., Irvine, W.M., Ziurys, L.M., 1988, ApJ 334, 175
Minh, Y.C., Brewer, M.K., Irvine, W.M., Friberg, P., Johansson, L.E.B., 1991, A&A 244, 470
Mitchell, G.F., Curry, C., Maillard, J.-P., Allen, M., 1989, ApJ 341, 1020
Mitchell, G.F., Maillard, J.-P., Allen, M. 1990, ApJ 363, 554
Paso, R., Kauppinen, J., Antilla, R., 1980, J. Mol. Spectrosc. 79, 236
Reichle, H.G., Young, C., 1972, Can. J. Phys. 50, 2662
Rothman, L.S., Gamache, R.R., Tipping, R.H. et al., 1992a, J. Quant. Spectrosc. Radiat. Transfer 48, 469
Rothman, L.S., Hawkins, R.L., Wattson, R.B., Gamache, R.R., 1992b, J. Quant. Spectrosc. Radiat. Transfer 48, 537
Sandford, S.A., Allamandola, L.J., 1990, ApJ 355, 357
Thaddeus, P., Guelin, M., Linke, R.A. 1981, ApJ 246. L41
Tielens, A.G.G.M., Tokunaga, A.T., Geballe, T.R., Baas. F., 1991, ApJ 381, 181
van Dishoeck, E.F., Helmich. F.P., 1996, this volume

This article was processed by the author using Springer-Verlag LaTeX A&A style file *L-AA* version 3.

MID INFRARED HYDROGEN RECOMBINATION LINE EMISSION
FROM THE MASER STAR MWC 349A

Howard A. Smith [1,3], V. Strelnitski [2,3], J.W. Miles [3,4], D. M. Kelly [3,5,6], and J.H. Lacy [3,5]

[1] Harvard-Smithsonian Center for Astrophysics, 60 Garden Street, Cambridge, MA 02138

[2] Martha Mitchell Observatory, Nantucket, MA

[3] Visiting Observer at the NASA Infrared Telescope Facility, Mauna Kea, HI

[4] Lockheed Martin Advanced Technology Center, 3251 Hanover Street, Palo Alto, CA 94304

[5] Department of Astronomy, University of Texas, Austin, Texas 78712

[6] Current Address: Dept. of Physics and Astronomy, Univ. of Wyoming, Laramie, WY 82071-3905

August 20, 1997

1

ABSTRACT

We have detected and spectrally resolved the mid-IR hydrogen recombination lines H6α (12.372μm), H7α (19.062μm), H7β(11.309μm) and H8γ(12.385μm) from the star MWC349A. This object has strong hydrogen maser emission reported in the millimeter and submillimeter hydrogen recombination lines from H36α to H21α, and laser emission seen in the H15α, H12α and H10α lines. The lasers/masers are thought to arise predominantly in a Keplerian disk around the star. The mid-IR lines we measure do not show evident signs of lasing, and can be adequately modeled as arising from the strong stellar wind, with a component arising from a quasi-static atmosphere around the disk, similar to what is hypothesized for the near IR ($\leq 4\mu$m) recombination lines. Since population inversions are expected to exist in the levels producing these mid-IR transitions, even at electron densities where they could produce significant amplification (from 10^8 cm^{-3} even up to 10^{11} cm^{-3}), our results imply that the disk does not contain such high-density ionized gas over long enough path lengths to produce a gain ≥ 1. More modest laser emission might be present from smaller zones, for example from high density clumps within the disk, but is minor compared to the spontaneous background line emission from the rest of the source. The results reinforce the interpretation of the three reported far-IR lines as true lasers.

Subject Headings: circumstellar matter - stars: emission-line, Be - stars: individual (MWC349A) - stars: mass loss - infrared: sources - infrared: spectra, masers

2

I. INTRODUCTION

MWC349A, the brightest radio continuum star in the sky, has a strong bipolar wind with mass loss estimated at $\sim 10^{-5}$ $M_{\odot} yr^{-1}$ (Cohen *et al.*, 1985), or even as much as $\sim 9 \times 10^{-5}$ $M_{\odot} yr^{-1}$ (Martin-Pintado, Bachiller, Thum and Walmsley, 1989). It is surrounded by a Keplerian disk of ionized gas seen edge-on (e.g., Hamann and Simon, 1986; Gordon, 1992; Thum, Martin-Pintado and Bachiller, 1992; Ponomarev, Smith and Strelnitski, 1994, hereafter Paper I; Strelnitski, Smith and Ponomarev, 1996, hereafter Paper III). The source is so far the only confirmed emitter of strong hydrogen recombination line masers and lasers in the millimeter (e.g., Martin-Pintado *et al.*, 1989a,b) and far infrared (Strelnitski *et al.*, 1996, hereafter Paper IV). Laser emission (for simplicity we will use the term laser when both maser and laser are meant) is seen in a series of Hnα lines (that is, transitions with n+1 $\rightarrow$ n) starting from about the H40α line at 135GHz (2.22 mm) and extending down at least as far as the H15α line at 169μm (Paper IV), with likely amplification seen even at the H10α line at 52.5μm (op cit.), and in one Hnβ line, the H32β at 366 GHz (Thum *et al.*, 1995).

Continuing from both ends of this string of lasing lines are many other recombination lines which have been reported from this source. At radio wavelengths lines have been reported out to the H92α line at 3 cm (Rodriguez and Bastian, 1994), and from the opposite extreme they continue through the near infrared H4α (4.05μm, Hamann and Simon 1986) into the visible H2α=Hα (6524Å, Kelly, Rieke and Campbell, 1994). In addition in the near IR higher order recombination lines are seen — Hnβ, Hnγ, and above (e.g., Kelly, Rieke and Campbell; Hamann and Simon, 1988). Absent from this long series of transitions, covering over four orders of magnitude in wavelength, are the lines in the critical region between 4μm and 52.5μm. The mid-IR range is important for two reasons. First, somewhere in this region the detected lasing disappears, despite theoretical indications that the populations of the corresponding levels are inverted. Observationally the strength of the lasing is seen to decrease from its peak in the submillimeter, where the excess above the expected spontaneous emission is a factor of ~200 (Paper III and Paper IV), towards shorter wavelengths

3

where it has a values of ~6 at 52μm. Similarly on the long wavelength side the maser action dies off longward of about the H40α line (e.g., Paper III). The second reason for the importance of the mid-IR lines is that, if lasing, they would be sampling higher density gas thought to arise at the inner edges of the disk, closer in than the ~5AU modeled for the H15α line (Paper IV). In this paper we report on velocity resolved infrared spectra of four recombination lines in this interval, and discuss their relative intensities and profiles.

A great advantage of the masing transitions has been that the strong, velocity resolved emission of this sequence enables detailed modeling of the environment, although these models are complicated by the fact the lines show substantial, rapid and complex time variations. The bipolar wind is recognized as being the source of the strong radio continuum flux, and of the non-masing centimeter radio recombination lines (Rodriguez and Bastian, 1995). Although early suggestions also proposed it as the source of the intense maser lines (Martin-Pintado *et al.*, 1989a,b) it is now clear that at least the strong, double-peaked emission arises from the disk and not the wind (e.g., Gordon, 1992; Thum, Martin-Pintado and Bachiller, 1992). A portion of the "pedestal component" may also arise in the wind. A specific model has been proposed for such "photoevaporated" Keplerian disk structures by Hollenbach *et al.* (1994), and has been used to obtain physical parameters of the disk (Paper IV). The non-masing near-IR and optical hydrogen recombination lines, as well as a plethora of other atomic lines, have been attributed to various zones of ionization along the radius of the Keplerian disk (Hamann and Simon, 1986), as have the lasing far-IR lines (Paper IV).

Maser and laser amplification in the submillimeter and FIR lines implies quite high densities, $N_e > 10^{6-7}$ cm^{-3} (e.g., Paper I; Strelnitski, Ponomarev and Smith, 1966, hereafter Paper II). The presence of very high densities of circumstellar ionized gas in this source, even as high as $N_e \geq 10^{10}$ cm^{-3}, was proposed by Hamann and Simon (1986; 1988) to explain the emission from [FeII] and [FeIII]. Kelly, Rieke and Campbell (1994) also found evidence for densities $N_e \geq 10^6$ cm^{-3} in their near-IR spectra. Smith, Larson and Fink (1979) had earlier suggested lasing in the abnormally bright infrared hydrogen Pfβ line from Orion/BN, but noted that at the high densities implied (>10^{10} cm^{-3}) improved models for the hydrogen levels populations were needed to model the line strengths.

4

Hummer and Storey (1992) and Storey and Hummer (1995) have recently provided such calculations, with densities that extend beyond $N_e \geq 10^{10}$ cm^{-3}. We have used their tables (Papers I, II and III) to model the maser and laser emission from MWC349, and to confirm in particular the prediction that population inversions persist to these high densities. The transitions having maximal laser gain shift steadily towards lower quantum number n as the density increases, and so at densities above $N_e >$ $10^{7.4}$ cm^{-3} the far and mid infrared Hnα lines are expected to be efficient amplifiers. Moreover very large gain coefficients are expected from even modest sized regions because the densities are so high. Since the gain is nominally proportional to the density squared, the H7α line for example has its characteristic length (i.e., where τ=1) as only 3×10^9 cm at $N_e \geq 10^{10}$ cm^{-3} (c.f. Paper II), suggesting these lines might be detectable and useful probes of the inner few AU.

We observed a set of mid-IR recombination lines to determine whether, given the theoretical possibility of inverted populations and high gains, the trend of observable lasing lines continues down into the mid IR in MWC349A, and to determine whether this enables us to refine further the parameters of the Keplerian disk. The result might help shed further light on the remarkable fact that despite the ubiquitous inversions predicted in hydrogen only MWC349A to date shows unambiguous and strong laser emission. In this paper we report our results: velocity resolved observations of four mid-IR hydrogen recombination lines from MWC 349A -- the H7α line at 19.062μm, the H6α line at 12.372μm, the H7β line at 11.309μm, and the H8γ line at 12.385μm.

5

II. OBSERVATIONS AND ANALYSIS

a) Instrumental and Observational Summary

The hydrogen recombination lines were measured from the NASA Infrared Telescope Facility on the nights of June 7 and 8, 1994, with a followup search for time variability one year later, in July 10, 1995. Table 1 shows a log of the observations. The Irshell spectrometer used a 1" slit width and had a resolution of 20-30 kms^{-1}. Flatfielding was done using a dome-temperature card chopped against the sky. Atmospheric corrections were done by observing the standard χ Cyg immediately before and after each observation, flatfielding in the same way as the source spectrum, normalizing the average spectrum to unity, and dividing it into the source spectrum. Flux calibration was done by normalizing the continuum flux of the observed spectra to an average spectrum generated by fitting the photometric observations between 9 and 20 μm of Simon (1974), Simon and Dyck (1977), Herzog, Gehrz and Hackwell (1980), and Aitken *et al.*, (1990). Velocity calibration was done using the telluric lines in each spectrum. In general the fluxes are precise to 5-10%. Data files were processed using Irshell's own software; further information on the instrument and software can be found in Lacy *et al.* (1989), and Achtermann (1992).

Figure 1a shows the 19μm spectrum, as well as four gaussian profiles into which it can be decomposed. Figure 1b shows the 12.4μm spectrum containing both the H6α and H8γ lines, along with gaussian decompositions. Figure 1c shows the 11.3μm spectrum containing the H7β line. The locations of telluric features are also marked throughout. Table 1 lists the observed parameters of the four measured lines and their decompositions; repeat observations in 1995 showed no variations.

6

b) Lasing, or Optically Thin Emission ?

In presenting their analysis of the FIR lasing lines H15α, H12α and H10α, Strelnitski *et al.* (Paper IV) point out the trend, first described by them in Paper III, that the integrated Hnα lines fluxes in the millimeter and far IR regime (H36α - H10α) deviate in intensity from that expected from optically thin, spontaneous emission. The latter is shown to be a smooth curve nominally proportional to n^{-6} to n^{-4}, where n is the principal quantum number, and the range in exponent is due to the increasing importance of free-free absorption at the longer wavelengths. Strelnitski *et al.* use this excess emission over the optically thin value to show that the FIR lines measured from the KAO are lasing, but with a smaller amplification than the maximal amplification values seen in the submillimeter. The integrated values of the two mid-IR α-lines presented here fall close to the expected spontaneous emission values predicted by the aforementioned dependence, providing evidence that the net emission in these lines has indeed not been significantly amplified. In the next section we show this in more detail.

c) Emission from the Wind and the Disk

The source structure of MWC349A is complex. Hamann and Simon (1988) delineate at least five different emission regions, and Kelly, Rieke and Campbell (1994) also find evidence for each of them in the near-IR. Rodriguez and Bastian (1994) observed the H92α line and conclude the bipolar wind is itself rotating. Finally the variability and asymmetries of the maser line profiles (e.g., Thum *et al.*, 1994) indicate both complex substructure in the disk and possible infall. Many of these structural subtleties are still under debate, but we think it is safe to admit that at least two distinct regions contribute to the recombination line fluxes we present here: the bipolar wind, and the quasi-static, ionized atmosphere of the Keplerian disk.

In order to calculate the absolute flux contribution to the mid-IR fluxes from the bipolar wind we normalize the flux calculation to one of the observed wind line fluxes in an attempt to correct for parametric uncertainties, but chosing a reference line is not straightforward. The millimeter lines are

7

dominated by masing in the disk. Even for the longer wavelength H66α line there is a suggestion that it has some component of masing, but in the wind (Martin-Pintado *et al.*, 1993). We therefore select the H92α line measured by Rodriguez and Bastian (1994), and Rodriguez (private communication) at $(7.6 \pm .8) \times 10^{-27}$ W/cm². It shows no evidence for anything except normal emission from a strong, ionized wind. Indeed the radio *continuum* emission from MWC349A follows an $L_\nu \propto \nu^{0.6}$ law down to wavelength of about 100μm, as is characteristic of such an optically thick flow. The hydrogen lines from such a wind sample surfaces of optical depth $\tau \approx 1$. We calculate their fluxes assuming the wind has a constant velocity flow $V = V_i (r/r_i)^s$ with s=0 (e.g., Smith, Fischer, Geballe and Schwartz, 1987; Panagia and Felli, 1975), and we then normalize the values to the H92α flux. The results are plotted as the solid line in Figure 2; fluxes for the entire series of Hα lines from H4α to H16α (wavelengths indicated by triangles on the x-axis), including those lines not yet reported, have also been calculated and plotted. The measured fluxes are close to those extrapolated from the H92α flux; the Brα line flux is about 90% higher than the wind prediction, and the H6α and H7α lines are stronger by a factor of 1.8 and 2.0 respectively. The same model finds the H7β and H8γ line fluxes are consistent with a wind to within their measurement errors, and these results are shown in Figure 2 as small open inverted triangles that virtually overlap the measured data points (since the curve refers only to the α-line transitions, a box is drawn around these two line fluxes to separate them.) The lasing H15α line is, of course, 35 times brighter than this model. The 10% uncertainty in the H92α flux we have used as a reference is not adequate to explain any of these deviations from the wind prediction.

There are several possible sources for these deviations from wind model predictions. First, even a small change in the wind parameters, for example a modest acceleration like s=0.5 instead of s=0, would be more than enough to boost the near and mid-IR line fluxes when extrapolated from the H92α line which is produced so far away (see the discussion and relations in Smith, Fischer, Geballe and Schwartz, 1987). However, Hamann and Simon (1988) note that their [FeII] emission might suggest deceleration; this would push the predicted fluxes of the H lines even further from those observed. Alternatively, as noted above, the wind itself may have very complex structures and/or motions. We have generally adopted (see also Paper IV) the generic "weak wind" model of

8

Hollenbach et al., (1994) for this source to describe aspects of the disk flaring and wind, but note that they too call attention to the fact that for MWC349A their model has difficulty describing the observed emission within the inner 30 AU. We note that their model predicts an $n \propto r^{-3/2}$ dependence to the flow, whereas the continuum data seem to be consistent with a $1/r^2$ wind (e.g., Cohen et al.) which we have adopted to fit the line fluxes.

After considering these alternative wind scenarios, we conclude that the most probable reason the line fluxes deviate from wind models is that the emitting ionized gas around MWC 349A is not limited to the wind. In particular, the Hollenbach et al. (1994) model has stellar ionizing photons maintaining an HII-region like atmosphere above the disk, including the region of the inner zone where the near and mid-IR lines are expected to arise. Hamann and Simon (1986) attribute the location of the Brα line to such a location: the double-peaked profiles and/or asymmetries of the shorter wavelength lines are strong indications the lines originate in a rotating disk rather than in a bipolar wind. We therefore modeled the remainder of the line fluxes, not produced by the bipolar wind, as arising from a static, optically thin HII region, normalized in turn to the observed IR line flux from this region. We calculated values from the Hummer and Storey Case B emissivities for the case of $T=10^4$K and $N_e=1\times10^7$ cm^{-3}; the conclusions are not particularly sensitive to the exact values of either T or N_e.

If we normalize the fluxes to the intrinsic total Brα flux, whose wavelength is at 4 μm, the extinction to the source contributes uncertainty. Using the canonical value for extinction in this source of $A_V=10$ mag (Cohen et al., 1985), the total Brα flux is 3.0×10^{-17} W/cm^2 (Hamann and Simon, 1986), with about half this flux contributed from the strong wind. The total modeled fluxes for the H6α and H7α lines then come out about 20% higher than those observed. If the assumed extinction is too high, the intrinsic flux of Brα is reduced and the predictions for the other lines fall even closer to the measured values. The current extinction value is derived by Cohen et al.'s analysis of the photospheres of both MWC349A and MWC349B. They find the extinction to MWC349A is about 2 mag larger than that for MWC 349B, and they speculate that this extra extinction is likely due to the effects of the edge-on disk, while that of the other 8 mag of extinction is probably

9

foreground dust. If the Brα and mid-IR lines arise in a region outside of the disk, they might not experience all of this additional extinction. Given the other general uncertainties in the physical structure of this inner region, and the wavelength dependence of the extinction itself, we conclude that an extinction between A_V=6-10 mag can adequately describe all the mid-IR line fluxes. We note that Kelly *et al.*(1994) also estimate an $A_V \approx 11$ mag from the near-IR hydrogen and helium line ratios. Because at the longer wavelengths we report here these extinction uncertainties produce negligible flux variations, we instead normalized the HII region contributions to the H7α line flux, that is, the total flux observed minus that contributed by the wind as calculated above. In Figure 2 the solid curve plots the contributions to the lines from the wind alone, while the dotted curve shows the total fluxes, wind plus "HII region". The predicted total mid-IR line fluxes, when calculated and normalized in this way, are close to all those observed including the Brα flux. We did not attempted to fit or model the many shorter wavelength line fluxes that have been seen because at wavelengths shorter than 4.05μm the size of the extinction correction becomes very large and sensitive.

The plots in Figure 2 also illustrate that no combination of wind and static atmosphere such as we have considered here is able to explain the very strong measured FIR fluxes in the H15α, H12α, and H10α lines reported by Strelnitski *et al.* (Paper IV). Our results confirm that these lines do indeed show sign of significant amplification: hence, lasing -- and that somewhere in the parameter space between H10α to H7α the lasing stops or becomes undetectable.

III. THE VELOCITY COMPONENTS

The four observed mid-IR lines show velocity structure spanning as much as 170 kms^{-1} (figures 1a-d). When the lines are fit to a single gaussian profile their peak velocities and their widths closely match (see Table 3): $V_{LSR} \approx +12\pm2$ kms^{-1}, $\Delta V(FWHM) \approx 90\pm8$ kms^{-1}. This value for V_{LSR} is comfortably close to that of the star: +8kms^{-1} (Thum *et al.*, 1995). The high SNR of the data make it tempting to try to attribute some of the velocity structure we observe, especially in the H7α line, to the several wind or disk components of the emission. A two component fit to the profile of H7α

10

gives +30 kms^{-1} (strong component) and -17 kms^{-1} (weak component), quite close to the values seen in the double-peaked Brγ line (Hamann and Simon, 1986), and to the weakly defined ~+37kms^{-1} feature they find in the Brα line, and which they attribute to the surface of an inner wind evaporated from the disk. Hamann and Simon show that a bipolar flow viewed approximately edge-on, as in the case of MWC 349A, is not by itself able to explain the line structure they observe, and conclude some disk-like rotation is needed; indeed this is the origin of the submillimeter lines' structures. If we compare the fluxes in the bright (that is, the positive velocity) components of our two mid-IR α-lines with those predicted from our previous wind model calculations, we find agreement to within 30%. The high velocity component of the H6α is weak, however, and cannot by itself account for the flux from an ionized, static atmosphere component. The negative velocity components are themselves weakly subdivided (Table 1): each of the two α-lines contains a doublet at high negative velocities separated by about 65±5 kms^{-1} . (We note that possible contamination from the He I 7-6 line at this velocity should be 10 times weaker.) In a Keplerian disk, such as that considered by Strelnitski, Smith and Ponomarev (Paper III), the velocity at 30AU from the star is ~50 kms^{-1} (as measured by the H30α maser line velocity and the interferometric observations of Planesas *et al.*, 1992). Hence if the velocity pair structure we see in the IR line emission arises from the disk, the velocity separation suggests a region located at about 25-30 AU from the star. Strelnitski, Smith and Ponomarev show however that laser emission in the H7α line is expected from a much denser region closer in and therefore with higher velocities than observed: at a distance of more like 3×10^{12} cm, within the static atmosphere of the Hollenbach model but much closer to the stellar photosphere. Of course the dense regions might (also) exist as knots of material located further out in the disk; the strong temporal flux variability seen even in the maser lines might be related to such substructures. Temporal monitoring at high spectral resolution to follow variations of individual line components would be helpful in sorting out this possibility.

11

IV . CONCLUSIONS

We present new observations of four mid-IR hydrogen recombination lines, whose strengths are consistent with conventional emission from the ionized atmosphere around the Keplerian disk of the star, the strong bipolar wind, or contributions from both. There is even mild agreement in the observed velocity structure of the lines. No amplification (lasing) is required in these new lines reported here, but the results confirm and strengthen our earlier conclusions that the FIR lines are lasing. The detailed conditions needed in the source to produce detectable laser emission in the mid-IR lines are discussed in Strelnitski, Ponomarev and Smith (Paper II). Although the theory of Hummer and Storey (1995) indicates inversions can be present between the levels of all the transitions we report here, considerations of laser saturation and/or possible beaming may make it hard to produce or detect significant amplification (Paper II). Alternatively it might just be that the densities needed for inversions at, say, the H7α line -- between about 2×10^{10} and 2×10^{11} cm^{-3} (*op cit.*) -- don't exist as a distinct disk annular region, either because as suggested in Paper IV the disk may only extend down to ~40AU, or perhaps because at these high values the material is too close to the star to retain its Keplerian character (see the "weak wind" model of Hollenbach *et al.*, 1994). The results presented here fill in a portion of the critical infrared wavelength interval within which this remarkable source switches from conventional emission to shining in laser lines from its disk.

12

References

Actermann, J.M., in *Astronomical Data Analysis Software*, ed. D.M. Warrall, C. Biemsderfer, and
    J. Barnes (A.S.P. Conference Series 25), p.451, 1992

Aitken, D.K., Smith, C.H., Roche, P.F., and Wright, C.M., 1990, *Monthly Notices, Royal
    Astronomical Society*, **247**, 466

Cohen, M., Bieging, J.H., Dreher, J.W., and Welch, W.J., 1985, *Ap.J.* , 292, 249

Gordon, M.A., *Ap.J.* , **191**, 93, 1992

Lacy, J.H., 1989, *P.A.S.P.*, **101**, 1166

Hamann, F., and Simon, M. 1986, *Ap.J.* , 311, 909

Hamann, F., and Simon, M., 1988, *Ap.J.* , 327, 876

Herzog, A.D., Gehrz, R.D., and Hackwell, J.A., 1980, *Ap.J.* **236**, 189

Hollenbach, D., Johnstone, D., Lizano, S., and Shu, F., 1994, *Ap.J.* **428**, 654

Hummer,D.G., and Storey, P.J., 1992, MNRAS, 254, 277

Kelly, D.M., Rieke, G.H., and Campbell, B., 1994, *Ap.J.* , **425**, 231

Planesas, P., Martin-Pintado, J., and Serabyn, E., *Ap.J.* , 386, L23

Ponomarev, V.O., Smirnov, G.T., and Strelnitski, V.S., 1989, *Astron. Tsirk.*, **1540**, 5

Ponomarev, V.O., Smith, H.A., and Strelnitski, V.S., 1994, *Ap.J.*, **424**, 976, (Paper I)

Rodriguez, L.F., and Bastian, T.S., 1994, *Ap.J.* , 428, 324

Simon, T., 1974, *A.J.*, 79, 1054

Simon, T., and Dyke, H.M., 1977, *A.J.*, **82**, 725

Strelnitski, V.S., Haas, M.R., Smith, H.A., Erickson, E.F., Colgan, S.W.J., and Hollenbach, D.J.,
    1966, *Science*, **272**, 1459, (Paper IV)

Strelnitski, V.S., Ponomarev, V.O., and Smith, H.A., 1996, *Ap.J.* , **470**, 1134 (Paper II)

Strelnitski, V.S., Smith, H.A., and Ponomarev, V.O., 1996, *Ap.J.* , **470**, 1118 (Paper III)

Smith, H.A., Larson, H.P., and Fink, U., 1979, *Ap.J.* , **233**, 132

Smith, H.A., Strelnitski, V.S., and Ponomarev, V.O., 1966, in *Amazing Light*, p. 603, ed.
    R.Y.Chiao, Springer-Verlag, New York,

Storey, P.J., and Hummer, D.G., 1995, MNRAS, 272, 41

Thum, C., Martin-Pintado, J., and Bachiller, R., 1992, *Astr. Ap*, **256**,507

13

Thum, C., Strelnitski, V.S., Martin-Pintado, J., Matthews, H.E., and Smith, H.A., *Astr. Ap.*, 1995, **300**, 843

White, R.L. and Becker, R.H., 1985, *Ap.J.* 297, 677

14

Figure 1 a-c: Irshell spectra of the four hydrogen recombination lines detected. Solid and dotted lines show the result of gaussian fitting. The locations of telluric features are also indicated.

Figure 2: Observed mid- and far-IR lines, also including the $Br\alpha$ line. The three FIR points are taken from Strelnitski *et al.*, 1966 (Paper IV). The solid line shows the predicted flux in the $Hn\alpha$ line sequence from a bipolar wind of constant velocity, normalized to the observed flux in the $H92\alpha$ transition at 3.1 cm. The dotted line shows the predicted flux in the $H\alpha$ lines from both the wind plus a component from a thin HII-region, with the latter contribution scaled to the flux in $H7\alpha$. The x-axis is marked with diamonds showing the wavelength locations of all the $Hn\alpha$ lines ($H16\alpha$ - $H4\alpha$); the two theoretical curves were produced by calculating fluxes for each of these thirteen lines, and connecting the points with straight line segments. Also plotted at the corresponding fluxes and wavelengths are the $H7\beta$ and $H8\gamma$ lines, with open inverted triangles showing the predicted fluxes from a "wind only" model; these non-α lines are drawn in a box to indicate the curves do not refer to them.

15

Table 1. Log of Observations

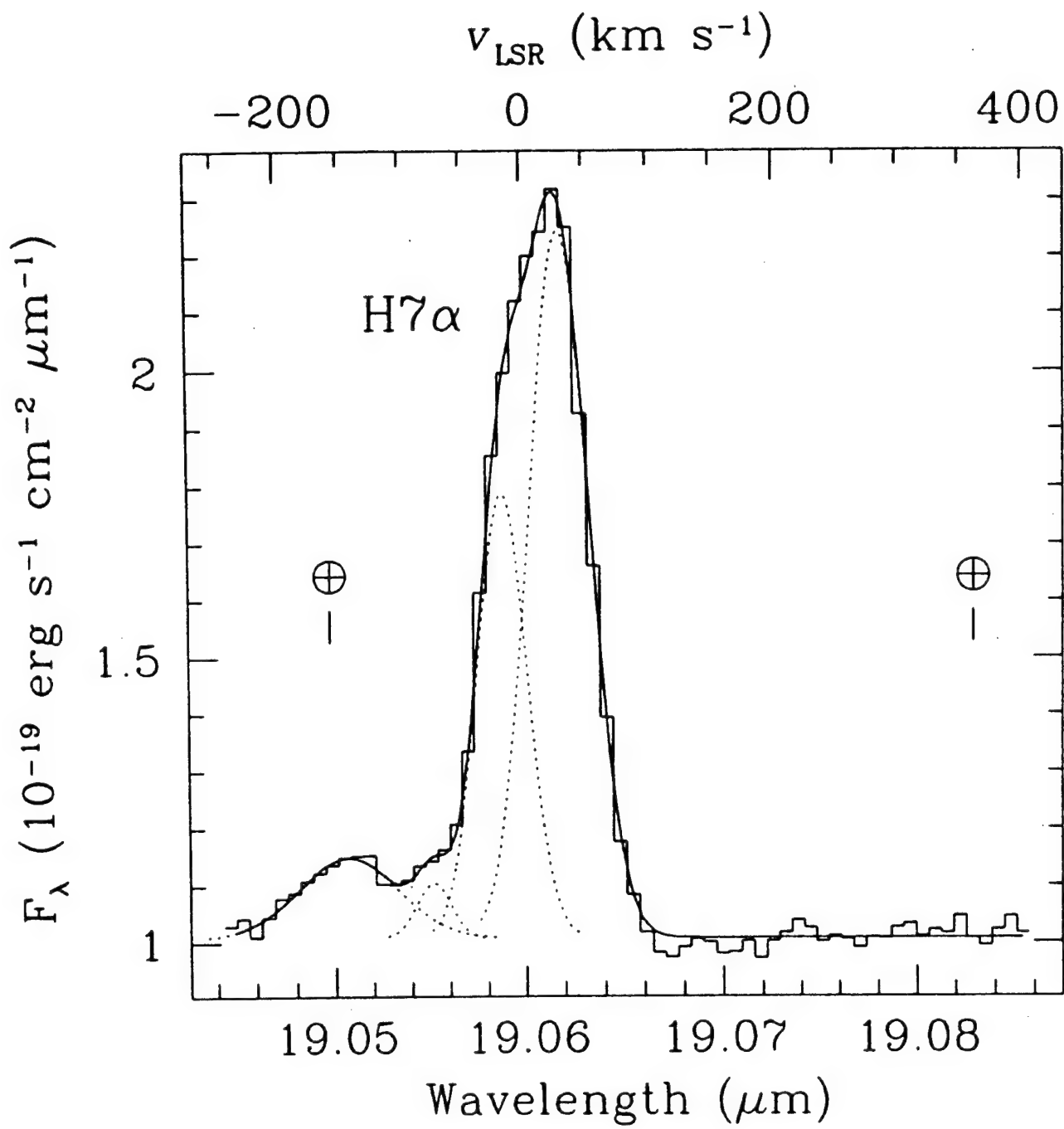| Transition	$\lambda(\mu m)$	UT Date (1994)	$T^a_{integration}$ (sec)	Resolution (kms^{-1})
H7α	19.062	June 7	1258	15
H6α	12.372	June 7	419	25
H6α	12.372	June 8	1258	25
H7β	11.309	June 8	210	15

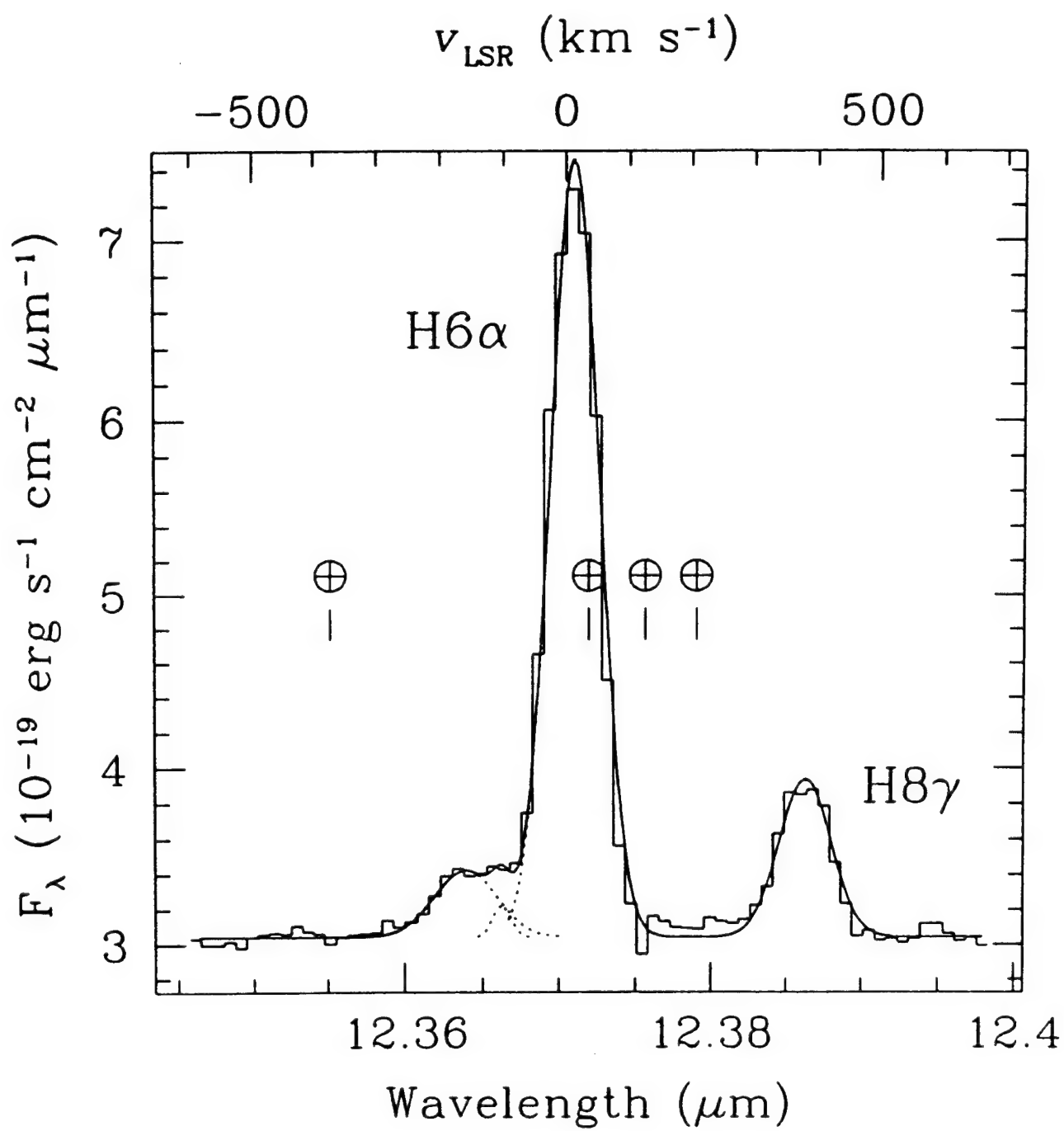[a] Total on source integration time

Table 2. Integrated Line Fluxes

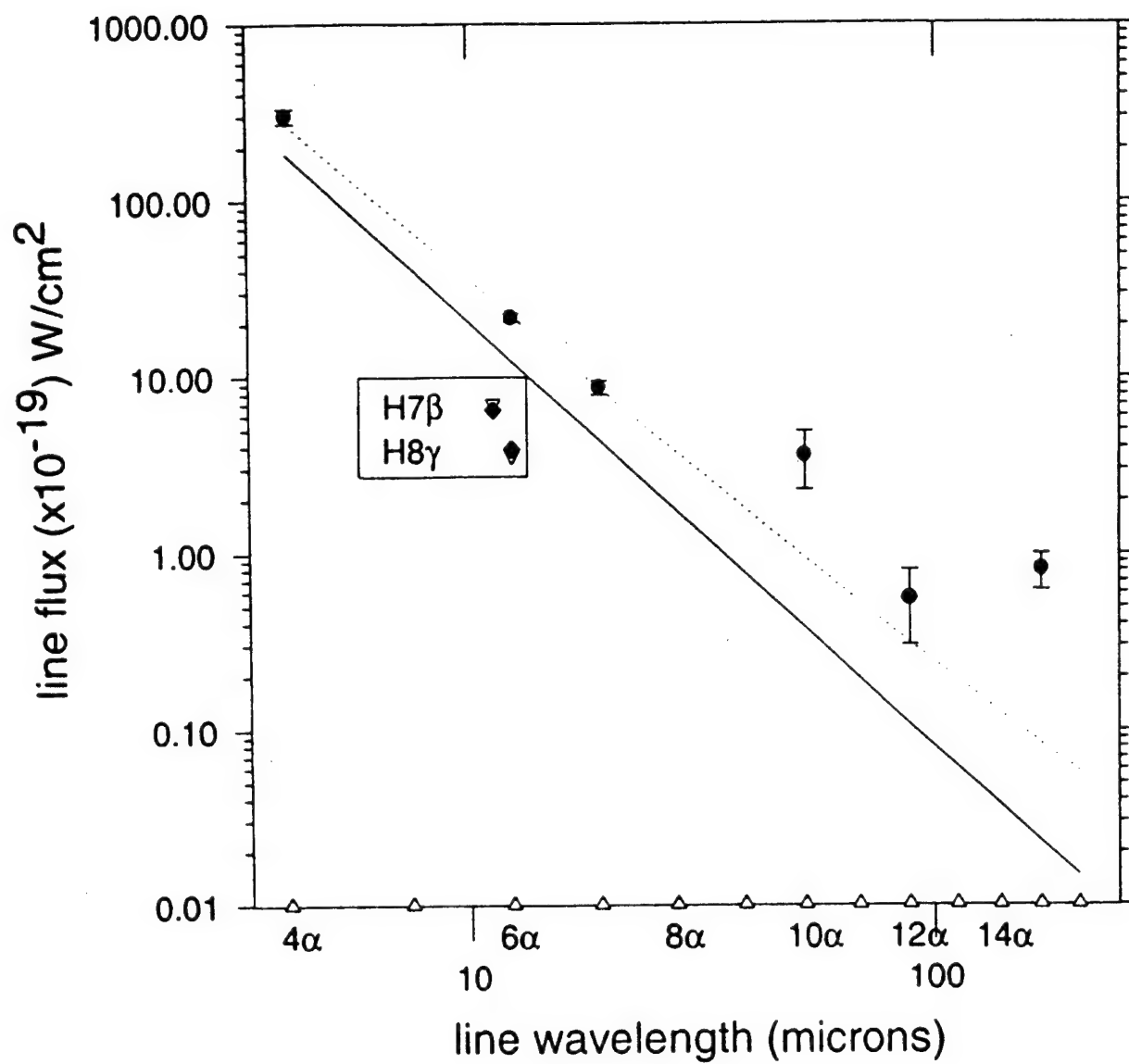| Transition	$\lambda(\mu m)$	Integrated Line Fluxes[a] ($\times 10^{-15}$ Wm^{-2})
H7α	19.062	8.7
H6α	12.372	22.0
H7β	11.309	6.5
H8γ	12.387	3.9

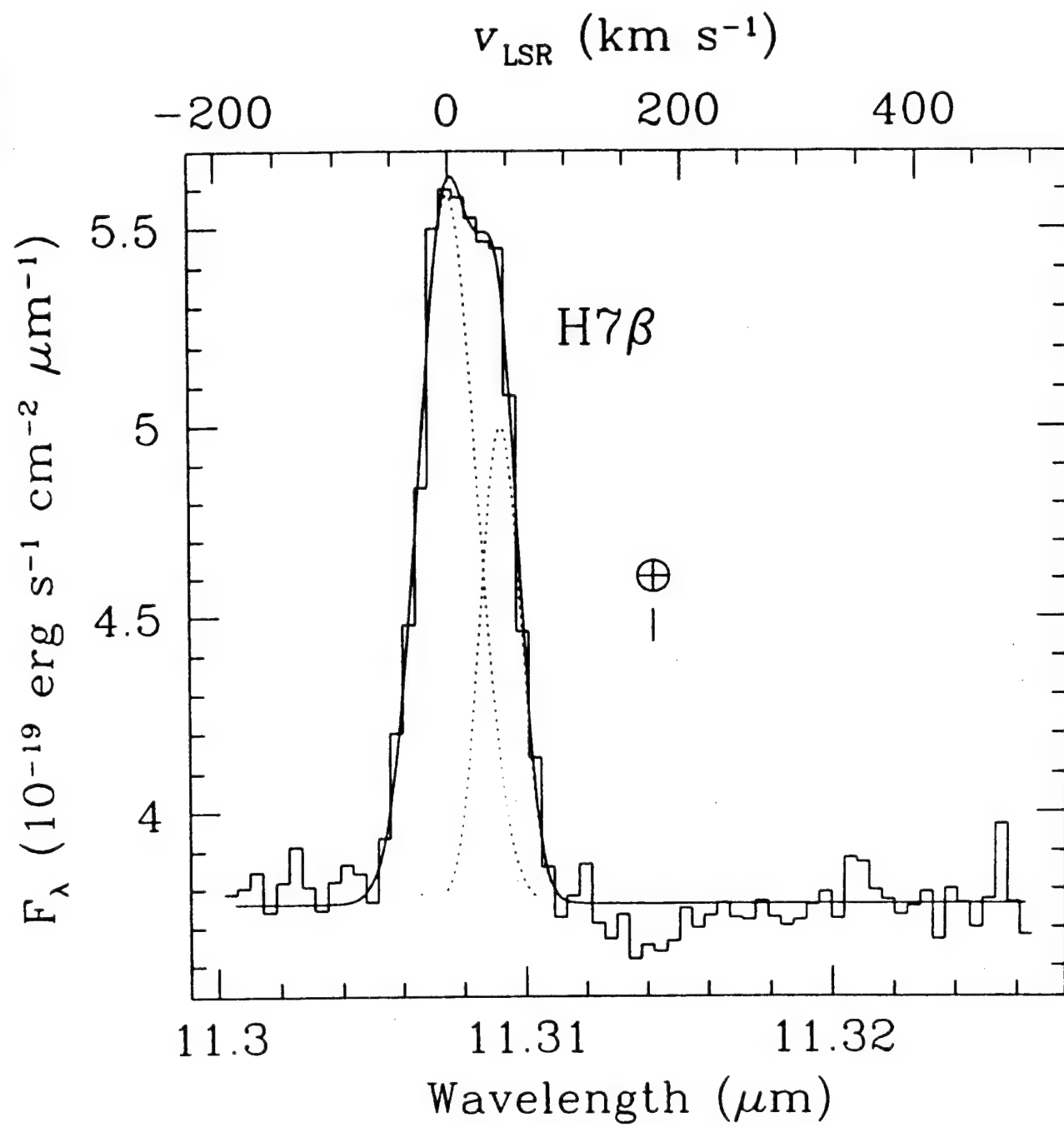[a]Systematic uncertainties are estimated to be ~15%; relative uncertainties are <5%.

16

Table 3. Line Component Parameters

Transition	V_{LSR} (kms^{-1})	ΔV_{FWHM} (kms^{-1})	Flux ($\times 10^{-15}$ Wm^{-2})
H7α	30 ± 2	57 ± 3	4.8 ± .3
	-17 ± 2	48 ± 4	2.5 ± .3
	-74 ± 4	33 ± 11	0.2 ± .1
	-144 ± 5	95 ± 13	0.9 ± .1
(single gaussian fit:	13.5	82.4 ± 3	8.7)
H6α	13 ± 1	90 ± 1	17.4 ± 0.3
	-103 ± 7	35 ± 32	0.3 ± 0.3
	-160 ± 17	116 ± 31	1.9 ± 0.6
H7β	14.3 ± 3	82.6 ± 4	6.5 ± 0.6
H8γ	11 ± 2	98 ± 6	3.9 ± 0.3

17

line flux (x10^{-19}) W/cm^2

1000.00

100.00

10.00

1.00

0.10

0.01

H7β

H8γ

4α   6α   8α   10α   12α 14α

10   100

line wavelength (microns)

The Infrared Nucleus of the Wolf-Rayet

Galaxy Henize 2-10[1]

S. C. Beck[2]

and

D. M. Kelly[2,3], J. H. Lacy

S. C. Beck[2]

School of Physics and Astronomy of the Sackler Faculty of Exact Sciences and Wise

Observatory; Tel Aviv University, 69978 Ramat Aviv, Israel

and

D. M. Kelly[2,3], J. H. Lacy

Department of Astronomy/McDonald Observatory, University of Texas, Austin, TX 78712

93

ABSTRACT

We have obtained near-infrared images and mid-infrared spectra of the starburst core of the dwarf Wolf-Rayet galaxy He 2-10. We find that the infrared continuum and emission lines are concentrated in a flattened ellipse 3-4″ or 150 pc across which may show where a recent accretion event has triggered intense star formation. The ionizing radiation from this cluster has an effective temperature of 40,000 K, corresponding to $30 M_\odot$ stars, and the starburst is $0.5 - 1.5 \times 10^7$ years old.

Subject headings: Galaxies: Individual (He 2-10) — Galaxies: Starburst — Infrared: Galaxies

1. Introduction and Observations

He 2-10 is a blue compact dwarf galaxy and the first galaxy in which Wolf-Rayet emission features were seen (Allen, Wright, & Goss 1976). It contains a bright star cluster A and a fainter cluster B 380 pc (8″ at the assumed distance of 9.2Mpc) to the east of A. The outer isophotes of the galaxy are smoothly elliptical. The kinematics of the molecular and atomic gas (Kobulnicky et al. 1995) show that He 2-10 is probably the moderately advanced merger of two dwarf galaxies. Optical spectroscopy (Vacca & Conti 1992) found hundreds of WR and thousands of O stars in the brighter cluster A, and HST UV images (Conti & Vacca 1994) show that the hot stars are grouped into knots the size and mass of globular clusters but from 1 to 10 Myr old. He 2-10 is thus a "starburst dwarf". Starburst dwarfs differ in important ways from other starburst galaxies: they are objects whose non-burst star formation rate is almost nil, they have low metallicity compared with larger galaxies, and their star formation is not driven by the dynamical mechanisms that dominate in spiral galaxies.

We set out to study the current stellar population of the starburst in He 2-10, with the hope of deducing the history of star formation activity in this galaxy and finding what may have caused it. It is known (Kawara, Nishida, & Phillips 1989) that the brightest region of He 2-10 is actually heavily obscured. We therefore observed this galaxy in the infrared where the extinction will be relatively small. We obtained spectra of the important infrared emission lines in the $8 - 13\mu$m region with the Irshell spectrograph (described in Lacy et al. 1989) at the NASA IRTF in May 1995. A wavelength region equivalent to 950 km s^{-1} was scanned around each of the [Ne II] 12.8μm, [Ar III] 8.99μm, and [S IV] 10.5μm lines. The spectral resolution was about 30 km s^{-1}. The slit was 2″ wide and sampled by 11 pixels along its 11″ length. It was oriented NS for the [Ne II] measurements and EW for the others. The telescope drifted by as much as 1-2″ during a ten minute observation. The

weather was good for the [Ne II] and [Ar III] observations but unstable for the [S IV], so we will use a [S IV] measurement with the same instrument from ESO made available to us by J.M. van der Hulst. The infrared line fluxes and details of the observations are in Table I and a typical [Ne II] spectrum is shown in Figure 1. We used a card at ambient temperature and standard stars for flux calibration and the results are accurate to 20%. The data were reduced and analysed with the SNOOPY package (Achtermann 1992).

We also present in Figure 2 J, H and K band continuum images obtained for us as a service observation by Mr. Charles Kaminski using the NSFCAM on the NASA IRTF. The spatial scale on these figures is 0.3″ per pixel, and the FWHM of stars in the field is 0.9″. The images were reduced and analysed with the VISTA package. Each image in figure 2 is the sum of two or three exposures in that band which were flatfielded with dome flats. The exposure times were different in each band and totalled 6 sec at J, 48 sec at H, and 60 sec at K; the galaxy was at least 35000 counts above the sky background even in these short exposures. We have not attempted to flux-calibrate the images.

2. Spatial Extent and Structure of the Starburst

2.1. The Infrared Continuum

Optical observations of He 2-10 show that continuum and line emission are strongly concentrated in a small clump (Vacca & Conti's A) in the center of the main body of the galaxy. Corbin, Korista, & Vacca's (1993) images show that the central source in the inner 10″ extends towards PA 127 (in degrees east of north) in $H\alpha$ and in the V band. The V-band image of the entire galaxy has a halo at PA 168, which Corbin et al. believe is the major axis of the object. At 10μm Sauvage, Lagage, & Thuan (1995) found an HII region NW of the main clump which they identify with the $H\alpha$ extension in that direction. The

near-infrared images in J,H, and K bands are less affected by extinction than is the optical and have the further advantage that they are good bands for locating giant and supergiant stars and dust-obscured O and B stars. The J,H, and K images in Figure 2 look very much alike; they each show an elongated ellipse of dimension (defined from the contour which is 10% of peak above the background) about 5x3 arcsec extended in PA 130, which we will hereafter call "the disk" (because it looks like a disk, not because there is any data on its rotation). If the brightest point of the disk is the center of the galaxy then the disk is not symmetric around the center but extends further to the NW than to the SE, and on the NW side of the center has a slightly less acute (to NS) angle. We believe that both these effects are due to unresolved subsources, notably the 10μm H II region, probably the small clusters of hot stars seen in the UV images, but possibly others which are still unknown, rather than to a bar structure. The logs of the ratios of J/K, J/H and K/H, which are equivalent modulo a constant to the relative J-K, J-H and K-H colors, are in Figure 3. There are no obvious structures that could be attributed to dust lanes. (It should be noted that the infrared aperture photometry of Johansson (1987) is on a much larger scale; the entire disk lies inside the smallest aperture used there.)

We see that all the tracers of active star formation are concentrated in the NIR disk. In addition to the near and middle infrared emission and the $H\alpha$ described above, the UV star clusters found by Conti & Vacca (1994) appear to lie across the disk in a bent line (bent in the same sense as the shift across the center seen in the NIR). We suggest that the UV star clusters lie on the near, less-heavily obscured side of the disk.

How does the NIR disk, the locus of current star formation, relate to the overall structure of the galaxy and its merger history? The accreted CO has a velocity structure reminiscent of a galaxy disk with the maximum velocity gradient in PA 130, agreeing with the NIR disk. The brightest CO is at PA 150, much closer to the PA 160 angle of the

galactic halo (Kobulnicky et al. 1995). We suggest that the NIR disk is the original disk of the galaxy and that accreted CO falling onto it is fueling the burst of star formation seen in the UV and IR. That the galactic halo is at a different angle than the disk may record an offset between disk and halo that predates the accretion event. It is also possible that the accretion process itself, which is well-advanced and probably at least 10^8 years old, distorted the angle of the galactic halo. This form of merger has been little studied so this suggestion must remain tentative.

It should be noted that the 3.6 cm radio continuum observations of Kobulnicky (1996), the CO observations of Kobulnicky et al. (1995), and the H_2 measurements of Baas, Israel, & Koorneef (1994) do not agree with the infrared continuum and emission lines. The peak of CO emission is $2''$ ENE of A, as is a strong source of 3.6 cm radio emission, and the peak of shocked H_2 is offset 1-$3''$ east from A. It is probable that the CO marks a body of gas not currently forming stars and that the H_2 is shock excited by winds from the starburst impacting the molecular cloud. It is harder to explain the offset between the 3.6 cm radio continuum and the starburst. That region of the galaxy may be so blanketed by extinction that even the 2 and 10 μm continua and 12.8μm [Ne II] emission cannot penetrate; this would be consistent with the concentration of molecular gas in that area. Or, the 3.6 cm emission may be from supernovae and trace an older stage of the starburst which does not currently have detectable infrared continuum or line emission, in which case it should be strong at 20cm (although measurements at 20cm with the spatial resolution needed to separate the 3.6 cm emission peak from A will be hard to achieve).

2.2. The [Ne II] Lines

We attempted to derive the size of the [Ne II] emission line source by comparing the Irshell data on [Ne II], the strongest line observed, to stellar profiles. The PSF for the run in which these data were obtained was somewhat elliptical due to an optical misalignment, which limits the accuracy of this method, but we can say that the [Ne II] emission on peak A is 3″ in diameter in both dimensions (with a probable error of 0.5″). The spatial resolution of the [Ne II] is enough lower than the infrared and UV images that the disk structure seen in the infrared and the small star clusters seen in the UV could not be distinguished even if present. We will therefore refer to the emission source detected in [Ne II] as the star cluster. This will provide consistency with the accepted use of cluster A and B for the bright optical sources. But we think it possible and even likely that it will break up into smaller and more structured sources under higher resolution.

The secondary 10μm H II region was not mapped in [Ne II]. We looked for [Ne II] on B and did not detect it, which is consistent with the relative strengths of the two clusters in other wavelengths and is further argument that star formation in cluster B, while it exists, is at too low a level to be called a starburst.

If the kinematics of the [Ne II] are like those of the CO and HI, the FWHM would be 50-80 km s^{-1}. Our lines were broadened by a misalignment of the dewar optics, but they showed similar profiles to the [Ne II] observed on the same night in the Galactic H II region W33. The lines in W33 are expected to be no more than 50 km s^{-1} wide, so we place an upper limit on the lines in He 2-10 of FWHM $\leq$ 100 km s^{-1}.

The common practise of quoting "the" extinction to a galaxy is misleading: galaxies and the dust within them can have complex three-dimensional structures. It is somewhat more precise to discuss the extinction to a given component of a galaxy. Vacca & Conti's

(1992) optical spectroscopy of He 2-10 found $E_{(B-V)} = 0.56$ or $A_v = 1.7$ mag to region A. Such a high value for A_v implies that the optical observations could not see through the source. The infrared Brackett line measurements of Kawara et al. (1989), which will probe deeper into the source, found A_v of about 17 mag, which is consistent with the depth of the 10μm silicate feature and the molecular column observed by Kobulnicky et al. (1995). He 2-10 is therefore like NGC 5253 (Beck et al. 1996) and many other galaxies where optical and UV observations see the near side of the star forming region and longer wavelength measurements see deeper in. The extinction in the infrared, while lower than in the optical, is not negligible. Unfortunately the mid-infrared extinction law is not well known and seems to differ in different environments (Draine 1989); furthermore, the dependance of extinction on the metallicity is unknown. Extinction laws in the literature give results ranging from 0.6 mag at [Ne II] and about 1.7 mag at [Ar III] and [S IV] (Becklin et al. 1978) to 0.22 mag at [Ne II] and 0.55 mag at [Ar III] (Roche & Aitken 1984) for $A_v = 17$ mag. We will discuss the importance of this uncertainty below.

3. Stellar Population and Star Burst History

3.1. Stellar Population

The O star population of the obscured region can be found from the mid-infrared and Brackett lines. First, we compared the ratios of the [Ne II], [Ar III] and [S IV] line fluxes to the model H II region grid of Sutherland, Shull, & Beck (1996) to find the effective temperature of the exciting stars. We use models with $z = 0.1z_\odot$, the closest in the grid to the almost $0.2z_\odot$ oxygen value of He 2-10 (Conti & Vacca 1994), and assume that Ne:Ar:S is solar. The models have $log(n_e) = 4.0$, which is typical of dense starburst regions, and log U (the ionization parameter) -2.5 and -1.5.

100

The [Ne II]/[Ar III] ratio is a good stellar temperature diagnostic for temperatures less than 45,000 K as it is fairly insensitive to density, ionization parameter and filling factor. The [Ar III] and [Ne II] were not observed in identical locations nor at the same slit angles, so we have compared the total flux in the EW slit position on region A where [Ar III] was observed to the total [Ne II] flux observed in each of the NS [Ne II] slit positions. This assumes that the distribution of the infrared lines is spherically symmetric, which within the resolution of the observations it appears to be; the uncertainties introduced by possible small asymmetries will be less than those from other factors such as extinction. The results uncorrected for reddening between 12.8 and 8.99 μm give stellar temperatures of 36-38,000 K for the different [Ne II] slit positions. Any extinction correction will increase [Ar III] relative to [Ne II] and give hotter temperatures; both the Becklin et al. (1978) and the Roche & Aitken (1984) extinction curves give stellar temperatures 38-40,000 K. These results are very insensitive to the metallicity and will be the same within the uncertainties for solar metal content. The weakness of [Ne II]/[Ar III] ratio is that it is relatively insensitive to small temperature shifts in precisely the 36,000 K to 41,000 K range where He 2-10 falls. The [Ne II]/[S IV] ratio (comparing the total observed [Ne II] flux to the total observed [S IV] flux) gives stellar temperatures above 37,000 K, but this ratio, although it has a large dynamic range, is very sensitive to the ionization parameter and the metallicity. If we compare the ratios of [Ar III], [S IV], and [Ne II] to those seen in the Galactic Center and NGC 3256 where the effective stellar temperature has been derived from the much more sensitive [Ne II]/[Ne III] ratio (Kunze et al. 1996) and interpolate, we find a temperature of $39,000 \pm 1400$ K, consistent with what the [Ne II]/[Ar III] ratio gives.

The stellar temperatures (38,000-40,000 K) found from the infrared lines are equivalent to O6.5 ZAMS stars (Panagia 1973). The ionizing spectrum of a cluster of stars will differ from that of a single star, so it is only an approximation to treat the cluster as if it were

composed only of one stellar type. While we expect there to be many stars cooler than 40,000 K the weak [Ar III] and [S IV] rule out the presence of more than a very few stars hotter than 40,000. Cluster simulations (Kunze et al. 1996) show that the upper mass cutoff in a cluster is typically about $5M_\odot$ greater than the single-star equivalent mass, so the upper mass cutoff is about $35M_\odot$. We can use Ho, Beck, & Turner's (1990) result which relates the total luminosity of a star cluster to the ionization (with a slight correction because we use a different upper mass cutoff) and find that the total stellar luminosity needed for the Lyman continuum flux N_{Lyc} of 7.6×10^{52} to 1.1×10^{53} s^{-1} (found from the extinction corrected $Br\alpha$ flux) is $3.7 - 5.3 \times 10^9 L_\odot$. This is quite close to the $8 \times 10^9 L_\odot$ of total luminosity from the IRAS FIR flux of He 2-10. The FIR beam of course contains the whole galaxy while the Brackett lines are limited to the core; He 2-10 is another example of the common starburst galaxy phenomenon that the bulk of the infrared luminosity observed by IRAS with large beams is generated by massive stars in a very small area (Ho et al. 1990).

The stellar luminosity derived from the infrared lines may be compared to that observed at optical and ultraviolet wavelengths. The cluster observed in the infrared is about a factor of 10 more luminous than the 5500 O stars that Vacca & Conti (1992) find from optical spectra. The ultraviolet observations of Conti & Vacca (1994) find about 6 times as many O stars as their optical measurements; this may be due, as Conti & Vacca suggest, to a combination of larger area coverage and contributions from evolved stars, but the dependance of their result on the very large extinction correction at 220nm may also be a factor; a small change in the proper extrapolation from E_{B-V} to A_{220} can change the final luminosity by more than a factor of two. In any case, the luminosity of the star cluster derived from the infrared lines is at least twice as great and may be 5-10 times as great as the optical luminosity. This is the expected result when the extinction is so great that the

102

optical measurements do not see through the source.

The total mass of the obscured star cluster can be calculated from the observed ionization if we assume a mass function. If we take a mass function that goes as $M^{-3.2}$, assume that stars smaller than $10_\odot$ do not contribute significantly to the ionization and sum the ionization of stars from 35 to 10 $M_\odot$ using Panagia's (1973) results for the ionizing flux of a ZAMS star of a given temperature and spectral type, we find the total mass of stars between $10M_\odot$ and $35M_\odot$ is $4.7 - 6.9 \times 10^6 M_\odot$ (where the spread in mass reflects the range of total ionization found from the Brackett lines). Giant and supergiant stars produce more ionization at a given spectral type; taking the extreme case that all the stars are luminosity class III reduces the total mass by about a factor of 2. The ZAMS case implies a mass density of $8 M_\odot pc^{-3}$ in a 130 pc radius, although since the young stars are probably clumped into small clusters like the ones seen in the UV (this may be confirmed when higher spatial resolution infrared observations become possible) this average density is only a lower limit. Kobulnicky et al. (1995) find a dynamical mass of 3.2×10^6 to $4.8 \times 10^7 M_\odot$ in the inner 70 pc, but caution that those are only lower limits due to beam size effects. But even within the large uncertainties of both the CO and the infrared measurements, it is clear that a substantial fraction of the dynamical mass in the center is in the form of young massive stars.

3.2. Starburst History

The effective stellar temperature of the cluster, as derived from the mid-infrared lines above, can be used in combination with a set of cluster evolution models to estimate the age and nature of the starburst. The other important constraint on the starburst age is the non-thermal radio flux, which we find by subtracting the 5 GHz thermal flux of $9 - 11 mJy$

(derived from the Brackett lines, the range reflects uncertainty in the extinction and the electron temperature) from the total $55 mJy$ observed by Allen et al. (1976). (While the radio fluxes were observed with much larger beams than the infrared, we will assume that the radio emission is dominated by the young star cluster and not by extended emission; this is usually the case in star-forming dwarfs.) We follow Allen et al. that the non-thermal radio emission is due to supernovae remnants rather than to the more extreme mechanisms which occur in radio galaxies; this agrees with the spectral index, the size and structure of the radio emission in the 3.6 cm maps, and the nature of the host galaxy. Then the non-thermal flux shows that a large number, which cannot be calculated exactly because of the wide range of supernova radio brightnesses but which we estimate at a few thousand, of supernovae have exploded in He 2-10. (We believe that the objection of Allen et al. that a large number of supernovae is not consistent with the low metal content of the galaxy may not be valid; He 2-10 has a relatively high abundance of oxygen for a dwarf, 50% higher than NGC 5253 for example, and the amount of O produced in the required number of supernova is consistent with the observed. It would be highly desirable to observe the [O/Fe] ratio in He 2-10 to constrain the contribution of supernovae to the metal content.)

The observations combined with the cluster evolution models of Sutherland et al. (1996) show that the cluster in He 2-10 is unlikely to have formed coevally. A coeval star cluster cools off so fast that its effective temperature will be as high as the observed only at ages less than 2×10^6 yrs, which is not enough time for the SNe needed for the non-thermal radio emission. We turn to gaussian burst models, where the total mass of stars formed is a gaussian function of time, with its peak at 5×10^6 yrs from the start of the burst and a FWHM in time of 4×10^6 yrs, and the chances of a star of a given mass forming at a given time are found from Monte Carlo simulations. (Other scenarios for long-lived star bursts, such as exponentially decaying rates, are of course possible; the gaussian models

are at present the best studied.) The effective stellar temperature found from the infrared lines does not constrain the burst age tightly; the cluster age can be from 5×10^6 to 1×10^7 years since the start of the burst in the absence of WR stars and as old as 1.5×10^7 yrs if WR stars are important in the infrared cluster. It similarly does not rule out longer-lived bursts. (It is at present very difficult to detect WR stars in the infrared and there is only a very high upper limit on the possible number of WR stars in the infrared cluster (Lumsden, Puxley, & Doherty 1994), nor can we assume that the stellar population in the obscured region is like that in the optically visible region.) If we assume that we do not see stars more massive than about $30 M_\odot$ because they have become supernovae, the cluster must be at least 5×10^6 yrs old (Woosley, Langer & Weaver 1993). The optical and infrared colors indicate that the cluster is about 2×10^7 years old (Johansson 1987); this is somewhat older than our results for the infrared cluster but considering how ill-constrained the age of the infrared cluster is the discrepancy may not be significant. We should remember that only in very unusual cases can a star formation episode be given a unique age; the above numbers probably reflect a star formation rate generally high but fluctuating with time over the last $1 - 2 \times 10^7$ yrs. The optical cluster, for example, contains many WR stars much younger than the cluster age derived from the colors.

3.3. Conclusion

We have found that the infrared emission of He 2-10 is produced by a star cluster 130×180 pc in size, with its ionizing radiation dominated by O6.5 stars, and less than 1.5×10^7 years old. He 2-10 resembles NGC 5253, the most famous bright infrared WR galaxy, in that they are both dominated by condensed central clusters of young OB stars of similar (to within a factor of two) sizes. It appears however to have had a very different

history. The star cluster in NGC 5253 probably formed in a coeval burst; star formation in He 2-10 appears to have been a more sustained process. The galaxies are also at different evolutionary stages; the star cluster in He 2-10 may be almost 10 times as old as that in NGC 5253. The young star cluster in He 2-10 has a disk shape and lies at the same angle as the steepest velocity gradient of the recently accreted molecular gas, which is different from the orientations of the galactic halo and the bulk of the CO. We believe that the recent burst of star formation we have observed lies in the original galactic disk and was triggered by the infall of molecular gas from the accretion event. The offset between the disk and the halo may be the result of the merger process or may have predated the merger.

REFERENCES

Achtermann, J.M., in ADASS p 451, A.S.P.Conference 25, 1992.

Allen, D.A., Wright, A.E., & Goss, W.M. 1976, MNRAS, 177, 91

Baas, F., Israel, F.P., & Koorneef, J. 1994, A&A, 284, 403

Beck, S.C., Turner, J.T., Ho, P.T.P., Lacy, J.H., & Kelly, D.M. 1996, ApJ, 457, 610

Becklin, E.E., Matthews, K., Neugebauer, G., & Willner, S.P. 1978, ApJ, 220, 831

Conti, P.S. & Vacca, W.D. 1994, ApJ, 423, L97

Corbin, M.R., Korista, K.T., & Vacca, W.D. 1993, AJ, 105, 1313

Draine, B.L., in Infrared Spectroscopy in Astronomy p 93, ESA SP-290, 1989.

Ho, P.T.P., Beck, S.C., & Turner, J.T. 1990, ApJ, 349, 57

Johansson, L. 1987, A&A, 182, 179

Kawara, K., Nishida, M., & Phillips, M.M. 1989, ApJ, 337, 230

Kobulnicky, H.A., Dickey, J.M., Sargent, A.I., Hogg, D.E., & Conti, P.S. 1995, AJ, 110, 116

Kobulnicky, H.A. 1996, private communication

Kunze, D. et al,1996, in press at A&A.

Lacy, J.H., Achtermann, J.M., Bruce, D.E., Lester, D.F., Arens, J.F., Peck, M.C., & Gaalema, S.D. 1989, PASP, 101, 1166

Lumsden, S.L., Puxley, P.J., & Doherty, R.M. 1994, MNRAS, 268, 82

Panagia, N. 1973, AJ, 78, 929

Roche, P.F. & Aitken, D.K. 1984, MNRAS, 215, 269

Sauvage, M., Lagage, P.O., & Thuan, T.X. 1995. Exp. Astr., 3, 165

Schaller, P.G., Schaerer,D.,Meybet,G, & Maeder,A. 1993, A&AS, 96, 269

Sutherland, R.S., Shull, M. & Beck, S.C. 1996, in prep.

Vacca, W.D. & Conti, P.S. 1992, ApJ, 401, 543

Woosley, S.E., Langer, N., & Weaver, T.A. 1993, ApJ, 448, 315

This manuscript was prepared with the AAS LaTeX macros v4.0.

Fig. 1.— The spectrum of [Ne II] observed with a $2'' \times 11''$ NS slit across the center of peak A.

Fig. 2.— J, H, and K band images of He 2-10 obtained with NSFCAM on the IRTF. a) J band: the first contour is at 16000 counts and the interval is 2500 counts. b) H band: the first contour is at 53000 and the interval is 2000. c) K band: the first contour is at 55000 and the interval is 3000.

Fig. 3.— The logarithms of the a)J/H, b)J/K, and c)K/H map ratios. These are equivalent to the relative J-H, J-K and K-H colors up to a constant.

TABLE 1. Observed Line Fluxes

Species	Wavelength	Date, Site	Slit	Flux($erg\ s^{-1}\ cm^{-2}$)
[Ne II]	12.8μm	May 1995, IRTF	2.0″ NS	$2 \pm 0.2 \times 10^{-12}$
[Ne II]	12.8μm	April 1993, ESO	1.6″ EW	$2.5 \pm 0.5 \times 10^{-12}$
[Ar III]	8.99μm	May 1995, IRTF	2.0″ EW	$1.6 \pm 0.5 \times 10^{-13}$
[S IV]	10.5μm	April 1993, ESO	1.6″ EW	$5 \pm 3 \times 10^{-14}$

Fig 1

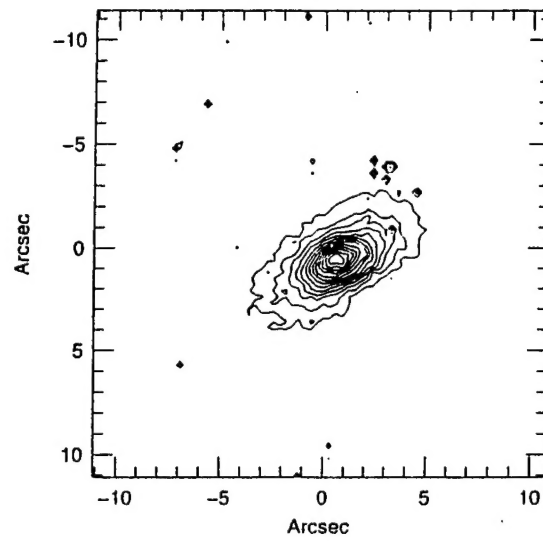Flux (10^{-12} ergs / sec cm^2 cm^{-1})

Wavenumber (cm^{-1})

Fig. 2a

Fig. 2b

Fig. 2c

Fig. 3a

Fig. 3b

Fig. 3c

113